

**Improved One-Dimensional Model of Blood Flow
in the Human Arterial Network,
with Application to Cerebral Flow**

by

John Fillenwarth

A thesis submitted to the Faculty of the University of Delaware in partial fulfillment of the requirements for the degree of Honors Bachelor of Science in Chemical Engineering with Distinction

Spring 2016

© 2016 John Fillenwarth
All Rights Reserved

**Improved One-Dimensional Model of Blood Flow
in the Human Arterial Network,
with Application to Cerebral Flow**

by

John Fillenwarth

Approved: _____
Antony N. Beris, Ph.D.
Professor in charge of thesis on behalf of the Advisory Committee

Approved: _____
Millicent Sullivan, Ph.D.
Committee member from the Department of Chemical and Biomolecular
Engineering

Approved: _____
Susan Groh, Ph.D.
Committee member from the Board of Senior Thesis Readers

Approved: _____
Michael Arnold, Ph.D.
Directory, University Honors Program

ACKNOWLEDGMENTS

Many, many thanks to Dr. Beris for allowing me to work with and learn under him for the past two and a half years. I've learned more than I ever thought possible in such a short time. Thank you also to Drs. Sullivan and Groh for their time and feedback throughout this process. Finally, thanks to my friends and family who have always supported me in all my endeavors.

TABLE OF CONTENTS

| | |
|---|------|
| LIST OF TABLES | vii |
| LIST OF FIGURES | viii |
| ABSTRACT | x |
| | |
| 1 INTRODUCTION | 1 |
| 1.1 Overview and Motivation | 1 |
| 1.2 Objectives | 3 |
| 1.3 Relevant Literature | 3 |
| 1.3.1 Original Model | 8 |
| Endnotes | 9 |
| 2 EXTENSION TO RECIRCULATION | 17 |
| 2.1 Expanded Network and Cerebral Arteries | 17 |
| 2.2 Simultaneous Solution and Recirculation | 19 |
| Endnotes | 21 |
| 3 MODELING THE FAHRÅEUS EFFECT | 22 |
| Endnotes | 28 |
| 4 CURRENT 1D MODEL PRESENTATION BASED ON WOMERSLEY SOLUTION OF TRANSIENT FLOW PROBLEM..... | 29 |
| 4.1 Womersley’s Method Setup | 29 |
| 4.1.1 User-defined Parameters | 31 |
| 4.1.2 Governing Equations | 32 |
| 4.1.2.1 Additional Transient Equations | 34 |
| 4.1.3 Model Input and Preliminary Calculations..... | 35 |
| 4.1.4 Test Case Description..... | 39 |

| | | |
|-------|---|----|
| 4.2 | Steady State Solution..... | 39 |
| 4.2.1 | Alternate Method for Single Vessel | 41 |
| 4.3 | Transient Solution | 41 |
| 4.3.1 | Alternate Method for Single Vessel | 47 |
| | Endnotes | 51 |
| 5 | ALTERNATE NUMERICAL APPROACH TO THE 1D VISCOUS FLOW IN AN ELASTIC TUBE | 53 |
| 5.1 | Governing Equations and Problem Setup..... | 53 |
| 5.1.1 | Dimensionless Conversion | 54 |
| 5.2 | Steady State Solution..... | 56 |
| 5.2.1 | Test Case | 56 |
| 5.3 | Transient Solution and Numerics | 60 |
| | Endnotes | 65 |
| 6 | RESULTS AND DISCUSSION..... | 66 |
| 6.1 | Womersley-like Method..... | 66 |
| 6.2 | Numerical Method..... | 68 |
| 6.2.1 | Steady State Validation | 68 |
| 6.2.2 | Simple Oscillatory Input..... | 71 |
| 6.2.3 | Full Pulse Solution | 74 |
| 6.3 | Model Comparison | 78 |
| 6.3.1 | Single Harmonic Comparison | 80 |
| 6.4 | Discussion..... | 84 |
| 7 | CONCLUSIONS AND RECOMMENDATIONS FOR FUTURE WORK | 85 |
| 7.1 | Conclusions | 85 |
| 7.2 | Recommendations for Future Work | 85 |

| | |
|---------------------------------|----|
| REFERENCES | 87 |
| RECIRCULATION MATLAB CODE | 95 |

LIST OF TABLES

| | | |
|-----------|---|----|
| Table 1: | Physical parameters used in the current model. | 31 |
| Table 2: | Scaling of dimensionless variables..... | 55 |
| Table 3: | Scaling of other dimensionless parameters | 57 |
| Table 4: | Test case reference conditions, all constant | 57 |
| Table 5: | Zero-order solution of perturbation expansion..... | 58 |
| Table 6: | 1 st -order solution of perturbation expansion | 59 |
| Table 7: | Model input parameters for test case; both methods | 66 |
| Table 8: | Steady state values, numerical code | 68 |
| Table 9: | Model results obtained using both methods, steady state | 78 |
| Table 10: | Average flowrate values, both methods | 80 |

LIST OF FIGURES

| | | |
|------------|---|----|
| Figure 1: | New arterial network, from Reymond <i>et al.</i> Fig.2 | 18 |
| Figure 2: | Alternate Circle of Willis networks, with estimates of their probability of occurrence; from Alastruey <i>et al.</i> | 20 |
| Figure 3: | Comparison of two empirical relationships between vessel diameter and discharge hematocrit: Barbee dissertation ⁴ (o) vs. Pries <i>et al.</i> (-) ³ ... | 23 |
| Figure 4: | Wall stress vs. pseudo-shear rate, Barbee dissertation data ⁴ (o) versus our model results | 24 |
| Figure 5: | Root of wall stress versus root of shear rate, Barbee dissertation data ⁴ (o) plotted against sample <i>cf</i> values using a Couette geometry | 25 |
| Figure 6: | Barbee dissertation piecewise Equation 18 ⁴ vs. bounds from Goldsmith <i>et al.</i> ⁷ | 26 |
| Figure 7: | Total transient pressures at various points along test vessel, Womersley method..... | 67 |
| Figure 8: | Volumetric flow rates at various points along test vessel, Womersley method..... | 68 |
| Figure 9: | Numerical solution for pressure, steady state boundary conditions | 69 |
| Figure 10: | Numerical solution for fluid velocity, steady state boundary conditions | 70 |
| Figure 11: | Numerical solution for area, steady state boundary conditions..... | 70 |
| Figure 12: | Numerical solution for pressure, oscillatory boundary conditions..... | 72 |
| Figure 13: | Numerical solution for fluid velocity, oscillatory boundary conditions . | 72 |
| Figure 14: | Numerical solution for area, oscillatory boundary conditions | 73 |
| Figure 15: | Boundary conditions for \underline{z} vector, oscillatory case..... | 74 |
| Figure 16: | Numerical solution for pressure, full pulse | 75 |

| | | |
|------------|--|----|
| Figure 17: | Pressure boundary conditions, full pulse..... | 76 |
| Figure 18: | Numerical solution for fluid velocity, first three periods of full pulse.... | 77 |
| Figure 19: | Numerical solution for fluid velocity, periods four through six of full pulse..... | 77 |
| Figure 20: | Numerical solution for area, full pulse | 78 |
| Figure 21: | Transient flowrate results, Womersley method..... | 79 |
| Figure 22: | Transient flowrate results, numerical method | 80 |
| Figure 23: | Single harmonic solution of the Womersley method, full pulse. | 81 |
| Figure 24: | Single harmonic solution of the numerical method, full pulse..... | 82 |
| Figure 25: | Womersley solution for the low Reynolds number case, three periods .. | 83 |
| Figure 26: | Numerical solution for the low Reynolds number case, three periods.... | 83 |

ABSTRACT

A one dimensional model of blood flow in the human arterial system has been reformulated to handle recirculation of blood, a phenomenon that occurs in the cerebral arteries of the brain. This model has also been made modular and the input requirements have been streamlined, thus allowing an easy adaptation to any particular system. Information on blood rheology and the vessel network has been updated to accurately reflect physiological conditions.

Most importantly, an alternate approach to develop and solve the (approximate) governing equations has been successfully implemented. The approach is based on a nonlinear system of hyperbolic equations that are now solved through a specially developed numerical method. This complements the original analytical solution, which requires a linearized version of the problem in order to be applied successfully. By incorporating nonlinear fluid mechanic effects, the new method may be used to validate the previous version, or replace it where the analytical assumptions break down. The results of the two methods on a single test vessel indicate that for low Reynolds numbers both are in agreement, but at high Reynolds numbers small nonlinear inertial effects do exist that create sizeable differences in the outcomes.

Chapter 1

INTRODUCTION

1.1 Overview and Motivation

Developing an accurate model for blood flow provides medical professionals and scientists with an extremely useful tool for diagnostics and research. An individual's pressure pulse patterns can be recorded and be compared over time, allowing doctors to quickly detect abnormalities. A model tailored to a specific patient could also be a useful tool for determining risk for a dangerous surgery. The list of applications extends far past these examples.

We already have the ability to construct a 3D image of an artery bifurcation and examine the pressure and flow profiles around it. However, these 3D simulations are limited in scope by the computational power and time required for them to converge. A full three dimensional model would be too complex to accurately take into account the full arterial system. A one dimensional model of blood flow is computationally much simpler, yet can still provide accurate pressure and flow information on human arteries. However, the majority of one-dimensional blood flow models that have been put forth thus far make rather severe simplifications on the blood flow problem. Physical data on human arteries are very scarce, and any that can be found in literature are usually only measured to two or three digits. Thus, simplifications are needed that may introduce unacceptable errors on the solution. Our goal for this research project was to refine a recently developed blood flow model to

be as accurate as possible, while simultaneously extending its applicability to more complex arterial networks, such as those in the brain that also possess recirculation.

A main focus during the software development was keeping as much physiological information as possible in input files rather than in the code itself. We hope that this software, implemented in MATLAB (as before, but now in a more modular and user-friendly fashion) may eventually be used in a diagnostic setting, where it can be applied to individual patients. Every person has unique vessel characteristics and network topologies. Therefore the software must be user-friendly and designed in a way that allows it to provide accurate outputs for different networks and parameters. The MATLAB framework also facilitates its portability.

A direct application of the new model's capabilities to handle brain arterial flow may eventually be to analyze how blood flow irregularities in the brain will affect cognitive function. With an accurate flow model, one can make simple changes to allow for the partial or full occlusion of arteries that supply the brain or bridge the two hemispheres. The model will then be able to compute the new results for flow to a given vessel, and correlations between blockages and reduced flows can be made. If the model is combined with data about where various cognitive functions take place and what vessels supply these areas, the model can even be used to predict effects on cognition in patients by copying the unique topology of their cerebral arterial system. This one dimensional model is a relatively simple yet extremely powerful tool for analyzing the behavior of blood in not only the brain, but any bodily tissue.

1.2 Objectives

- To reformulate the original 1D blood arterial flow model developed by Johnson *et al.* (2011) so that it is capable of handling flow recirculation, which is present in the Circle of Willis in the brain.
- To reformulate the original MATLAB code to be modular, with separate input files, thus allowing seamless extension to more extensive arterial network descriptions as well as patient personalization.
- To update crucial information on
 - the arteries (involving the most important brain arteries and the Circle of Willis)
 - the blood flow rheology, involving the latest steady state viscoplastic rheology modeling by Apostolidis and Beris (2014).
 - the vessel elasticity
 - the Fahraeus and Fahraeus-Lindqvist effects
- To develop an alternative method of solving the 1D model equations that then can be used to check the previous approach and/or substitute for it as needed on an individual vessel-based case.

1.3 Relevant Literature

Cardiovascular diseases represent the leading cause of non-accidental death in the United States, causing roughly one out of three deaths and contributing more than three hundred billion dollars annually to health costs¹. This explains the enormous interest and the many research activities centered on the investigation of blood flows today, as it can be testified from the many books that have been dedicated partly or

fully to this subject^{2,3,4,5,6,7,8,9,10,11,12,13,14,15,16}, many of which have appeared within the last decade .

Unfortunately, when it comes to understanding the exact local fluid dynamics of the cardiovascular system, there is much difficulty in reproducing the *in vivo* flow profiles for simulation purposes, or even using simulations to effectively represent the arterial flow in regions of higher risk. Three-dimensional (3D) computational fluid dynamic simulations have been performed with increasing frequency on various vascular geometries, ranging from the carotid^{17,18,19,20,21,22,23,24,25,26,27,28}, the coronary^{29,30,31,32,33,34,35,36,37,38,39}, the abdominal aorta^{40,41}, as well as the cerebral^{42,43,44,45,46}, and pulmonary^{47,48} arteries to name a few. However, even here, the physical accuracy of the simulations is questionable as crucial issues such as the non-Newtonian nature of the blood rheology⁴⁹, the inhomogeneous red blood cell concentration⁵⁰, and the appropriate conditions describing the blood vessel wall⁵¹ and their tethering within the human body² are often neglected or at best severely simplified. Characteristically, non-Newtonian blood rheology effects are at best approximated through generalized Newtonian models^{19,22,27,52,53,54}. However, as we know from theory⁵⁵ and given the historical dependence of blood rheology⁵⁶, such a description is only valid for steady shear flows. Moreover, even without taking all of these physical effects into account, the full time-dependent and three-dimensional solution within a system of vessels corresponding to real patient data (as extracted, for example, through MRI), represents such a geometrical complexity as to typically necessitate large-scale massively parallel and grid-distributed computational resources⁵⁷.

Another issue associated with appropriately capturing the *in vivo* nature of blood fluid dynamics comes from the specification of the appropriate outflow boundary conditions. One way to address this issue involves 3D MRI velocity profiles^{18,25,37,58,59,60}. These are very accurate and detailed data but also expensive and time consuming; they can only be used to reproduce the existing flow. A different route^{14,38,61} is to couple the 3D to more approximate, typically one dimensional (1D) blood flow models developed to represent the entire arterial tree. Reymond *et al.*⁴⁵ have concisely tabulated the principal components of the major 1D blood flow models that were available at the time for that use.

Distributed 1D models have merit on their own, however. They were the first to develop, especially after the pioneering work of Womersley^{62,63} in the 1950s based on the analytical solution for pulsatile flow in an elastic vessel. Several publications eventually extended the work to cover the full arterial tree^{9,45,51,64,65,66,67,68,69}. 1D models have the flexibility of being easily adapted to various patients and vascular systems. They allow simple and elegant solutions to the pressure and flow profiles across the network to be readily obtained with minimum computational resources, while allowing for the closed network condition to still be met. In a short time, the sophistication of the 1D models has improved significantly.

With the use of simplified 1D models to generate the boundary conditions in full scale 3D simulations, one can consider the final result as a hybrid method¹⁴. This definitely represents a significant step forward, although these methods tend to be even more computationally demanding. As a step to decrease the computational workload, yet simultaneously make those hybrid methods more versatile, a novel approach has very recently been developed for matching the outlet 3D flow boundary

conditions to the 1D model requirements³⁸. This method utilizes a special simulant as a connection between the full 3D and the outlet impedance-type conditions supplied from the use of a 1D blood flow model⁶⁸. This allows for the easy and efficient implementation of the outlet impedance conditions in commercial Computational Fluid Dynamics (CFD) software, such as FLUENT. However, because of their use of 1D simplified models, they also suffer from the same limitations. At best those models can be used to obtain certain trends, such as those seen in the pressure profiles as a result of pathological increases in certain critical parameter values like viscosity or arterial wall elasticity⁶⁹. More involved nonlinear 1D models have also been developed, as well as approaches to combine them in a consistent fashion to 3D simulations (see the review by Berger⁷⁰ and the recent comprehensive account for those methods in Formaggia *et al.*¹⁴). These however require quite sophisticated methods that involve even more computational resources and consequently have not been tried in an extensive simulation.

Despite the tremendous amount of efforts in this area, especially in the last decade (see the recent monograph on this subject by Formaggia *et al.*¹⁴) there are several issues concerning the existing state of the art of blood flow modeling and simulations. First, in relation to even the most detailed 3D and time dependent simulations (besides the fact that most of them use a rigid wall assumption), most of them rely to the assumption of Newtonian flow, which is not accurate for blood, a viscoelastic/viscoplastic material. Even when non-Newtonian effects were considered¹⁹ these simulations typically only included shear-thinning and only for the steady state flow. Valencia *et al.*²² tried to also include some non-Newtonian (viscoplastic; through the Herschel-Bulkley phenomenological constitutive equation)

flow effects in a numerical study of a secular aneurism. Incidentally, this type of effect has also been considered within our previous 1D model, but with old parametrization of the model parameters.

Moreover, just being able to perform more accurate 3D simulations cannot possibly be considered transformative of this field, to enhance our capabilities to control and understand blood flow arterial circulation with or without macromolecular additives. Many applications still demand simulations that can be performed quickly and require minimal physical information. This information can be more easily generated from existing statistics and scaling analyses, and is amenable to an easily personalized adaptation based on limited and readily accessible patient-specific data. For example, there is a tremendous push towards a lower health cost, a significant component of which is triggered by unnecessary and expensive medical diagnostic tests. Of course, one does not want to lower our capabilities for early detection of diseases, as this greatly contributes not only to an increased life span and a better quality of life, but also to lowering the health cost by potentially eliminating the need for much more expensive treatment, often required at later stages of disease detection. Nowhere is this more true than in cardiovascular diseases, especially atherosclerosis. Developing a model that can potentially help the interpretation of easily acquired measurements in the general physician's office (as simple as measuring the blood pressure at a few locations), and therefore providing advice as for the likelihood of diseased arteries and the need or lack thereof for further testing, can be invaluable.

This is, however, something that can only be accomplished with simpler, lower dimensional blood flow models that result in simulations which can be run quickly and reliably on an arbitrary PC. Such a plan requires development of this model to allow

for a representation of recirculation, such as occurs in the brain. The model also requires a solution method, or combination of methods, that is appropriate for all vessels. Moreover, there is information to be transferred from the recent Beris NSF-sponsored research that addresses the full non-Newtonian character of blood flow rheology. A significant result obtained from that work was a new parametric representation of the steady state shear flow behavior for blood, which for the first time quantitatively represents the effect of both hematocrit and fibrinogen concentration (as well as temperature) on the rheological model parameters³⁹. These relationships, derived on a large number of available blood flow data from the literature, represent the first improvement over the previously widely used but rather obsolete relations offered by Pries *et al.*⁴⁹. This new non-Newtonian model has not as of yet been incorporated into the original 1D model on which this work is based.

1.3.1 Original Model

Before my work began on this model, it was originally developed over several years by researchers at the University of Delaware³⁸. The majority of code written for this model was used at first for my work as well. Sections were replaced or deleted as deemed necessary during the process of updating the model. The governing equations for the Womersley-like method were used directly from Johnson *et al.*³⁸, with a few modifications that will be discussed later. This work set out the mathematical analysis behind the model code, but it relied on outside sources for physical data of the major arteries of the human body. This information was taken exclusively from Alastruey *et al.* (2007)⁴³, which included physical data on 45 major arteries, and well as a diagram of the network. To simulate the remainder of the arterial network, biological scaling laws were utilized^{66,71}.

Endnotes

- ¹ American Heart Association, Heart Disease and Stroke Statistics (2014 Update), <http://circ.ahajournals.org/content/125/1/e2.full>
- ² Pedley, T. J. *The Fluid Mechanics of Large Blood Vessels*. Cambridge: Cambridge UP, 1980.
- ³ Cheer, A. Y., and Van Dam C. P. *Fluid Dynamics in Biology*. Providence: American Mathematical Society, 1993.
- ⁴ Fung, Y. C. *Biomechanics*. New York: Springer, 1997.
- ⁵ Nichols, Wilmer W., and Michael F. O'Rourke. *MacDonald's Blood Flow in Arteries: Theoretical, Experimental and Clinical Principles*. London: Arnold, 1998.
- ⁶ Drzewiecki, Gary M., and John Li. *Analysis and Assessment of Cardiovascular Function*. New York: Springer-Verlag, 1998.
- ⁷ Li JK-J, *The Arterial Circulation: Physical Principles and Clinical Applications*. Humana Press: Totowa,NJ. 2000.
- ⁸ Li, John K-J. *Dynamics of the Vascular System*. River Edge, NJ: World Scientific, 2004
- ⁹ Zamir, M. *The Physics of Pulsatile Flow*. New York: AIP, 2000.
- ¹⁰ Waite, Lee, and Jerry Michael Fine. *Applied Biofluid Mechanics*. New York: McGraw-Hill, 2007.
- ¹¹ Batzel, Jerry J., Franz Kappel, Daniel Schneditz, and Hien T. Tran. "Cardiovascular and Respiratory Systems." (2007)
- ¹² Galdi, Giovanni P. *Hemodynamical Flows: Modeling, Analysis, and Simulation*. Basel:, Birkhäuser 2008.

-
- ¹³ Truskey, G. A., F. Yuan, and D. F. Katz. *Transport Phenomena in Biological Systems*. Upper Saddle River: Prentice Hall, 2004.
- ¹⁴ Formaggia, L., Alfio Quarteroni, and A. Veneziani. *Cardiovascular Mathematics: Modeling and Simulation of the Circulatory System*. Vol. 1. Milan: Springer, 2009.
- ¹⁵ Chandran, K. B., Stanley E. Rittgers, and A. P. Yoganathan. *Biofluid Mechanics: The Human Circulation*. Boca Raton: CRC/Taylor & Francis, 2007.
- ¹⁶ Peattie, Robert, Robert Fisher, Joseph Bronzino, and Donald Peterson. "Transport Phenomena in Biomedical Engineering." (2012)
- ¹⁷ Rindt, C. C. M., and A. A. V. Steenhoven. "Unsteady Flow in a Rigid 3-D Model of the Carotid Artery Bifurcation." *Journal of Biomechanical Engineering J. Biomech. Eng.* 118.1 (1996): 90.
- ¹⁸ Milner, Jaques S., Jennifer A. Moore, Brian K. Rutt, and David A. Steinman. "Hemodynamics of Human Carotid Artery Bifurcations: Computational Studies with Models Reconstructed from Magnetic Resonance Imaging of Normal Subjects." *Journal of Vascular Surgery* 28.1 (1998): 143-56.
- ¹⁹ Gijssen, F.j.h., E. Allanic, F.n. Van De Vosse, and J.d. Janssen. "The Influence of the Non-Newtonian Properties of Blood on the Flow in Large Arteries: Unsteady Flow in a 90° Curved Tube." *Journal of Biomechanics* 32.7 (1999): 705-13.
- ²⁰ Steinman, David A., Jonathan B. Thomas, Hanif M. Ladak, Jaques S. Milner, Brian K. Rutt, and J. David Spence. "Reconstruction of Carotid Bifurcation Hemodynamics and Wall Thickness Using Computational Fluid Dynamics and MRI." *Magnetic Resonance in Medicine Magn. Reson. Med.* 47.1 (2001): 149-59.
- ²¹ Kato, Masaya, Keigo Dote, Koichi Nakaoka, Kenji Goto, Hiroaki Takemoto, and Seiji Habara. "Clinical Implication of Carotid Artery Remodeling in Acute Coronary Syndrome: Ultrasonographic Assessments of Positive Remodeling." *Journal of the American College of Cardiology* 41.6 (2003): 287.
- ²² Valencia, Alvaro, Alvaro Zarate, Marcelo Galvez, and Lautaro Badilla. "Non-Newtonian Blood Flow Dynamics in a Right Internal Carotid Artery with a Saccular Aneurysm." *International Journal for Numerical Methods in Fluids Int. J. Numer. Meth. Fluids* 50.6 (2006): 751-64.

-
- ²³ Nguyen, Kien T., Christopher D. Clark, Thomas J. Chancellor, and Dimitrios V. Papavassiliou. "Carotid Geometry Effects on Blood Flow and on Risk for Vascular Disease." *Journal of Biomechanics* 41.1 (2008): 11-19.
- ²⁴ Gay, Mickaël, and Lucy T. Zhang. "Numerical Studies of Blood Flow in Healthy, Stenosed, and Stented Carotid Arteries." *International Journal for Numerical Methods in Fluids Int. J. Numer. Meth. Fluids* 61.4 (2009): 453-72.
- ²⁵ Wake, Amanda K., John N. Oshinski, Allen R. Tannenbaum, and Don P. Giddens. "Choice of In Vivo Versus Idealized Velocity Boundary Conditions Influences Physiologically Relevant Flow Patterns in a Subject-Specific Simulation of Flow in the Human Carotid Bifurcation." *Journal of Biomechanical Engineering J. Biomech. Eng.* 131.2 (2009): 021013.
- ²⁶ Bevan, R. L. T., P. Nithiarasu, R. Van Loon, I. Sazonov, H. Luckraz, and A. Garnham. "Application of a Locally Conservative Galerkin (LCG) Method for Modelling Blood Flow through a Patient-specific Carotid Bifurcation." *International Journal for Numerical Methods in Fluids Int. J. Numer. Meth. Fluids* 64.10-12 (2010): 1274-295.
- ²⁷ Morbiducci, Umberto, Diego Gallo, Diana Massai, Raffaele Ponzini, Marco A. Deriu, Luca Antiga, Alberto Redaelli, and Franco M. Montevecchi. "On the Importance of Blood Rheology for Bulk Flow in Hemodynamic Models of the Carotid Bifurcation." *Journal of Biomechanics* 44.13 (2011): 2427-438.
- ²⁸ Kamenskiy, Alexey V., Jason N. Mactaggart, Iraklis I. Pipinos, Jai Bikhchandani, and Yuris A. Dzenis. "Three-Dimensional Geometry of the Human Carotid Artery." *Journal of Biomechanical Engineering J. Biomech. Eng.* 134.6 (2012): 064502.
- ²⁹ Hutchins, G. M., M. M. Miner, and J. K. Boitnott. "Vessel Caliber and Branch-angle of Human Coronary Artery Branch-points." *Circulation Research* 38.6 (1976): 572-76.
- ³⁰ Nissen, S. E., J. C. Gurley, C. L. Grines, D. C. Booth, R. McClure, M. Berk, C. Fischer, and A. N. Demaria. "Intravascular Ultrasound Assessment of Lumen Size and Wall Morphology in Normal Subjects and Patients with Coronary Artery Disease." *Circulation* 84.3 (1991): 1087-099.
- ³¹ Brinkman, A. M., P. B. Baker, W. P. Newman, R. Vigorito, and M. H. Friedman. "Variability of Human Coronary Artery Geometry: An Angiographic Study of

-
- the Left Anterior Descending Arteries of 30 Autopsy Hearts." *Annals of Biomedical Engineering Ann Biomed Eng* 22.1 (1994): 34-44.
- ³² Friedman, M. "Relationship between the Geometry and Quantitative Morphology of the Left Anterior Descending Coronary Artery." *Atherosclerosis* 125.2 (1996): 183-92.
- ³³ Perktold, K., M. Hofer, G. Rappitsch, M. Loew, B.d Kuban, and M.h Friedman. "Validated Computation of Physiologic Flow in a Realistic Coronary Artery Branch." *Journal of Biomechanics* 31.3 (1997): 217-28.
- ³⁴ Changizi, Mark A., and Christopher Cherniak. "Modeling the Large-scale Geometry of Human Coronary Arteries." *Can. J. Physiol. Pharmacol. Canadian Journal of Physiology and Pharmacology* 78.8 (2000): 603-11.
- ³⁵ Seron, Francisco J., Elsa Garcia, and Jorge Del Pico. "MOTRICO Project – Geometric Construction and Mesh Generation of Blood Vessels by Means of the Fusion of Angiograms and IVUS." *Pattern Recognition and Image Analysis Lecture Notes in Computer Science* (2003): 951-61.
- ³⁶ Ramaswamy, S. D., S. C. Vigmostad, A. Wahle, Y. -G. Lai, M. E. Olszewski, K. C. Braddy, T. M. H. Brennan, J. D. Rossen, M. Sonka, and K. B. Chandran. "Fluid Dynamic Analysis in a Human Left Anterior Descending Coronary Artery with Arterial Motion." *Annals of Biomedical Engineering Ann Biomed Eng* 32.12 (2004): 1628-641.
- ³⁷ Frauenfelder, Thomas, Evangelos Boutsianis, Thomas Schertler, Lars Husmann, Sebastian Leschka, Dimos Poulikakos, Borut Marincek, and Hatem Alkadhi. "In-vivo Flow Simulation in Coronary Arteries Based on Computed Tomography Datasets: Feasibility and Initial Results." *Eur Radiol European Radiology* 17.5 (2006): 1291-300.
- ³⁸ Johnson, David A., Justin R. Spaeth, William C. Rose, Ulhas P. Naik, and Antony N. Beris. "An Impedance Model for Blood Flow in the Human Arterial System. Part I: Model Development and MATLAB Implementation." *Computers & Chemical Engineering* 35.7 (2011): 1304-316.
- ³⁹ Apostolidis, Alex J. and Antony N. Beris. "Modeling of the Blood Rheology in Steady-state Shear Flows." *Journal of Rheology* 58 (2014): 607-633.
- ⁴⁰ Taylor, Charles A., Thomas J. R. Hughes, and Christopher K. Zarins. "Finite Element Modeling of Three-Dimensional Pulsatile Flow in the Abdominal

-
- Aorta: Relevance to Atherosclerosis." *Annals of Biomedical Engineering* 26.6 (1998): 975-87.
- ⁴¹ Gohil, Trushar, Robert H. P. McGregor, Dominik Szczerba, Kathrin Burckhardt, Krishnamurthy Muralidhar, and Gábor Székely. "Simulation of Oscillatory Flow in an Aortic Bifurcation Using FVM and FEM: A Comparative Study of Implementation Strategies." *International Journal for Numerical Methods in Fluids Int. J. Numer. Meth. Fluids* 66.8 (2010): 1037-067.
- ⁴² Moore, S., T. David, J.g. Chase, J. Arnold, and J. Fink. "3D Models of Blood Flow in the Cerebral Vasculature." *Journal of Biomechanics* 39.8 (2006): 1454-463.
- ⁴³ Alastruey, J., K. H. Parker, J. Peiró, S. M. Byrd, and S. J. Sherwin. "Modelling the Circle of Willis to Assess the Effects of Anatomical Variations and Occlusions on Cerebral Flows." *Journal of Biomechanics* 40.8 (2007): 1794-805.
- ⁴⁴ Passerini, Tiziano, Mariarita De Luca, Luca Formaggia, Alfio Quarteroni, and Alessandro Veneziani. "A 3D/1D Geometrical Multiscale Model of Cerebral Vasculature." *Journal of Engineering Mathematics J Eng Math* 64.4 (2009): 319-30.
- ⁴⁵ Reymond, Philippe, Fabienne Perren, François Lazeyras, and Nikos Stergiopoulos. "Patient-specific Mean Pressure Drop in the Systemic Arterial Tree, a Comparison between 1-D and 3-D Models." *Journal of Biomechanics* 45.15 (2012): 2499-505.
- ⁴⁶ Fahy, Paul, Patrick Delassus, Peter Mccarthy, Sheriff Sultan, Niamh Hynes, and Liam Morris. "An In Vitro Assessment of the Cerebral Hemodynamics Through Three Patient Specific Circle of Willis Geometries." *Journal of Biomechanical Engineering J Biomech Eng* 136.1 (2013): 011007.
- ⁴⁷ Spilker, Ryan L., Jeffrey A. Feinstein, David W. Parker, V. Mohan Reddy, and Charles A. Taylor. "Morphometry-Based Impedance Boundary Conditions for Patient-Specific Modeling of Blood Flow in Pulmonary Arteries." *Annals of Biomedical Engineering Ann Biomed Eng* 35.4 (2007): 546-59.
- ⁴⁸ Clipp, R. B., and B. N. Steele. "Impedance Boundary Conditions for the Pulmonary Vasculature Including the Effects of Geometry, Compliance, and Respiration." *IEEE Transactions on Biomedical Engineering IEEE Trans. Biomed. Eng.* 56.3 (2009): 862-70.

-
- 49 Pries, A. R., T. W. Secomb, P. Gaehtgens, and J. F. Gross. "Blood Flow in Microvascular Networks. Experiments and Simulation." *Circulation Research* 67.4 (1990): 826-34.
- 50 Turitto, Vincent T. *The Measurement of the Transport Kinetics of Platelets in Flowing Blood*. Ann Arbor, MI: U Microfilms, 1982.
- 51 Olufsen, M. S. "Modeling Flow and Pressure in the Systemic Arteries." In: Ottesen, J. T., Olufsen, M. S., & Larsen, J. K. (Eds.) *Applied Mathematical Models in Human Physiology*, Philadelphia: SIAM, 2004.
- 52 Lee, S.-W., and D.a. Steinman. "On the Relative Importance of Rheology for Image-based CFD Models of the Carotid Bifurcation." *Journal of Biomechanics* 39 (2006)
- 53 Wang, Sheng-Zhang, Jia-Liang Chen, Guang-Hong Ding, Gang Lu, and Xiao-Long Zhang. "Non-newtonian Computational Hemodynamics in Two Patient-specific Cerebral Aneurysms with Daughter Saccules." *Journal of Hydrodynamics, Ser. B* 22.5 (2010): 639-46.
- 54 Seo, Taewon. "Numerical Simulations of Blood Flow in Arterial Bifurcation Models." *Korea-Australia Rheology Journal Korea-Aust. Rheol. J.* 25.3 (2013): 153-61.
- 55 Bird, R. Byron. *Dynamics of Polymeric Liquids*. 2nd ed. Vol. 1. New York: Wiley, 1987.
- 56 Bureau, M., J. C. Healy, D. Bourgoïn, and M. Joly. "Etude Expérimentale *in vitro* Du Comportement Rhéologique Du Sang En Régime Transitoire à Faible Vitesse De Cisaillement." *Rheologica Acta Rheol Acta* 17.6 (1978): 612-25.
- 57 Grinberg, Leopold, and George Em Karniadakis. "Outflow Boundary Conditions for Arterial Networks with Multiple Outlets." *Annals of Biomedical Engineering Ann Biomed Eng* 36.9 (2008): 1496-514.
- 58 Xu, X. Y., Q. Long, M. W. Collins, M. Bourne, and T. M. Griffith. "Reconstruction of Blood Flow Patterns in Human Arteries." *Proceedings of the Institution of Mechanical Engineers, Part H: Journal of Engineering in Medicine* 213.5 (1999): 411-21.
- 59 Boutsianis, Evangelos, Sumeet Gupta, Kevin Boomsma, and Dimos Poulidakos. "Boundary Conditions by Schwarz-Christoffel Mapping in Anatomically

Accurate Hemodynamics." *Annals of Biomedical Engineering Ann Biomed Eng* 36.12 (2008): 2068-084.

- ⁶⁰ Torii, Ryo, Nigel B. Wood, Nearchos HadjiIoizou, Andrew W. Dowsey, Andrew R. Wright, Alun D. Hughes, Justin Davies, Darrel P. Francis, Jamil Mayet, Guang-Zhong Yang, Simon A. Mcg. Thom, and X. Yun Xu. "Fluid-structure Interaction Analysis of a Patient-specific Right Coronary Artery with Physiological Velocity and Pressure Waveforms." *Communications in Numerical Methods in Engineering Commun. Numer. Meth. Engng.* 25.5 (2009): 565-80.
- ⁶¹ Quarteroni, Alfio, and Alessandro Veneziani. "Analysis of a Geometrical Multiscale Model Based on the Coupling of ODE and PDE for Blood Flow Simulations." *Multiscale Modeling & Simulation Multiscale Model. Simul.* 1.2 (2003): 173-95.
- ⁶² Womersley, J. R. "Method for the Calculation of Velocity, Rate of Flow and Viscous Drag in Arteries When the Pressure Gradient Is Known." *The Journal of Physiology* 127.3 (1955): 553-63.
- ⁶³ Womersley, J. R. "Oscillatory Flow in Arteries: The Constrained Elastic Tube as a Model of Arterial Flow and Pulse Transmission." *Physics in Medicine and Biology Phys. Med. Biol.* 2.2 (1957): 178-87.
- ⁶⁴ Duan, B., and M. Zamir. "Viscous Damping in One-dimensional Wave Transmission." *The Journal of the Acoustical Society of America J. Acoust. Soc. Am.* 92.6 (1992): 3358.
- ⁶⁵ West, Geoffrey B. "The Origin of Universal Scaling Laws in Biology." *Physica A Statistical Mechanics and Its Applications* 263.1-4 (1999): 104-13.
- ⁶⁶ Formaggia, Luca, Daniele Lamponi, and Alfio Quarteroni. "One-dimensional Models for Blood Flow in Arteries." *Journal of Engineering Mathematics* 47.3/4 (2003): 251-76.
- ⁶⁷ Vosse, Frans N. Van De, and Nikos Stergiopoulos. "Pulse Wave Propagation in the Arterial Tree." *Annu. Rev. Fluid Mech. Annual Review of Fluid Mechanics* 43.1 (2011): 467-99.
- ⁶⁸ Johnson, David A., Justin R. Spaeth, William C. Rose, Ulhas P. Naik, and Antony N. Beris. "An Impedance Model for Blood Flow in the Human Arterial

System. Part I: Model Development and MATLAB Implementation." *Computers & Chemical Engineering* 35.7 (2011): 1304-316.

- ⁶⁹ Johnson, David A., William C. Rose, Jonathan W. Edwards, Ulhas P. Naik, and Antony N. Beris. "Application of 1D Blood Flow Models of the Human Arterial Network to Differential Pressure Predictions." *Journal of Biomechanics* 44.5 (2011): 869-76.
- ⁷⁰ Cheer, A. Y., and Van Dam C. P. *Fluid Dynamics in Biology: Proceedings of an AMS-IMS-SIAM Joint Summer Research Conference Held July 6-12, 1991 with Support from the National Science Foundation and NASA Headquarters*. Providence, RI: American Mathematical Society, 1993.
- ⁷¹ West, Geoffrey B., James H. Brown, and Brian J. Enquist. "A General Model for the Origin of Allometric Scaling Laws in Biology." *Science* 276.5309 (1997): 122-26.

Chapter 2

EXTENSION TO RECIRCULATION

Prior to the 2015-2016 academic year, I worked on refining the model used for the Womersley-like calculations. These changes did not affect the mathematical concepts involved. Rather, they improved empirical relationships that we already used and incorporated a more detailed network, in an attempt to maximize the accuracy of our model.

2.1 Expanded Network and Cerebral Arteries

One of the first changes to the model was the network data used as input. The data from Alastruey *et al.*¹ included only 45 vessels. We wanted to increase the accuracy of our model, which means delaying the implementation of scaling laws until absolutely necessary. Thus, we want to include as many explicitly defined vessels as possible. We chose to input the data from Reymond *et al.*² which contains information on 103 vessels, including the cerebral arteries around the Circle of Willis (subnetwork D, Figure 1). The inclusion of the cerebral arteries is especially important because of the possibility of recirculation of blood. This phenomenon will be discussed further in Section 2.2.

The new network is shown in Figure 1, which corresponds to Fig.2 in Reymond *et al.* The Circle of Willis can be seen on the far right.

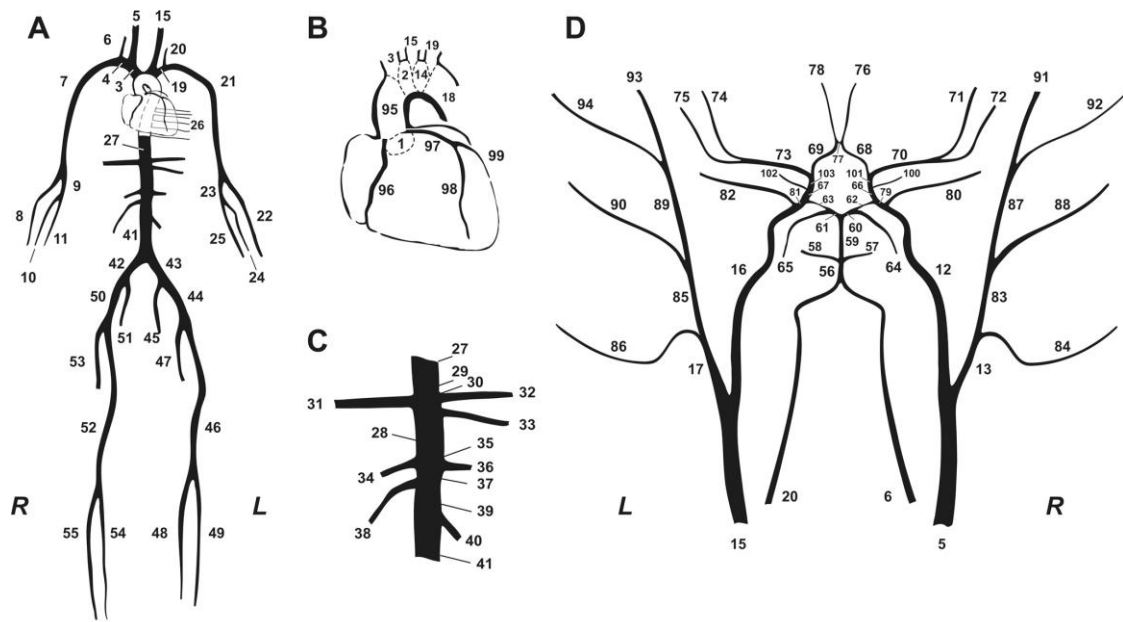


Figure 1: New arterial network, from Reymond *et al.* Fig.2

The network expansion went hand in hand with adding modularity to the model code. Any information specific to the given system was moved to input files, and the code now reads in these files and constructs the network itself. In this way, the main software does not have to be changed for any network or set of parameters, so long as the user inputs files constructed in the correct way. This makes it dramatically easier to apply the model to networks of various sizes or to the different networks of various patients. The pressure data is input through a simple text file with two columns. Physical data of the blood vessels is recorded in a MATLAB.m file. A small .m file with the necessary connectivity information is also required. Every other piece of information is calculated by the code.

2.2 Simultaneous Solution and Recirculation

In the original model, the network always branched downstream. Thus, the entire system could be solved recursively by starting at the pressure boundary condition of the capillaries and working upstream until the aorta was reached. The new network does not allow for this recursion-only method. This is due to the inclusion of the Circle of Willis (Figure 1). The CoW is an arterial loop made up of the cerebral arteries. Because blood has the ability to flow all the way around, there is no “upstream” or “downstream.” The vessels generated with scaling laws can be solved for recursively as before. However, once the main vessels are reached, the entire system of 103 vessels must be solved simultaneously, so as not to assume a particular direction of flow anywhere in the CoW. This required coding a system of 206 equations, to account for the forward and backward pressure waves in each vessel. More specifics about the calculations will be discussed in Chapter 4.

Including recirculation capabilities has additional impact on future studies of blood flow in the CoW. Only about 50% of the human population has a full Circle of Willis. Common alternate topologies are shown in Figure 2. By changing our network to match these variations, it is possible to analyze the effect they have on blood flow profiles in the brain, which was an original goal of this research project.

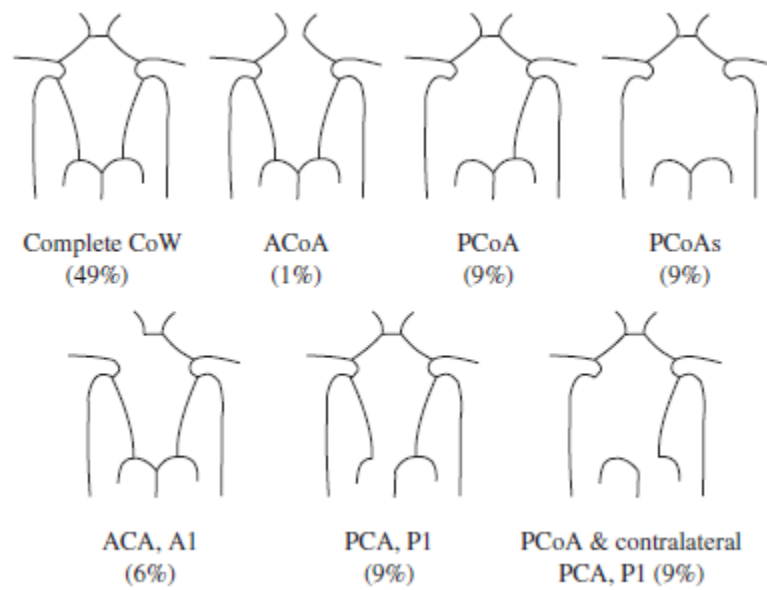


Figure 2: Alternate Circle of Willis networks, with estimates of their probability of occurrence; from Alastruey *et al.*

Now that the new model uses a simultaneous solution to find pressures, a subnetwork involving recirculation could be added to other areas in the body as well. Abstracting from the assumed direction of flow is just another way that this model has been improved and its possible uses extended.

Endnotes

- ¹ Alastruey, J., K. H. Parker, J. Peiró, S. M. Byrd, and S. J. Sherwin. "Modelling the Circle of Willis to Assess the Effects of Anatomical Variations and Occlusions on Cerebral Flows." *Journal of Biomechanics* 40.8 (2007): 1794-805.
- ² Reymond, P., F. Merenda, F. Perren, D. Rufenacht, and N. Stergiopoulos. "Validation of a One-dimensional Model of the Systemic Arterial Tree." *AJP: Heart and Circulatory Physiology* 297.1 (2009): H208-222.

Chapter 3

MODELING THE FAHRÆUS EFFECT

The Fåhræus effect describes the decrease in relative concentration of red blood cells as the diameter of a vessel decreases. In blood vessels with diameters less than about 600 μm , the hematocrit decreases with decreasing capillary diameter^{1,2}. This effect contributes to the Fåhræus–Lindqvist effect, where red blood cells are excluded from the volume near the tube wall, leading to an increase in relative viscosity along the center line.

To model the Farhåeus effect in the code, the hematocrit was calculated as a function of the vessel diameter following an expression provided by Pries *et al.*³:

$$\frac{H_T}{H_D} = H_D + (1 - H_D)(1 + 1.7e^{-0.415D} - 0.6e^{-0.011D}), \quad (3-1)$$

where H_T is the local tube hematocrit, H_D is the discharge hematocrit, and D is the vessel diameter in microns. We undertook a study to check that expression based on other data from the literature. The first test involved plotting this equation from Pries *et al.* against Eq.18 from James Barbee's PhD dissertation⁴:

$$\frac{H_T}{H_D} = \begin{cases} -0.024 + 0.1754 \ln(D) + (-0.046D + 1.15)(H_f - 0.45) & 8 < D \leq 25 \\ -0.019 + 0.1899 \ln(D) + (0.25 - 0.00195D)(H_f - 0.45) & 25 < D \leq 60 \\ 0.1171 + 0.1562 \ln(D) + (0.25 - 0.00195D)(H_f - 0.45) & 60 < D \leq 125 \\ 0.1171 + 0.1562 \ln(D) & 125 < D \leq 280 \\ 1 & 280 < D \end{cases}, \quad (3-2)$$

where H_f is the feed hematocrit, assumed to equal 0.45 for this test. The result is shown in Figure 3 below. There is general agreement for larger diameters, although

Barbee's equation underpredicts that of Pries *et al.* However, the Barbee data diverge sharply lower than 29 μm , indicating a possible error in his piecewise formula.

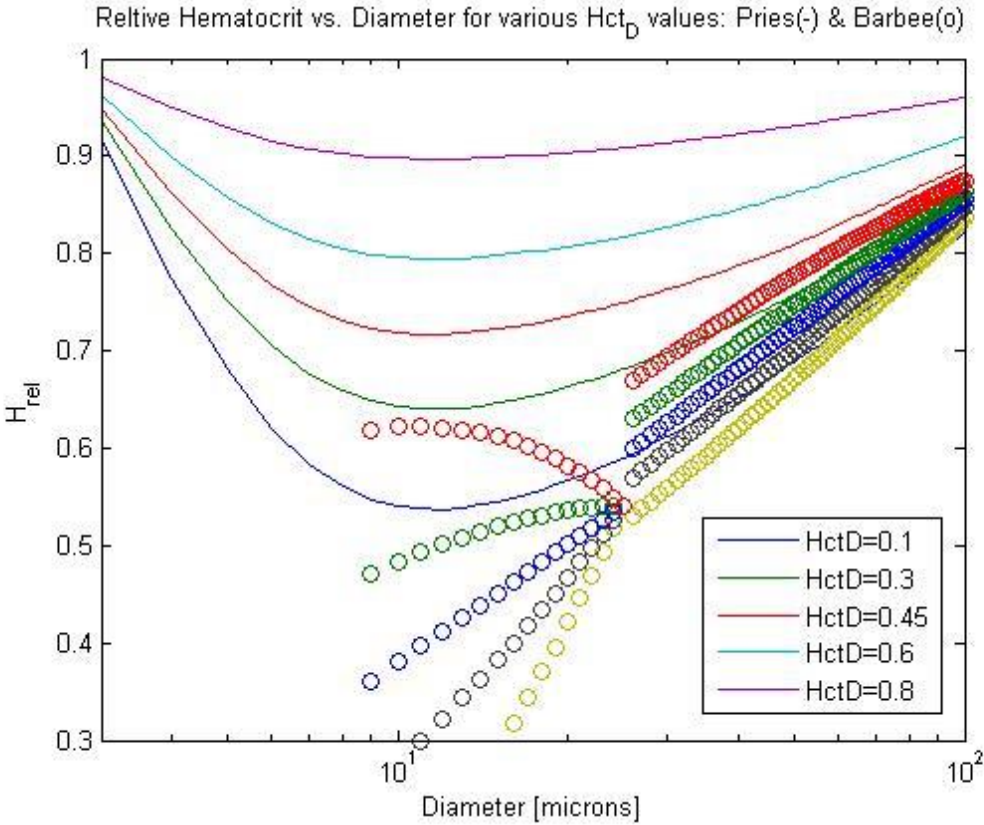


Figure 3: Comparison of two empirical relationships between vessel diameter and discharge hematocrit: Barbee dissertation⁴ (o) vs. Pries *et al.* (-)³

Additionally I tested if there was an ideal fibrinogen concentration (c_f) for our parametric relationships that would best recreate Fig.17 in Barbee's dissertation². The data was plotted for $Hct_D = 0.421$, the closest to the value of 0.45 which is used in our model. The results are in Figure 4 below. There is no obvious choice because the data create a line that runs right through those produced by our model equations. It

should be noted that the feed hematocrit reported by Barbee was assumed equal to the Hct_D we used, and the temperature correction was neglected because the difference was less than 0.05°F .

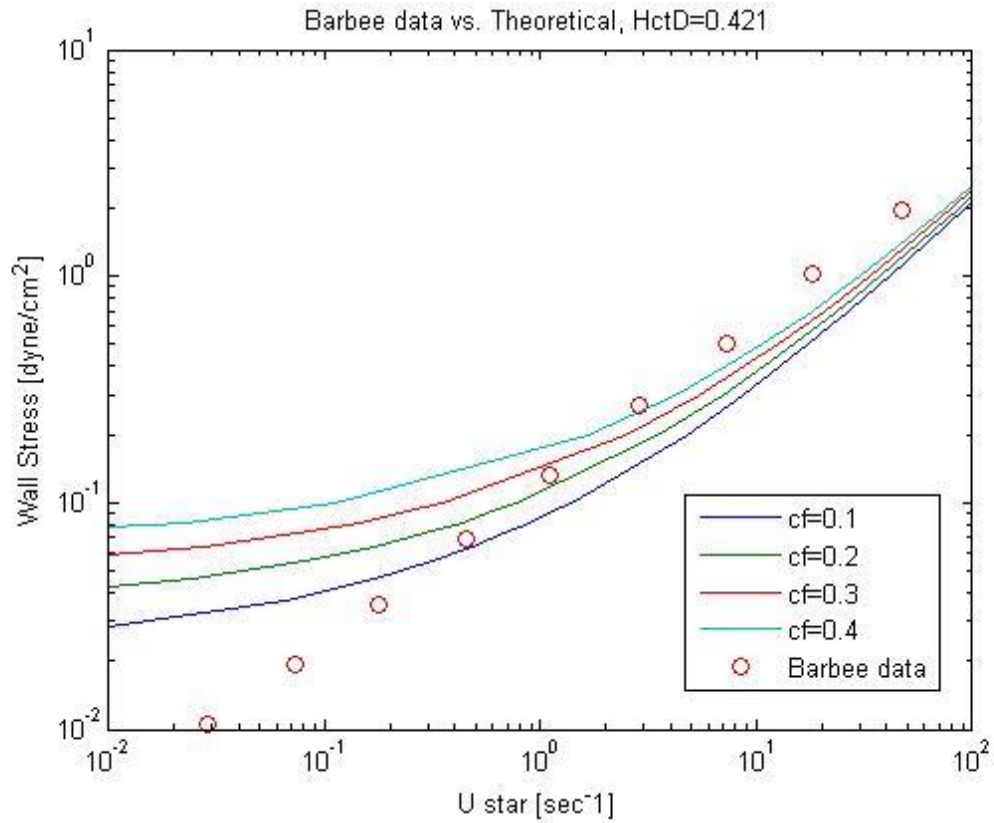


Figure 4: Wall stress vs. pseudo-shear rate, Barbee dissertation data⁴ (o) versus our model results

Lastly, I attempted to convert the data from Barbee Fig.17 to a Couette geometry, to more easily determine if the Casson model⁵ was accurate for this blood data. The yield stress was found with Eq.4 in Apostolidis and Beris (2014)⁶ (see Chapter 4), and the root of the wall stress was plotted against the root of the shear rate.

The data was plotted along with theoretical curves from our model with varying c_f values. The data does not exhibit a linear trend, indicating that the Casson model may not be valid. The shape is closer to a square root curve. This plot is shown in Figure 5.

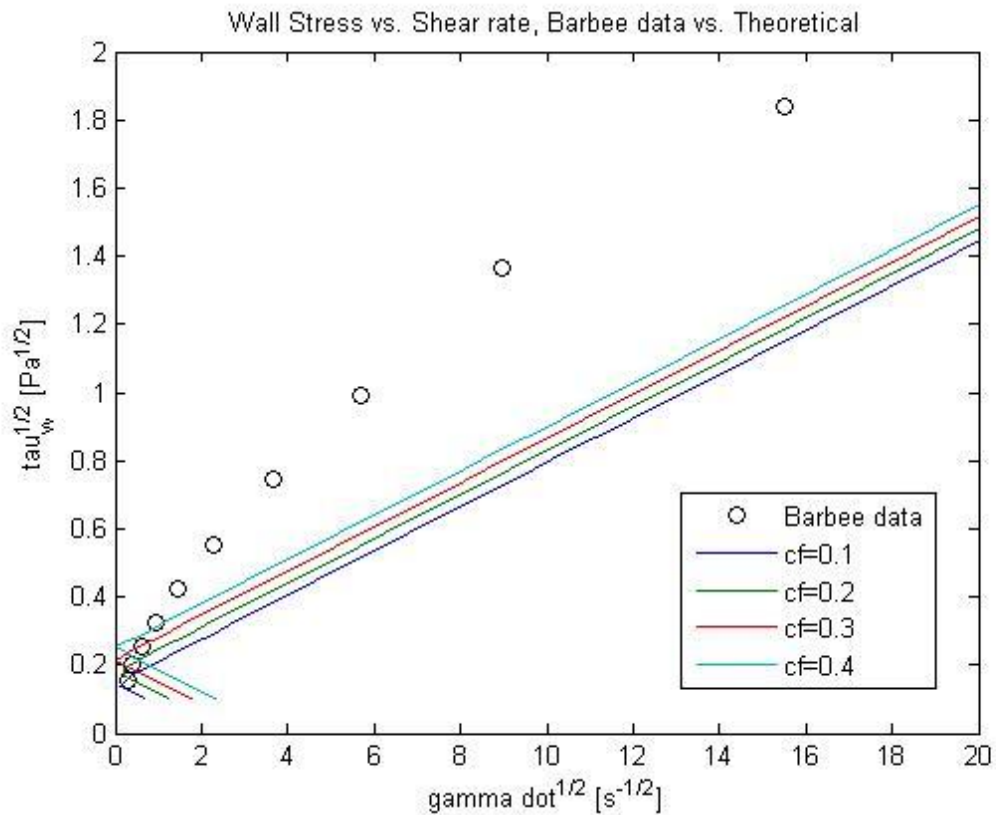


Figure 5: Root of wall stress versus root of shear rate, Barbee dissertation data⁴ (o) plotted against sample c_f values using a Couette geometry

Based on Figure 3, there seems to be some error with Barbee's piecewise characterization of local hematocrit. We can see that the equation breaks down below $d=18\mu\text{m}$, so we wanted to see for how large a diameter the other parts are valid. The

piecewise equation has five parts. The first we eliminated completely. Then we extended the second to include diameters down to 18 μ m.

Values using Barbee's equation with varying discharge hematocrits were plotted against the upper and lower bounds of relative hematocrit from Goldsmith *et al.* (1989), Fig.1⁷. The results are shown in Figure 6. Aside from the $Hct_D = 0.1$ case, Barbee's equations look valid up to 250 μ m. In the future, a new equation could be derived that exhibits a curve similar to the Goldsmith bounds as one approaches large diameters.

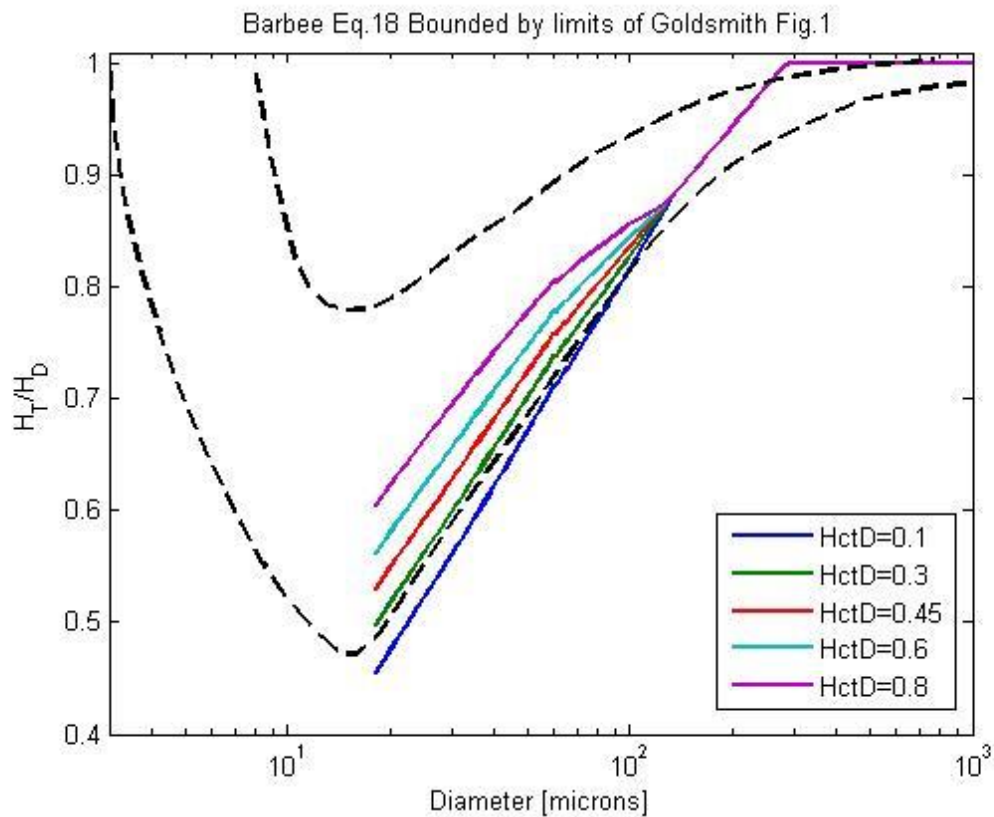


Figure 6: Barbee dissertation piecewise Equation 18⁴ vs. bounds from Goldsmith *et al.*⁷

Endnotes

- ¹ Seshadri, V., R.M. Hochmuth, P.A. Croce, and S.P. Suter. "Capillary Blood Flow." *Microvascular Research* 2.4 (1970): 434-42.
- ² Pries, Axel R., and Timothy W. Secomb. "Blood Flow in Microvascular Networks." *Comprehensive Physiology* (2011)
- ³ Pries, A. R., T. W. Secomb, P. Gaehtgens, and J. F. Gross. "Blood Flow in Microvascular Networks. Experiments and Simulation." *Circulation Research* 67.4 (1990): 826-34.
- ⁴ Barbee, James Henry. "The Flow of Human Blood Through Capillary Tubes with the Inside Diameters Between 8.7 and 221 Microns." Diss. California Institute of Technology, 1971.
- ⁵ Mill, C. C. *Rheology of Disperse Systems*. New York: Symposium Publications Division, Pergamon, 1959.
- ⁶ Apostolidis, Alex J. and Antony N. Beris. "Modeling of the Blood Rheology in Steady-state Shear Flows." *Journal of Rheology* 58 (2014): 607-633.
- ⁷ Goldsmith, Harry L., Giles R. Cokelet, and Peter Gaehtgens. "Robin Fåhræus: Evolution of his Concepts in Cardiovascular Physiology." *Journal of American Physiology* (1989): H1005-H1014

Chapter 4

CURRENT 1D MODEL PRESENTATION BASED ON WOMERSLEY SOLUTION OF TRANSIENT FLOW PROBLEM

4.1 Womersley's Method Setup

Our blood flow model is run entirely in MATLAB. All necessary information regarding the network of vessels or the governing equations is either inputted into, generated in, or computed by the MATLAB program. As discussed in Johnson *et al.* (2011)¹, which used an earlier version of this model, MATLAB is a powerful yet easy to use computational tool. It is equipped with many options for displaying the results of the model's computations. MATLAB also excels when operating with systems of equations, a necessary part of working with a network that incorporates redundancy (see Section 2.2). It is a natural choice as the computational system to carry out our work.

The code used in the current model has been adapted from the work of Johnson *et al.* Many of the governing equations used and discussed below, as well as references to their original works, are found in this paper. The previous version of this model incorporated the physiological data found in Alastruey *et al.* (2007)². We however opted to use data from Reymond *et al.* (2009)³. The data from the latter work includes physiological information on many more arteries as well as detailed schematics of the arterial network. This network, which we have used to refine our current model, contains 103 main vessels connected at 100 nodes. The corresponding information for the vessels of the remainder of the arterial system is generated using

biological scaling laws from West (1997, 1999)^{4,5}. To generate information for these “sub-networks,” we assume that every parent vessel either bifurcates or trifurcates into symmetric daughter vessels all the way to the capillary level.

An important goal of our model is the possibility of being applied diagnostically, and therefore it must be able to correctly compute pressures and flows for many patients with varying physiological parameters and unique arterial networks. Thus MATLAB must be provided with a way to construct the network itself (rather than incorporate it into the code) while still developing correct outputs. This was the largest change from the model used by Johnson *et al.* Other changes were much simpler, such as parameter values or coefficients of certain expressions, which were altered to correct mistakes found in referenced works and our own model. The original scaling laws were also altered to better match results found by West (1997).

The model code consists of a large script with several smaller routines that serve very specific purposes. For instance, the first of these routines computes steady state wall stress effects. Because wall stress (τ_w) and flow are interdependent, this routine runs iteratively until the values for wall stress converge to at least 5 significant digits. The final values for wall stress generated by this routine are then used in the main script. Other subroutines produce plots of pressure or flow rate in various arteries.

The model code requires several inputs, the first of which is a simple text file with two columns representing time and pressure over the time of a single heartbeat. This pressure information is used to develop the steady state and transient solutions to the model by solving systems of equations. The code also requires an input of physiological parameters, such as residual capillary pressure and the dimensions of

each main vessel. Ideally, this information would be provided in a unique input file representing a given patient. As long as the input data is formatted correctly, the model can be used for many patients with varying arterial network topologies. The final piece of necessary input is a small file that notes which vessels are connected to each other. The main script allows MATLAB to construct all other relevant connectivity information.

4.1.1 User-defined Parameters

Several physical parameters must be specified in MATLAB so that the necessary equations may be computed. Those used in our model are found in Table 1.

Table 1: Physical parameters used in the current model.

| Parameter | | Value | Units |
|-------------------------------------|--------------|-----------------------|--------------|
| Discharge Hematocrit | Hct_D | 0.45 | - |
| *Plasma Viscosity (at 296.16K) | μ_p | 1.67×10^{-3} | $Pa \cdot s$ |
| Plasma Density | ρ_p | 1030 | kg/m^3 |
| Red Blood Cell Density | ρ_{RBC} | 1090 | kg/m^3 |
| Minimum Capillary Radius | r_{MinCap} | 3×10^{-6} | m |
| *Capillary Length-to-Diameter Ratio | l/d | 35 | - |
| Residual Capillary Pressure | - | 2000 | Pa |
| *Fibrinogen Concentration | c_f | 1 | kg/m^3 |
| Poisson Ratio | σ | 0 | - |
| * "N bar" | \bar{N} | 16 | - |

Unless noted by a star (*), these parameters have the same value found in Johnson *et al.* The value for plasma viscosity used in that work was $1.35 \times 10^{-3} Pa \cdot s$, but we use a corrected value of $1.67 \times 10^{-3} Pa \cdot s$ from Apostolidis and Beris (2014)⁶. The hematocrit is equivalent to the volume fraction of red blood cells. Knowing the

concentration of fibrinogen in the blood (c_f) is necessary to compute the critical hematocrit (Hct_c) with the equation⁶

$$Hct_c = 0.3126c_f^2 - 0.468c_f + 0.1764 \quad (4-1)$$

We do not currently have an expression for c_f , but it commonly falls into the range of 0.1 to 0.4 g/dl⁷. In order to develop results for cardiac output and overall network resistance that best match values found in literature, the minimum value of 0.1 g/dl has been chosen. The expression for Hct_c (4-1) developed by Apostolidis and Beris and utilized by our model code is calculated using this value.

The capillary length-to-diameter ratio was also changed from Johnson *et al.* to better match the outputs discussed above. They used a value of 50 (the maximum value found in literature); we use 35. \bar{N} , which refers to the number of sub-network generations scaled by a one-third power law, was not used in their work.

4.1.2 Governing Equations

The steady state solution of the model relies heavily on the Hagen-Poiseuille formula for flow of a viscous fluid through a cylinder:

$$Q = |\Delta P| \frac{\pi r^4}{8\mu L}. \quad (4-2)$$

In this case, the radii r and lengths L of the main vessels are input directly into the model. An expression for the pseudo shear rate U^* can be found in Truskey *et al.*⁸:

$$U^* = \frac{Q}{\pi r^3}. \quad (4-3)$$

Wall stress is calculated using⁶

$$\tau_w = \frac{|\Delta P| r}{2L} \quad (4-4)$$

Combining (4-2), (4-3), and (4-4), we see that

$$U^* = \frac{\tau_w}{4\mu} \quad (4-5)$$

at steady state. This equation does not account for non-Newtonian effects of blood rheology. To encapsulate these effects as well, Merrill *et al.* include a coefficient dependent on the ratio of yield stress to wall stress:

$$U^* = \frac{\tau_w}{4\mu} \left[1 - \frac{1}{21} \left(\frac{\tau_y}{\tau_w} \right)^4 - \frac{16}{7} \left(\frac{\tau_y}{\tau_w} \right)^{1/2} + \frac{4}{3} \left(\frac{\tau_y}{\tau_w} \right) \right] \quad (4-6)$$

For a simple verification of the Poiseuille solution, (4-5) will suffice, but we use (4-6) in our model code.

The steady state viscosity may be calculated by an empirical relationship used by Apostolidis and Beris:

$$\mu_{SS} = \mu_p \left(1 + 2.0703 \times Hct + 3.7222 \times Hct^2 \right). \quad (4-7)$$

Using (4-4) and (4-7), the shear rate ($\dot{\gamma}$) can be found with the Casson model:

$$\dot{\gamma} = \frac{\left(\sqrt{\tau_w} - \sqrt{\tau_y} \right)^2}{\mu_{SS}}. \quad (4-8)$$

The yield stress (τ_y) is found with Equation 14 from Apostolidis and Beris:

$$\tau_y = \begin{cases} [(Hct - Hct_c)^2 \times (0.5084c_f + 0.4517)]^2 & Hct > Hct_c \\ 0 & Hct \leq Hct_c \end{cases} \quad (4-9)$$

The local hematocrit is calculated using⁹

$$\frac{Hct}{Hct_D} = Hct_D + (1 - Hct_D) \left(1 + 1.7e^{-0.415D} - 0.6e^{-0.011D} \right) \quad (4-10)$$

where D is the vessel diameter in μm .

The flow resistance of each main vessel can easily be calculated by a relationship similar to Ohm's Law¹, namely,

$$R_{SS} \equiv \frac{|\Delta P|}{Q} = \frac{8\mu L}{\pi r^4} \quad (4-11)$$

Here, the pressure drop corresponds to a voltage drop and flow rate to an electric current. For vessels with non-constant radii, a correction must be made to the resistance due to a changing pressure drop. The approach used by Johnson *et al.* (Equation 7) is the lubrication approximation, in which the resistance is a function of axial distance along the vessel:

$$R_{SS,tapered}(z) = \frac{8\mu}{\pi r_{top}^4} \left[\frac{e^{-4Kz} - 1}{-4K} \right]. \quad (4-12)$$

K in this expression is

$$K = \ln \left(\frac{r_{bottom}/r_{top}}{L} \right)$$

where r_{bottom} is the distal radius, r_{top} is the proximal radius, and L is the length of the vessel.

4.1.2.1 Additional Transient Equations

To develop time-dependent flow solutions, the characteristic (local) impedance Z must be found for each vessel. These values represent the local ratio of pressure to flow and are generally complex. To find these values, Johnson *et al.*¹ use the equation

$$Z = \left(\frac{1}{1 - \sigma^2} \right) \frac{c_0^2 \rho}{\pi r^2 c} \quad (4-13)$$

where ρ is the blood density, r is the vessel radius, and c_0 is the Moens-Korteweg wave velocity^{10,11}. The term $\frac{1}{1 - \sigma^2}$ is sometimes used as a correcting factor where σ is

the Poisson ratio, but in our code σ is set to 0 so the term cancels. To account for effects of viscosity, the complex wave speed c is also necessary. c_0 is found using the equation¹

$$c_0 \equiv \sqrt{\frac{Eh}{2\rho r}} \quad (4-14)$$

Here, E is the modulus of elasticity of the vessel and h is the vessel wall thickness. $\frac{Eh}{r}$ defines the characteristic “pseudo-compliance” of each vessel, denoted β . c_0 is generally real, but to account for viscoelastic effects we add an imaginary component to E equal to 15% of the real part. To find the complex wave speed c , Johnson *et al.* use

$$c = c_0 \sqrt{-\left(\frac{1}{1-\sigma^2}\right) \frac{J_2(i^{3/2}\alpha)}{J_0(i^{3/2}\alpha)}} \quad (4-15)$$

In this expression J_n is the Bessel function of the n^{th} order and

$$\alpha \equiv r \sqrt{\frac{\omega\rho}{\mu}} \quad (4-16)$$

is the dimensionless Womersley number.

A necessary part of finding the transient solution is knowing the reflection ratio R of each vessel. Zamir¹² defines this ratio as

$$R = \frac{\bar{p}_b(l,t)}{\bar{p}_f(l,t)} \quad (4-17)$$

\bar{p}_b is the backward pressure wave created when the forward wave hits the junction of the daughter vessels, while \bar{p}_f is the corresponding forward wave. The pressure wave equations are also found in Zamir:

$$\bar{p}_f(x,t) = \exp[i\omega(t-x/c)] \quad (4-18)$$

and

$$\bar{p}_b(x,t) = R \exp[i\omega(t+x/c-2l/c)] \quad (4-19)$$

4.1.3 Model Input and Preliminary Calculations

The first objective of the model is to extract the required input data from the files used. The text file containing the heartbeat information and the two MATLAB data files are loaded. Critical hematocrit is calculated using (4-1). The capillary length-to-radius ratio is then calculated for each main vessel. This parameter can be

changed within the model to account for higher or lower flows to specific tissues. For instance, due to the brain's high demand for blood, cerebral terminal arteries have been given a smaller capillary l/r ratio (50) than the rest of the network (70).

The code next generates additional connectivity information. The maximum number of main arteries connected at a single node is found, along with the total number of nodes. These include junctions between two main arteries or between a main artery and a branching secondary network. MATLAB then iterates through each node to find which arteries (and thus which other nodes) they are connected to. The connected vessels and nodes are stored separately in memory. The final piece of connectivity information is an array that tracks which main arteries are direct parents of a generated sub-network.

Input pressure data is then organized and the mean pressure and fundamental frequency of the signal are computed. Then several local parameters for each main vessel are found. The first is local hematocrit (Hct) which is calculated using (4-10).

The local density is found next:

$$\rho = \rho_p(1 - Hct) + \rho_{RBC}Hct . \quad (4-20)$$

The code then finds viscosity values using (4-7). An initial wall stress value of 1 is assigned to each main vessel. The iterative procedure for finding the actual wall stress values will be explained below.

The lubrication approximation (4-12) is applied to arteries with varying radii. The Poiseuille resistance (corrected for tapering) is calculated for all main vessels. An additional correction to the resistance values using the Casson relationship cannot be applied until after the wall stress has been calculated.

The code then uses scaling laws to generate sub-systems, completing the full closed arterial network. This allows the remaining resistances to be calculated. The

full network must be explicitly known so that parallel and series resistances can be calculated, much like in an electric circuit. The scaling laws used for our model are slightly modified versions of those found in West (1997 & 1999)^{4,5}. Lengths of generated vessels always scale down by a power of 1/3. Radii of generated vessels scale by a 1/2 power law until a critical generation \bar{k} is reached. At this point along the sub-network, viscosity effects in the smaller vessels take over and the cross-sectional areas of the daughter vessels must increase, rather than preserve the area of the parent vessels. The scaling thus changes to a power of -1/3 at \bar{k}^4 . The calculations to generate sub-networks are obviously only carried out for terminal main arteries, and each sub-network is associated with the index of its main parent vessel.

The first calculation finds the critical radius \bar{r} associated with the \bar{k} generation using

$$\bar{r} = \frac{r_{MinCap}}{\left(n^{-1/3}\right)^{\bar{N}}}, \quad (4-21)$$

where r_{MinCap} is the user-defined minimum capillary radius, n is the number of daughter vessels at the first junction (3 in our case), and \bar{N} is the number of generations (counted from the capillaries) that scale by a 1/3 power law. The value of \bar{N} is constant for all sub-networks, unless the total number of generations N is less than \bar{N} . In this case $\bar{N} = N$. \bar{r} may turn out to be larger than the distal radius of the main parent vessel of the given sub-network. This means that the terminal vessel is small, so the sub-network immediately scales by the -1/3 power law. If this is the case \bar{k} is set to 0 and the total number of generations N is found with

$$N = \frac{\ln\left(\frac{r_{MinCap}}{r_P}\right)}{-\frac{1}{3}\ln(n)} \quad (4-22)$$

rounded down to the nearest integer, where r_p is the parent radius. If $\bar{r} < r_p$,

$$\bar{k} = \frac{\ln\left(\frac{\bar{r}}{r_p}\right)}{-\frac{1}{2}\ln(n)} \quad (4-23)$$

and $N = \bar{N} + \bar{k}$. For our current model $n = 2$. We found that the best results occurred when a switch from bifurcations to trifurcations was made during the scaling process. We elected to apply this switch at the \bar{k} generation. Thus for scaling above \bar{k} (4-23), the value of n is 2, but for scaling below \bar{k} (4-22) $n = 3$.

Sub-network radii are then calculated with the laws discussed above. The methodology is straightforward. For the first vessel of the sub-network the radius is based off of the terminal main vessel; all others are based off the radius of the previous generation. As long as the generation number is less than or equal to \bar{k} , the -1/2 power law is used. Past this point a substitution is made for -1/3.

Finally, the lengths must be back-calculated based on the radii of the sub-network vessels. It is far more accurate to start at the capillaries and generate the lengths in an upstream direction rather than from the terminal vessel, because small differences in vessel dimensions can make large changes in the viscosity effects of the smallest vessels. The length of the last vessel (generation number N) is first found with the relation

$$l_N = r_N \times \frac{l_{cap,j}}{r_{cap,j}}, \quad (4-24)$$

where $\frac{l_{cap,j}}{r_{cap,j}}$ is the previously defined length to radius ratio for the sub-network

associated with terminal artery j . Once the capillary length is found, the rest may be easily computed by applying the 1/3 power law all the way up the sub-network, making sure to switch to bifurcations once \bar{k} is reached.

4.1.4 Test Case Description

For the purposes of refining our model using a simple case, we have applied our code to an arbitrary vessel designated “vessel₀.” This is a single artery whose dimensions exactly match those of the right common carotid artery, taken from Reymond *et al*³. We have also taken pressure information about this vessel from our previously developed 1D model code. The pressures (in Pa) at the inlet and outlet nodes have been recorded and are implemented into the new special-case code. They are kept in an Excel file, making them easier to load since there are now multiple sets of pressures as functions of time.

4.2 Steady State Solution

The initial step involves a subroutine which iteratively calculates wall stress. The total resistance of every main artery is first computed. Yield stress is found using (4-9). The total resistance is found using (4-6) and (4-11) (or (4-12) for tapered vessels) for both main and sub-network vessels with τ_w assumed to be 1 as mentioned previously. Because the sub-networks are regular in nature, the cumulative resistance of each tree may be found by using (4-11) recursively. The resistance of a parent vessel $R_{SS,p}$ will be equal to the resistance of the individual daughter vessels $R_{SS,d}/2$ at a bifurcation or $R_{SS,d}/3$ at a trifurcation. The cumulative resistance of every sub-network is calculated with this relationship by beginning at the capillary level and working upstream. The cumulative resistance of each tree is then simply added to the tree’s parent vessel resistance to account for the full network.

The subroutine then utilizes a system of equations to solve for the pressure at every node. The difference in the resistances between two connecting vessels is used to find the pressure drop over each artery. The equations take the form

$$\Delta P \left(\frac{1}{R_{SS,1}} - \frac{1}{R_{SS,2}} \right) = 0 .$$

Knowing the mean input pressure and every pressure drop, the pressure at each node can be found. Because flow is conserved at each node, the inverse of the resistances are used as the pressure coefficients. For terminal main arteries, the only difference is that the inverse cumulative resistance of the attached sub-network is also used.

Once the pressures of the nodes are computed, the pressure drops along each vessel are recalculated and stored by subtracting the pressures at the two connecting nodes. Several other pieces of information are then found such as the steady state flow and average velocity of the blood in each main vessel. Entrance resistances are currently excluded. Should an expression for this term be found, it may be easily incorporated into the model for increased accuracy. Excluding this term in our current model does not alter any values significantly. Wall stress is then found with (4-4). In the model code, Shank's transform is used to increase the rate at which τ_w converges. The shear rate is then calculated using the Casson model (4-8). The same calculations are performed for the vessels in the arterial trees. The code iterates 15 times, which is enough for wall stress to converge to 5 significant digits.

Upon completing the iterative procedure described above, the final values for resistance, steady state pressure drop, and flow rate are computed using the converged values of τ_w by following the exact procedure used in the subroutine. MATLAB then displays several key outputs, such as the total cardiac output (the pressure difference between the first two nodes divided by the resistance of the aorta), the total pressure drop, mean flow rate to the brain, and cumulative network resistance.

4.2.1 Alternate Method for Single Vessel

The new code is very similar to our previously developed model code. Many sections have been copied directly from that script. Specifically, the parts that solve for resistances and other variables of vessels in generated subnetworks have been left in. Since our test system is a single user-defined vessel, every calculation involving subnetworks is skipped over. All of the calculations for main vessels are the same as in our old code up to the iterative calculation of wall stress.

Wall stress is found using a separately coded function based on our older code, but is much simpler because it does not involve a system of equations to solve for pressure. The other calculations to find τ_w , including Shank's transform, are the same as before. The value of wall stress for this system converges after a single iteration, because we assign the pressure boundary conditions directly. Resistances and steady state flows are then found and reported just as in the old code.

4.3 Transient Solution

The Womersley method involves initially decomposing the transient signal into a set of harmonics using a Fourier transformation. This solution has complex values until it is transformed back into the time domain. It accounts for the pulsatile motion of the flow and pressure waves. The transient solution is ultimately found using the steady state results and an inverse Fourier transformation.

The model code first calculates variables for each vessel associated with the pulsatile nature of blood flow. First a value for pseudo-compliance $\left(\frac{Eh}{r}\right)$ is calculated based on an empirical relation from Olufsen¹³. E and h are computed based on which range of values the vessel radius falls within. c_0 can then be found for each vessel by solving(4-14). With these values, the dimensionless Womersley number,

complex wave speed, and impedance are calculated for each vessel and Fourier harmonic using (4-16), (4-15), and (4-13), respectively. These calculations of pulsatile characteristics are performed for the sub-network vessels using the same methods.

In order to incorporate the time-dependent behaviors of pressure and flow into our model, a Fourier transformation with 10 harmonics is used to convert the input pressure into the frequency domain. In every vessel (except at the capillary level) there is a forward and a backward pressure wave which together make up the total pressure in the vessel at any given axial distance and time. The forward and backward flows through each vessel are thus also based on axial distance and time. We next describe how to generate these time dependent outputs.

For each vessel, R must be found for all 10 harmonics used in the transformation. The reflection ratios of vessels in secondary networks are found first. We assume a perfect termination of the vessels at the capillary level, meaning the backward pressure is nonexistent and $R = 0$. R is found recursively for the other sub-network vessels by moving upstream and utilizing the pressures and reflection ratios found previously. With this information the reflection ratios of the terminal main arteries are also found, using the equation

$$R_0 = \frac{\frac{Z_{1,input} - Z_0}{\eta}}{\frac{Z_{1,input} + Z_0}{\eta}} \quad (4-25)$$

for a given main vessel and harmonic. The subscript 0 refers to the terminal main artery while the subscript 1 refers to the first generation after that vessel branches. η is a scaling factor: 2 for a bifurcation or 3 for a trifurcation. The $Z_{1,input}$ term is found using

$$Z_{1,input} = Z_1 \left[\frac{1 + R_1 \exp\left(-2i\omega \frac{L_1}{c_1}\right)}{1 - R_1 \exp\left(-2i\omega \frac{L_1}{c_1}\right)} \right] \quad (4-26)$$

The transient pressures of the main arteries are still unknown at this point, so a system of equations is necessary to solve for them simultaneously.

The number of equations in this system is twice the number of main vessels, because a forward and backward pressure component for each must be found. The equations that must be solved differ depending on if the vessel in question is terminal. If so, the equation

$$P_f R - P_b = 0 \quad (4-27)$$

is used. The forward pressure coefficient is thus the reflection ratio and the backward coefficient is -1. The reflection ratios of the main vessels have not been calculated, so an alternative method must be used for these arteries.

For every node, the number of equations to solve is equal to the number of main arteries connected to it. The first equation is

$$\sum Q_j = 0 \quad (4-28)$$

for node j . The others equations set the pressures in the connected ends of each vessel equal to each other. For the flux equation, the inverse complex impedances of the main vessels are used for the pressure coefficients because $\frac{P(t)}{Z} = Q(t)$. To stay consistent, each node must be designated as either the “beginning” or “end” of each vessel it connects. If it is the end of a vessel, a correction to the impedance must be applied that accounts for how the pressure changes as it travels along the artery to that point. The designation is arbitrary so long as it does not change for the entire system of equations. In the matrix that contains the connected nodes to each vessel, the first node is designated as the beginning.

If the specified node is the beginning of the vessel, the forward pressure does not need a correction and is simply P_f . However, the backward pressure must travel the length of the vessel before reaching the node, and therefore is corrected to $P_b \exp\left(\frac{-i\omega l}{c}\right)$, where ω is the frequency of the Fourier harmonic, l is the vessel length and c is the complex wave speed for the given vessel and harmonic (not to be confused with the Moens-Korteweg wave velocity). Similarly, if the node is at the end of a vessel, the forward pressure must be written as $P_f \exp\left(\frac{-i\omega l}{c}\right)$, while the backward pressure stays as P_b . Thus the expressions for flux are

$$-\frac{P_f}{Z} + \frac{P_b \exp\left(\frac{-i\omega l}{c}\right)}{Z} \quad (4-29)$$

and

$$\frac{P_f \exp\left(\frac{-i\omega l}{c}\right)}{Z} - \frac{P_b}{Z} \quad (4-30)$$

for beginning and end nodes, respectively. The end node expression(s) are subtracted from the beginning node expression(s) to give the left hand side of (4-28) for a given node.

The other equations involving pressure at a given node will have solutions with orders of magnitude close to 1. However, the values for impedance are much larger, meaning these solutions will have extremely small orders of magnitude (about 10^{-8}). The coefficients involving impedances must be weighted so that the orders of all numbers in the matrix stay close. Otherwise MATLAB may find a singularity error when attempting to solve the system. To avoid this issue, the inverse of the first coefficient for every node is stored as the weighting value. Each coefficient of the flux

equation is then multiplied by the weighting value. Since all of these terms are very small in magnitude, the re-weighting brings them much closer to 1. Additionally, since each coefficient is multiplied by the same factor, the overall system is not affected.

The remaining equations set the pressures of the connecting vessels equal to each other at the specified node. The *total* pressures must be equal, so the sum of the forward and backward pressures of one vessel must equal those of the other. However, the specified node will be at the beginning of one of these arteries and at the end of the others. Therefore a correction similar to the one applied before must also be applied here. If vessel 1 ends at the node and vessel 2 begins at the node, the pressure equation is

$$\left[P_{f,1} \exp\left(\frac{-i\omega l_1}{c_1}\right) + P_{b,1} \right] - \left[P_{f,2} + P_{b,2} \exp\left(\frac{-i\omega l_2}{c_2}\right) \right] = 0 \quad (4-31)$$

Likewise, if vessel 1 begins at the specified node and vessel 2 ends at the node the equation becomes

$$\left[P_{f,1} + P_{b,1} \exp\left(\frac{-i\omega l_1}{c_1}\right) \right] - \left[P_{f,2} \exp\left(\frac{-i\omega l_2}{c_2}\right) + P_{b,2} \right] = 0 \quad (4-32)$$

In the first case the pressure coefficients are $\exp(-i\omega l_1/c_1)$ (forward) and 1 (backward) for the first vessel, and -1 (forward) and $-\exp(-i\omega l_2/c_2)$ (backward) for the second vessel. In the second case these coefficients are 1 (forward) and $\exp(-i\omega l_1/c_1)$ (backward) for vessel 1, and -1 (forward) and $-\exp(-i\omega l_2/c_2)$ (backward) for vessel 2. The first vessel connected to the node will be designated as vessel 1 and this procedure will be carried out for each other connected vessel. After finding these coefficients, all of the equations will have been stated. The system is solved in this way for each harmonic.

To then find the reflection ratio for each non-terminal main artery, the equation

$$\frac{P_{b,j,n}}{P_{f,j,n}} \exp\left(\frac{i\omega_n l_j}{c_{j,n}}\right) \quad (4-33)$$

is used, where j is the vessel number and n is the harmonic. The total impedance of the network is calculated for each harmonic using

$$Z_{total} = Z_{top} \frac{1 + R_{top} \exp\left(\frac{-2i\omega l_{top}}{c_{top}}\right)}{1 - R_{top} \exp\left(\frac{-2i\omega l_{top}}{c_{top}}\right)} \quad (4-34)$$

The magnitude (modulus) and phase lag of the total impedance may now be found and plotted against experimental results to validate the model.

To find true transient pressures in specific main arteries, results of the system of equations (denoted by *) are altered for the specific vessel dimensions and then summed over each harmonic. For each vessel and time point, these equations are

$$P_{f,n} = P_{f,n}^* \exp(i\omega_n \times \text{step}) \quad (4-35)$$

and

$$P_{b,n} = P_{b,n}^* \exp\left[i\omega_n \left(\text{step} - \frac{l}{c_n}\right)\right] \quad (4-36)$$

for the n^{th} harmonic. The total forward and backward pressure components are found using

$$P_{total} = \frac{Q_{SS}}{R_{SS}} + P_{f,1}^* \sum_{n=1}^{10} \frac{2 \operatorname{Re}(P_{f,n} + P_{b,n})}{N} \quad (4-37)$$

where N is the number of steps in the input signal, P is the result of either (4-35) or (4-36), and Q_{SS} and R_{SS} are the steady state flow and resistance, respectively. The transient pressure contribution is relative to the first term in the transient system of equations, which we set equal to 1 for convenience. For any vessel, P_{total} must be multiplied by $P_{f,1}^*$. This total transient pressure still only accounts for the oscillations

in the flow. Therefore, the mean steady state pressure of the given vessel is added to the transient component. This result may be plotted against time to view the characteristic pressure and flow waves of each main artery.

4.3.1 Alternate Method for Single Vessel

We again utilize our single vessel₀ to test our model against a simple case. The changes to our model that allow for two distinct boundary conditions are described here.

First, a normalized Fourier transform of the two pressure input waves is found using the fast Fourier transform function (fft) and dividing by N , the number of time points. A completely new system of equations is then solved to find the complex coefficients of the transient pressures.

The principle behind these calculations is that both pressure waves (forward and backward) may be accurately approximated by a complex coefficient multiplied by a complex exponential term dependent on both time and linear distance. These two complex coefficients may be found at the end points by utilizing boundary conditions. They then may be applied to all interior points. The overall set up is as follows:

$$P_{inlet,k}(t) = C_f \exp(i\omega_k t - kx) \Big|_{x=0} + C_b \exp(i\omega_k t - kx) \Big|_{x=L} \quad (4-38)$$

and

$$P_{outlet,k}(t) = C_f \exp(i\omega_k t - kx) \Big|_{x=L} + C_b \exp(i\omega_k t - kx) \Big|_{x=0}, \quad (4-39)$$

where the *subscript* k indicates the Fourier harmonic. The pressure contributions from each harmonic are summed and added to the steady state pressure to give the full solution. The coefficients of the exponentials (C) are split into their real and imaginary parts, thus $C_f = C_{rf} + iC_{if}$ and $C_b = C_{rb} + iC_{ib}$. The coefficients of the length terms (k) are equal to the fundamental frequency divided by the complex wave speed

characteristic of this specific vessel. This term is also split into real and imaginary parts, thus $k = \frac{i\omega_k}{c} = (ic_r + c_i) \frac{\omega_k}{|c|^2}$ by multiplying the numerator and denominator by

the complex conjugate of c . The two components of k are $k_r = \frac{\omega_k c_i}{|c|^2}$ and $k_i = \frac{\omega_k c_r}{|c|^2}$

such that $k = k_r + ik_i$. The exponential term is manipulated as follows:

$$\exp(i\omega_k t \pm kx) = \exp(\mp k_i x) \exp[i(\omega_k t \pm k_r x)] = \exp(\mp k_i x) [\cos(\omega_k t \pm k_r x) + i \sin(\omega_k t \pm k_r x)]$$

by Euler's formula. The new forms of the forward and backward waves are

$$(C_{rf} + iC_{if}) [\cos(\omega_k t - k_r x) \exp(k_i x) + i \sin(\omega_k t + k_r x) \exp(k_i x)] \Big|_{x=0} \quad (4-40)$$

and

$$(C_{rb} + iC_{ib}) [\cos(\omega_k t + k_r x) \exp(-k_i x) + i \sin(\omega_k t + k_r x) \exp(-k_i x)] \Big|_{x=L}, \quad (4-41)$$

respectively.

These expressions may be simplified by expanding them and keeping only the real terms. The sinusoidal terms are further expanded by utilizing two sine identities:

$$\sin(x \pm y) = \sin(x) \cos(y) \pm \cos(x) \sin(y) \quad (4-42)$$

and

$$\cos(x \pm y) = \cos(x) \cos(y) \mp \sin(x) \sin(y). \quad (4-43)$$

This leads us to the final form of the pressure wave components as used in the system of equations within our code:

$$P_k(x, t) = \left[\begin{aligned} &C_{rf} \cos(\omega_k t) \cos(k_r x) \exp(k_i x) + C_{rf} \sin(\omega_k t) \sin(k_r x) \exp(k_i x) \\ &-C_{if} \sin(\omega_k t) \cos(k_r x) \exp(k_i x) + C_{if} \cos(\omega_k t) \sin(k_r x) \exp(k_i x) \end{aligned} \right] + \left[\begin{aligned} &C_{rb} \cos(\omega_k t) \cos(k_r x) \exp(-k_i x) - C_{rb} \sin(\omega_k t) \sin(k_r x) \exp(-k_i x) \\ &-C_{ib} \sin(\omega_k t) \cos(k_r x) \exp(-k_i x) - C_{ib} \cos(\omega_k t) \sin(k_r x) \exp(-k_i x) \end{aligned} \right], \quad (4-44)$$

where $P_k(t)$ is the pressure corresponding to the k^{th} Fourier harmonic at time t ,

evaluated at $x=0$ for the inlet or $x=L$ for the outlet.

To apply the boundary conditions, we must utilize the Fourier coefficients at the inlet and outlet found previously. After we applied Euler's formula above, we were left with a real coefficient of $\cos(\omega_k t)$ and an imaginary coefficient of $\sin(\omega_k t)$.

These sine and cosine terms are the common factors in our system. Taking the real part of the Fourier coefficient results in the cosine term; taking the imaginary part will give the sine term. Thus (4-38) and (4-39) may be rewritten as

$$P_{inlet,k}(t) = 2 \operatorname{Re}[\operatorname{fft}(P_{in})] \cos(\omega_k t) - 2 \operatorname{Im}[\operatorname{fft}(P_{in})] \sin(\omega_k t) \quad (4-45)$$

and

$$P_{outlet,k}(t) = 2 \operatorname{Re}[\operatorname{fft}(P_{out})] \cos(\omega_k t) - 2 \operatorname{Im}[\operatorname{fft}(P_{out})] \sin(\omega_k t). \quad (4-46)$$

The factor of 2 is included to account for the negative signal frequencies not captured by the Fourier transformation. We find P_k for each harmonic by evaluating (4-44) at the two boundary points. We are left with four equations: the real (cosine) and imaginary (sine) sets of terms at both the inlet and outlet(4-47).

$$\begin{pmatrix} 1 & 0 & 1 & 0 \\ 0 & 1 & 0 & 1 \\ \cos(k,L)\exp(k_i L) & \sin(k,L)\exp(k_i L) & \cos(k,L)\exp(-k_i L) & -\sin(k,L)\exp(-k_i L) \\ \sin(k,L)\exp(k_i L) & -\cos(k,L)\exp(k_i L) & -\sin(k,L)\exp(-k_i L) & -\cos(k,L)\exp(-k_i L) \end{pmatrix} \begin{pmatrix} C_{rf} \\ C_{if} \\ C_{rb} \\ C_{ib} \end{pmatrix} = \begin{pmatrix} 2 \operatorname{Re}[\operatorname{fft}(P_{in})] \\ 2 \operatorname{Im}[\operatorname{fft}(P_{in})] \\ 2 \operatorname{Re}[\operatorname{fft}(P_{out})] \\ 2 \operatorname{Im}[\operatorname{fft}(P_{out})] \end{pmatrix} \quad (4-47)$$

This system is solved for every harmonic. The pressure profile along the vessel is then split into 100 equal steps, and a linear gradient is assumed; this is the steady state value for the given length point. A correction for tapering will later be added in, since this vessel varies in radius. For each time and length point, the steady state and transient contributions are summed. The transient part is reconstructed from the complex coefficients using

$$\sum_{k=1}^{10} (C_r + iC_i) \exp\left[i\omega_k \left(t - \frac{x}{c}\right)\right] \quad (4-48)$$

and

$$\sum_{k=1}^{10} (C_r + iC_i) \exp \left[i\omega_k \left(t + \frac{L-x}{c} \right) \right] \quad (4-49)$$

for the forward and backward components, respectively. The final value for pressure is

$$P(x,t) = P_{ss}(x,t) + \text{Re} \left[P_f(x,t) + P_b(x,t) \right]. \quad (4-50)$$

Endnotes

- ¹ Johnson, David A., Justin R. Spaeth, William C. Rose, Ulhas P. Naik, and Antony N. Beris. "An Impedance Model for Blood Flow in the Human Arterial System. Part I: Model Development and MATLAB Implementation." *Computers & Chemical Engineering* 35.7 (2011): 1304-316.
- ² Alastruey, J., K. H. Parker, J. Peiró, S. M. Byrd, and S. J. Sherwin. "Modelling the Circle of Willis to Assess the Effects of Anatomical Variations and Occlusions on Cerebral Flows." *Journal of Biomechanics* 40.8 (2007): 1794-805.
- ³ Reymond, P., F. Merenda, F. Perren, D. Rufenacht, and N. Stergiopoulos. "Validation of a One-dimensional Model of the Systemic Arterial Tree." *AJP: Heart and Circulatory Physiology* 297.1 (2009): H208-222.
- ⁴ West, Geoffrey B., James H. Brown, and Brian J. Enquist. "A General Model for the Origin of Allometric Scaling Laws in Biology." *Science* 276.5309 (1997): 122-26.
- ⁵ West, Geoffrey B. "The Origin of Universal Scaling Laws in Biology." *Physica A: Statistical Mechanics and Its Applications* 263.1-4 (1999): 104-13.
- ⁶ Apostolidis, Alex J. and Antony N. Beris. "Modeling of the Blood Rheology in Steady-state Shear Flows." *Journal of Rheology* 58 (2014): 607-633.
- ⁷ Merrill, Edward W., Chon S. Cheng, and Gerard A. Pelletier. "Yield Stress of Normal Human Blood as a Function of Endogenous Fibrinogen." *Journal of Applied Physiology* 26.1 (1969): 1-3.
- ⁸ Truskey, G. A., F. Yuan, and D. F. Katz. *Transport Phenomena in Biological Systems*. Upper Saddle River: Prentice Hall, 2004.
- ⁹ Pries, A. R., T. W. Secomb, P. Gaehtgens, and J. F. Gross. "Blood Flow in Microvascular Networks. Experiments and Simulation." *Circulation Research* 67.4 (1990): 826-34.

-
- ¹⁰ Korteweg, D. J. "Ueber Die Fortpflanzungsgeschwindigkeit Des Schalles in Elastischen Röhren." *Ann. Phys. Chem. Annalen Der Physik Und Chemie* 241.12 (1878): 525-42.
- ¹¹ Moens, A. *Die Pulscurve*. Leiden: E.J. Brill, 1878.
- ¹² Zamir, M. *The Physics of Pulsatile Flow*. New York: AIP, 2000.
- ¹³ Olufsen, M. S. "Modeling Flow and Pressure in the Systemic Arteries." In: Ottesen, J. T., Olufsen, M. S., & Larsen, J. K. (Eds.) *Applied Mathematical Models in Human Physiology*, Philadelphia: SIAM, 2004.

Chapter 5

ALTERNATE NUMERICAL APPROACH TO THE 1D VISCOUS FLOW IN AN ELASTIC TUBE

5.1 Governing Equations and Problem Setup

An alternative method of solving the individual vessel flow problem is maintaining the nonlinear form of the governing equations. Our nonlinear method is more expensive computationally, but it allows us to identify any nonlinear effects that are not captured in our Womersley-like calculations. The three equations are as follows:

$$\text{Continuity: } \frac{\partial(\rho A)}{\partial t} + \frac{\partial}{\partial x}(\rho Au) = 0 \quad (5-1)$$

$$\text{Conservation of Momentum: } \frac{\partial(\rho u)}{\partial t} + \frac{\partial}{\partial x} \left(\frac{\rho u^2}{2} + P \right) + 8\pi\mu \frac{u}{A} = 0 \quad (5-2)$$

$$\text{Constitutive Relationship: } \sqrt{A} - \sqrt{A_0} = \gamma P \quad (5-3)$$

The three variables we must solve for are cross-sectional area A , fluid velocity u , and pressure P . The pressure terms here are all relative to the exterior so that A_0 is the vessel area at zero relative pressure. ρ is the total mass density. It is dependent on the local hematocrit Hct (the volume fraction of red blood cells) by (4-20), where the p subscript indicates plasma density. The local hematocrit is in turn found for a given vessel using Equation 1 from Pries *et al.* (1990)¹ (4-10), where D is the vessel diameter in μm . This correction only becomes significant at diameters greater than about 600 microns. Hct_D is the discharge hematocrit of larger arteries, a user defined parameter to which we assign a value of 0.45. The dependence of hematocrit on vessel

diameter is explained by the Fahraeus effect². The local viscosity μ is also dependent on Hct by (4-7)³. Variations in blood viscosity are caused by Fahraeus-Lindqvist effects². μ_p is the average plasma viscosity, defined by the user. γ is a small parameter equal to the inverse pseudo-compliance, a function of vessel viscoelasticity.

The constitutive relationship (5-3) may be solved for A , so that our system involves only two equations. The modified forms of the continuity and momentum equations are

$$\frac{\partial}{\partial t} \left[\rho (\gamma P + \sqrt{A_0})^2 \right] + \frac{\partial}{\partial x} \left[\rho u (\gamma P + \sqrt{A_0})^2 \right] = 0 \quad (5-4)$$

and

$$\frac{\partial(\rho u)}{\partial t} + \frac{\partial}{\partial x} \left(\frac{\rho u^2}{2} + P \right) + \frac{8\pi\mu u}{(\gamma P + \sqrt{A_0})^2} = 0, \quad (5-5)$$

respectively.

5.1.1 Dimensionless Conversion

In order to both gain a greater understanding of the fluid mechanics involved and simplify our calculations, we utilized dimensionless variables and parameters in our nonlinear equations. The relevant variables were scaled by characteristic constants to make them unitless. The conversions are found in Table 2.

Table 2: Scaling of dimensionless variables

| Dimensionless Variable | Physical Equivalent |
|--|---------------------|
| \hat{u} | u/u^* |
| $\hat{A}(\hat{x}, \hat{t}), \hat{A}_0(\hat{x}, \hat{t})$ | $A/A^*, A_0/A^*$ |
| \hat{P} | P/P^* |
| \hat{x} | x/L^* |
| \hat{t} | $t(u^*/L^*)$ |
| $\hat{\mu}(\hat{x}, \hat{t})$ | μ/μ^* |
| $\hat{\rho}(\hat{x}, \hat{t})$ | ρ/ρ^* |

Stars indicate reference values, which may be suitably chosen based on the given problem. The dimensionless area and viscosity include dependences on distance and time in case one wants to include phenomena such as vasodilation or viscoelastic effects, respectively. The density is dependent on the hematocrit (4-20), which may depend on distance and time as well. Thus, we list this dependence explicitly.

In order to make the relevant equations fully dimensionless, two dimensionless groups must be defined. These factors are listed in Table 3. Re_m represents a modified Reynolds number, which involves the radius-based Reynolds number $Re_r = \frac{\rho ur}{\mu}$ as well as the aspect ratio $\frac{\sqrt{A^*}}{\sqrt{\pi L^*}}$. The dimensionless $\hat{\gamma}$ will become very important to our analytical method used to validate the nonlinear numerical solution.

The two governing equations can now be rewritten in a dimensionless form. The continuity and momentum equations now become

$$\begin{aligned}
& 2\hat{\rho}\hat{\gamma}\frac{d\hat{P}}{d\hat{t}} + \left(\frac{\hat{\rho}}{\sqrt{\hat{A}_0}}\right)\frac{d\hat{A}_0}{d\hat{t}} + \left(\hat{\gamma}\hat{P} + \sqrt{\hat{A}_0}\right)\frac{d\hat{\rho}}{d\hat{t}} \\
& + 2\hat{\gamma}\hat{\rho}\hat{u}\frac{d\hat{P}}{d\hat{x}} + \frac{\hat{\rho}\hat{u}}{\sqrt{\hat{A}_0}}\frac{d\hat{A}_0}{d\hat{x}} + \hat{u}\left(\hat{\gamma}\hat{P} + \sqrt{\hat{A}_0}\right)\frac{d\hat{\rho}}{d\hat{x}} + \hat{\rho}\left(\hat{\gamma}\hat{P} + \sqrt{\hat{A}_0}\right)\frac{d\hat{u}}{d\hat{x}} = 0
\end{aligned} \tag{5-6}$$

and

$$\begin{aligned}
& \hat{\rho}\frac{d\hat{u}}{d\hat{t}} + \hat{u}\frac{d\hat{\rho}}{d\hat{t}} \\
& + \hat{\rho}\hat{u}\frac{d\hat{u}}{d\hat{x}} + \frac{1}{2}\hat{u}^2\frac{d\hat{\rho}}{d\hat{x}} + \frac{1}{\text{Re}_m}\frac{d\hat{P}}{d\hat{x}} + \frac{\hat{\rho}\hat{u}}{\text{Re}_m(\hat{\gamma}\hat{P} + \sqrt{\hat{A}_0})^2} = 0
\end{aligned} \tag{5-7}$$

respectively. (5-6) and (5-7) are a set of hyperbolic equations that require two initial conditions to solve. We accomplish this by setting explicit pressure boundary conditions at the inlet and outlet of the vessel. The steady state solution is found first, before moving to the time-dependent transient solution.

5.2 Steady State Solution

For the steady state solution, all time-dependent derivatives will reduce to zero, leaving

$$2\hat{\gamma}\hat{\rho}\hat{u}\frac{d\hat{P}}{d\hat{x}} + \frac{\hat{\rho}\hat{u}}{\sqrt{\hat{A}_0}}\frac{d\hat{A}_0}{d\hat{x}} + \hat{u}\left(\hat{\gamma}\hat{P} + \sqrt{\hat{A}_0}\right)\frac{d\hat{\rho}}{d\hat{x}} + \hat{\rho}\left(\hat{\gamma}\hat{P} + \sqrt{\hat{A}_0}\right)\frac{d\hat{u}}{d\hat{x}} = 0 \tag{5-8}$$

and

$$\hat{\rho}\hat{u}\frac{d\hat{u}}{d\hat{x}} + \frac{1}{2}\hat{u}^2\frac{d\hat{\rho}}{d\hat{x}} + \frac{1}{\text{Re}_m}\frac{d\hat{P}}{d\hat{x}} + \frac{\hat{\rho}\hat{u}}{\text{Re}_m(\hat{\gamma}\hat{P} + \sqrt{\hat{A}_0})^2} = 0. \tag{5-9}$$

5.2.1 Test Case

We again chose the representative artery vessel₀ as a test vessel on which to apply our model. The values for our dimensionless parameters are listed in Table 3, and reference conditions for this case are listed in Table 4.

Table 3: Scaling of other dimensionless parameters

| Dimensionless Parameter | Physical Equivalent | Test Case Values |
|-------------------------|--|------------------------|
| Re_m | $u^* \left(\frac{A^*}{8\pi L^*} \right) \left(\frac{\rho^*}{\mu^*} \right) = Re_r \left(\frac{\sqrt{A^*}}{8\sqrt{\pi} L^*} \right)$ | 3.434 |
| $\hat{\gamma}$ | $\frac{\gamma P^*}{\sqrt{A^*}}$ | 1.534×10^{-4} |

Table 4: Test case reference conditions, all constant

| Variable | Reference Condition | Value for Test Case |
|----------|---|-----------------------------------|
| u^* | Poiseuille velocity, $u_0 = \frac{A_0 (P_{in} - P_{out})}{8\pi\mu_0 L}$ | 0.3 m/s |
| A^* | average resting area (A_0), $d = 10.25\text{mm}$ | $8.25 \times 10^{-5} \text{ m}^2$ |
| P^* | steady state pressure drop | 29.0 Pa |
| L^* | entire vessel length | $9.4 \times 10^{-2} \text{ m}$ |
| μ^* | average local viscosity μ_0 | $3.3 \times 10^{-3} \text{ Pa s}$ |
| ρ^* | average density ρ_0 | 1057 kg/m^3 |

For our current case where both area and viscosity lack dependence on either \hat{x} or \hat{t} and hematocrit is constant, \hat{A}_0 , $\hat{\mu}$, and $\hat{\rho}$ will equal 1 and the governing equations further simplify to

$$2\hat{\gamma}\hat{u} \frac{d\hat{P}}{d\hat{x}} + (\hat{\gamma}\hat{P} + 1) \frac{d\hat{u}}{d\hat{x}} = 0 \quad (5-10)$$

and

$$\hat{u} \frac{d\hat{u}}{d\hat{x}} + \frac{1}{Re_m} \frac{d\hat{P}}{d\hat{x}} + \frac{\hat{u}}{Re_m (\hat{\gamma}\hat{P} + 1)^2} = 0 \quad (5-11)$$

Before the numerical method is applied, we generate an initial solution using an analytical perturbation expansion of \hat{P} , \hat{A} , and \hat{u} . We apply a Taylor-like series expansion beginning from the steady state values and continually adding more

coefficients that are respectively multiplied by increasing powers of the small parameter $\hat{\gamma}$. Thus $\hat{P} \approx \hat{P}_0 + \hat{P}_1\hat{\gamma} + \hat{P}_2\hat{\gamma}^2 + \hat{P}_3\hat{\gamma}^3 + \dots$ until the subsequent terms are so small that they no longer appreciably change the total value. Because $\hat{\gamma}$ is small to begin with, only terms up to the second or third order should be necessary.

The perturbation approach requires solving each variable for a given order before moving to the next higher power. Thus we must first solve the zero order terms. This calculation is mostly trivial; it will simplify to the steady state values. The zero order solution is found in Table 5 (reference area, viscosity, and density are again assumed constant).

Table 5: Zero-order solution of perturbation expansion

| | |
|-------------|---------------|
| \hat{u}_0 | 1 |
| \hat{A}_0 | 1 |
| \hat{P}_0 | $1 - \hat{x}$ |

The solution is trivial; it reduces to the Poiseuille solution which we used to set up the problem. Additionally, the results make physical sense; at steady state \hat{u} and \hat{A} are constant while \hat{P} is linearly dependent on \hat{x} .

The first order solution is obtained by expanding the variables in terms of $\hat{\gamma}$ and manipulating the equations so they are in polynomial form. Then all terms multiplied by $\hat{\gamma}^1$ are grouped and solved for using the zero-order solution. The results of these calculations are listed in Table 6.

Table 6: 1st-order solution of perturbation expansion

| | |
|-------------|---------------------------|
| \hat{u}_1 | $Re_m + 1/2 + x$ |
| \hat{A}_1 | $2(\hat{x} - 1)$ |
| \hat{P}_1 | $3/2(1 - \hat{x})\hat{x}$ |

Again, the results make sense, since each variable is now dependent on one additional power of \hat{x} . Area is expected to be highest when the pressure is at a maximum. A pressure drop occurs over the entirety of the vessel, and we can see that \hat{A}_1 also decreases with \hat{x} . For simplicity, we have only used the first two orders of this method in our expansion. The perturbation approach is only used as an initial guess for a numerical method, and a way to validate that scheme. However, the second or third order could easily be included after a few algebraic calculations, should we opt to add them later.

We now move to Newton's method, a numerical technique to solve our nonlinear system. The blood vessel in question is first discretized into small steps of length h . We will eventually use finite differences to solve the derivatives in the governing equations. Thus h must be sufficiently small to preserve accuracy.

The initial guesses from the perturbation expansion are added to a matrix denoted $\underline{y}_{initial}$. A system of equations is then solved:

$$\underline{g}(\underline{y}_{initial}) + \underline{J} \cdot (\underline{y} - \underline{y}_{initial}) = \underline{0}. \quad (5-12)$$

Here, $\underline{g}(\underline{y}_{initial})$ represents a residual function, the solution to the governing system minus $\underline{y}_{initial}$, leaving a small difference for all \hat{u} and \hat{P} . \underline{J} is the Jacobian matrix, thus $\underline{J} = \frac{\partial \underline{g}_i}{\partial y_i}(\underline{y}_{initial})$. A new set of variables \underline{y}_{new} is then found by adding the initial vector to $\underline{\Delta y}$ and the process iterates until a convergence criterion is reached. It should

be noted that for a single vessel system, we impose inlet and outlet pressure boundary conditions directly.

The nonlinear code currently incorporates physical information of the system (such as length, radius, density, etc.) directly into the script. This could easily be changed to loading data from another file just as in the Womersley method code. The steady state area is found by assuming an average radius over the length of the vessel. The Poiseuille velocity is then found by assuming a linear pressure gradient. Dimensionless parameters are then defined using these steady state values (Table 4). Tapering of the vessel is not accounted for at this time; a correction for this could be added after verifying this method against additional results from the alternative method. The initial y matrix is defined and the Newton function is called. We use 20 as our maximum number of iterations and a tolerance of 10^{-7} . Once convergence is reached, area is calculated from the pressure values.

5.3 Transient Solution and Numerics

(Unless otherwise noted, all variables are assumed to be in their non-dimensional forms for the entirety of this section.)

The numerical method for solving the transient pressure and flow in a blood vessel involves evaluating derivatives in the governing equations and tracking them from the boundaries along “characteristics.” The characteristics are defined by the first order wave equation:

$$\frac{\partial f}{\partial t} = \lambda \frac{\partial f}{\partial x}, \quad (5-13)$$

where f can be either u or P . For the forward moving characteristic, λ_1 defines the slope and s_f is the x -intercept such that $x = \lambda_1 t + s_f$. For the backward moving

characteristic, $x = \lambda_2 t + s_b$ (λ_2 is negative). The characteristics track how changes with respect to time and length propagate along the vessel from the end points. The velocity and pressure waves will propagate along these lines; thus, we can track and evaluate them at any x and t . In order for this method to be successful, the discretized time interval must be less than the maximum wave speed.

Initially, the physical information used for the steady state solution is defined, including the linear pressure gradient. We also define a dimensionless characteristic time,

$$\hat{t} = \frac{u^* T}{L^*}, \quad (5-14)$$

where T is the period of the pulse (we use 1.25 sec) and u^* is the reference velocity. A time step value is found by dividing \hat{t} by a suitable number, usually 10^3 - 10^4 . A characteristic frequency is also defined:

$$\hat{\omega}_0 = \frac{2\pi}{\hat{t}}. \quad (5-15)$$

Dimensionless groups are then defined and the initial solution based on the perturbation expansion is found, just as for the steady state solution. We then set up a system of equations in matrix form that loops for all time and length points:

$$\frac{\partial}{\partial t} \begin{bmatrix} u \\ P \end{bmatrix} = -\underline{\underline{A}} \frac{\partial}{\partial x} \begin{bmatrix} u \\ P \end{bmatrix} + \begin{bmatrix} \frac{-u}{(1 + \hat{\gamma}P)^2 \text{Re}} \\ 0 \end{bmatrix}, \quad (5-16)$$

where

$$\underline{\underline{A}} = \begin{bmatrix} u & \frac{1}{\text{Re}_m} \\ \frac{1 + \hat{\gamma}P}{2\hat{\gamma}} & u \end{bmatrix}.$$

$\underline{\underline{A}}$ is broken up into its eigenvalue and eigenvector matrices such that

$$\underline{\underline{A}} = \underline{\underline{Q}} \underline{\underline{\Lambda}} \underline{\underline{Q}}^{-1} = \underline{\underline{Q}} \underline{\underline{\Lambda}} \underline{\underline{R}}. \quad (5-17)$$

We assign $\underline{\underline{R}} = \underline{\underline{Q}}^{-1}$ simply to clarify notation. A bit of analysis reveals

$$\underline{\underline{Q}} = \begin{bmatrix} \frac{1}{\text{Re}_m} & \frac{1}{\text{Re}_m} \\ \sqrt{\frac{1+\hat{\gamma}P}{2\text{Re}_m\hat{\gamma}}} & -\sqrt{\frac{1+\hat{\gamma}P}{2\text{Re}_m\hat{\gamma}}} \end{bmatrix}, \underline{\underline{\Lambda}} = \begin{bmatrix} u + \sqrt{\frac{1+\hat{\gamma}P}{2\text{Re}_m\hat{\gamma}}} & 0 \\ 0 & u - \sqrt{\frac{1+\hat{\gamma}P}{2\text{Re}_m\hat{\gamma}}} \end{bmatrix}, \underline{\underline{R}} = \begin{bmatrix} \frac{\text{Re}_m}{2} & \frac{1}{2\sqrt{\frac{1+\hat{\gamma}P}{2\text{Re}_m\hat{\gamma}}}} \\ \frac{\text{Re}_m}{2} & \frac{-1}{2\sqrt{\frac{1+\hat{\gamma}P}{2\text{Re}_m\hat{\gamma}}}} \end{bmatrix}.$$

To evaluate the length-dependent derivatives in this system, we utilize the finite difference method. Assuming our step sizes are sufficiently small, this estimation should be a good approximation for the actual value. However, because the characteristic waves are propagating along the vessel in a certain direction, it is important to evaluate the finite difference from the correct side. The first equation contains the positive eigenvalue, which contains information traveling in the positive x -direction. Conversely, the second equation corresponds to the characteristic traveling along the negative x -direction.

We split the calculations at each point into two parts. First the vector \underline{v} is defined such that

$$\underline{v} = \begin{bmatrix} -\lambda_1 \left(r_{11} \frac{\partial u}{\partial x} + r_{12} \frac{\partial P}{\partial x} \right) \\ -\lambda_2 \left(r_{21} \frac{\partial u}{\partial x} + r_{22} \frac{\partial P}{\partial x} \right) \end{bmatrix}. \quad (5-18)$$

We evaluate a one-sided finite difference for each derivative in \underline{v} . For the first equation,

$$\frac{\partial u_i}{\partial x} = \frac{3u_i - 4u_{i-1} + u_{i-2}}{2h} \quad (5-19)$$

and

$$\frac{\partial P_i}{\partial x} = \frac{3P_i - 4P_{i-1} + P_{i-2}}{2h}. \quad (5-20)$$

For the second equation,

$$\frac{\partial u_i}{\partial x} = \frac{-3u_i + 4u_{i+1} - u_{i+2}}{2h} \quad (5-21)$$

and

$$\frac{\partial P_i}{\partial x} = \frac{-3P_i + 4P_{i+1} - P_{i+2}}{2h}. \quad (5-22)$$

Then a vector \underline{z} is defined such that

$$\underline{z} = \underline{Q}\underline{v} + \underline{b}, \quad (5-23)$$

where

$$\underline{b} = \begin{bmatrix} \frac{-u}{(1 + \hat{\gamma}P)^2 \text{Re}_m} \\ 0 \end{bmatrix}.$$

\underline{z} can readily be solved with the information we have in MATLAB at this point.

The method described above works for most interior points, but as we near the boundaries we must alter our calculations somewhat. Specifically, for $N+1$ points in N increments of h , points 2 and N are problematic because there is insufficient information to compute a one-sided FD. For these two points, we instead calculate a 1st order finite difference. At point 2 the first equation has insufficient information, so we instead use

$$\frac{\partial u_2}{\partial x} = \frac{u_2 - u_1}{h} \quad (5-24)$$

and

$$\frac{\partial P_2}{\partial x} = \frac{P_2 - P_1}{h}. \quad (5-25)$$

At point N the second equation has insufficient information, so we use

$$\frac{\partial u_N}{\partial x} = \frac{u_{N+1} - u_N}{h} \quad (5-26)$$

and

$$\frac{\partial P_N}{\partial x} = \frac{P_{N+1} - P_N}{h}. \quad (5-27)$$

The values at points 1 and $N+1$ also cause trouble, but we go about the solution in a different way. At these two points, we impose the pressure conditions directly.

Thus $z_{1,P}$ and $z_{N+1,P}$ are the derivatives of the inlet and outlet pressures with respect to time, inputted directly by the user. We then calculate $z_{1,u}$ and $z_{N+1,u}$ using these

values. Specifically,

$$z_{1,u} = \frac{-r_{22}z_{1,P} + v_{1,P} + r_{21}b_1 + r_{22}b_2}{r_{21}} \quad (5-28)$$

and

$$z_{N+1,u} = \frac{-r_{12}z_{N+1,P} + v_{N+1,u} + r_{11}b_1 + r_{12}b_2}{r_{11}} \quad (5-29)$$

\underline{z} is now specified for every length point. To update the model with time, we employ Euler's method:

$$\underline{y}_{t+\Delta t} = \underline{y}_t + \underline{z}_t \Delta t \quad (5-30)$$

We continue with this method for every time point, recording the values for u and P at every t and x . Finding the dimensional values of velocity or pressure simply involves multiplying by the reference value. Additionally, we can now get area by using the constitutive equation (5-3).

For the full pulse waveform, a derivative of the pressure boundary conditions is not available. For this case, we compute a finite difference using the input pressure conditions to obtain $z_{1,P}$ and $z_{N+1,P}$:

$$z_{j,P} = \frac{P_j(t_{k+1}) - P_j(t_k)}{\Delta t}. \quad (5-31)$$

We then simply implement (5-28) and (5-29) to get the corresponding velocity entries. The rest of the calculations follow as before.

Endnotes

- ¹ Pries, A. R., T. W. Secomb, P. Gaehtgens, and J. F. Gross. "Blood Flow in Microvascular Networks. Experiments and Simulation." *Circulation Research* 67.4 (1990): 826-34.
- ² Truskey, G. A., F. Yuan, and D. F. Katz. *Transport Phenomena in Biological Systems*. Upper Saddle River: Prentice Hall, 2004.
- ³ Apostolidis, Alex J. and Antony N. Beris. "Modeling of the Blood Rheology in Steady-state Shear Flows." *Journal of Rheology* 58 (2014): 607-633.

Chapter 6

RESULTS AND DISCUSSION

The results of the original analytical and numerical model solutions are reported and compared here based on our single vessel case. Relevant parameters are listed in Table 7, which correspond to the dimensionless values in Table 3.

Table 7: Model input parameters for test case; both methods

| Parameter | Value | Units |
|-----------------|--------|-------------------|
| Length | 0.094 | m |
| Average Radius | 0.0052 | m |
| Blood Viscosity | 0.0033 | Pa*s |
| Blood Density | 1057 | kg/m ³ |

6.1 Womersley-like Method

A sample plot (Figure 7) has been generated that shows the transient pressure waves at several points along the vessel. The graphs exhibit a slight pressure lag, which is to be expected for a vessel of this length. A plot of the corresponding volumetric flowrates (Figure 8) is also included.

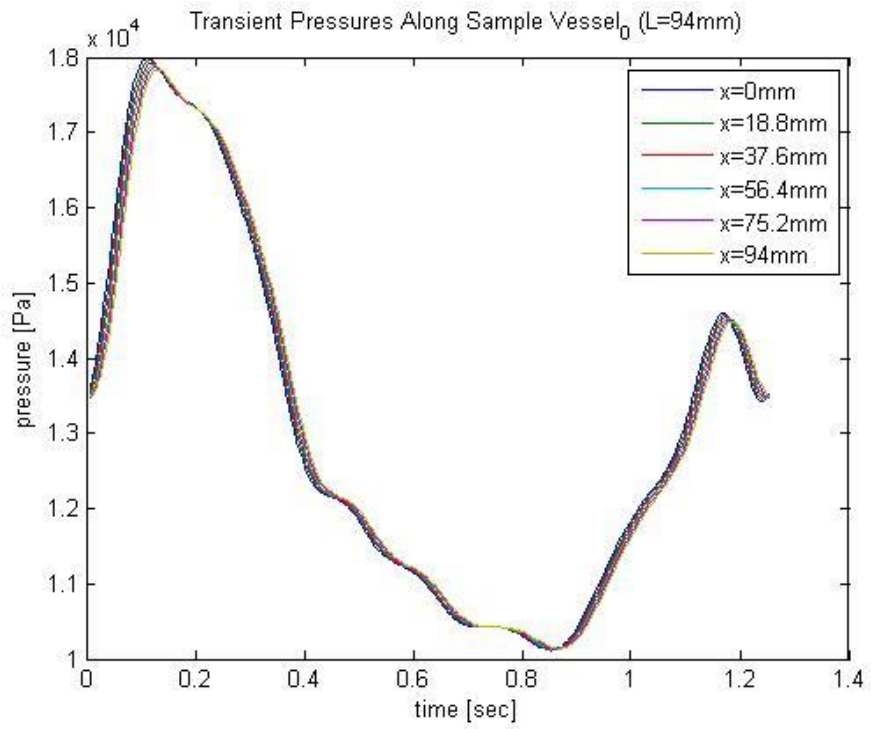


Figure 7: Total transient pressures at various points along test vessel, Womersley method

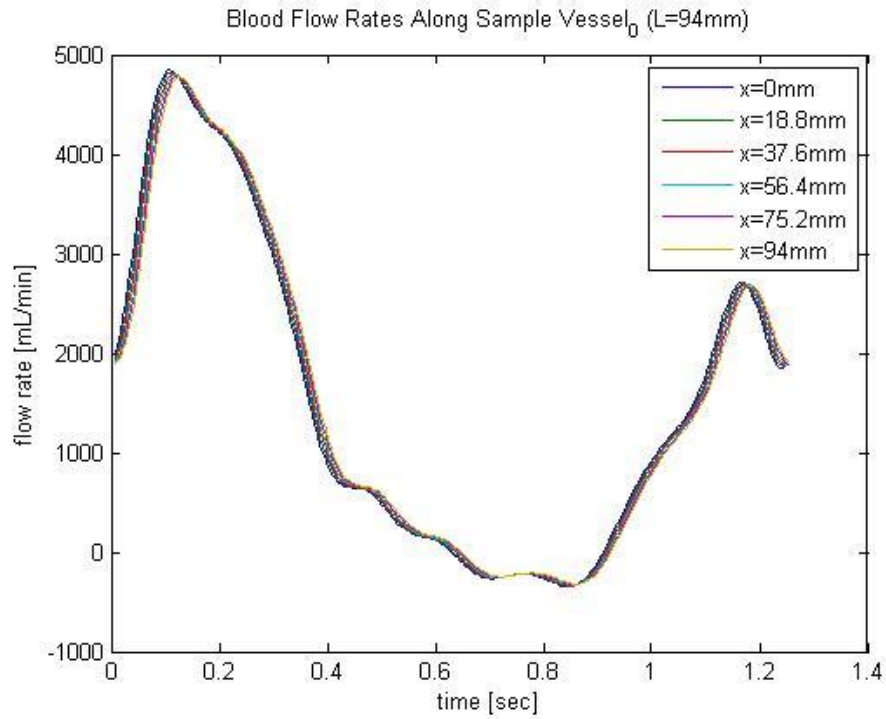


Figure 8: Volumetric flow rates at various points along test vessel, Womersley method

6.2 Numerical Method

6.2.1 Steady State Validation

We must first validate the transient code by running it for $\frac{\partial f}{\partial t} = 0$ and checking

that the result is equal to the steady state solution. The average steady state values from the numerical code are listed in Table 8.

Table 8: Steady state values, numerical code

| Pressure drop (Pa) | Velocity (m/s) | Cross-sectional Area (m ²) |
|--------------------|----------------|--|
| 29 | 0.3067 | 8.253x10 ⁻⁵ |

The values for pressure ,velocity, and area over time and space for constant pressure boundary conditions are shown in Figures 9, 10, and 11, respectively.

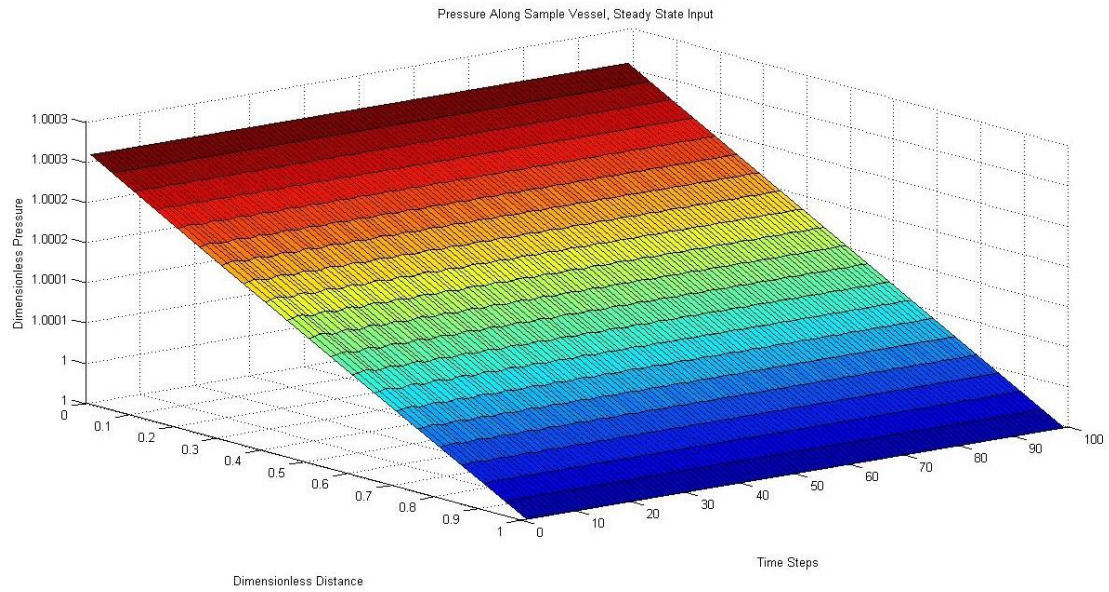


Figure 9: Numerical solution for pressure, steady state boundary conditions

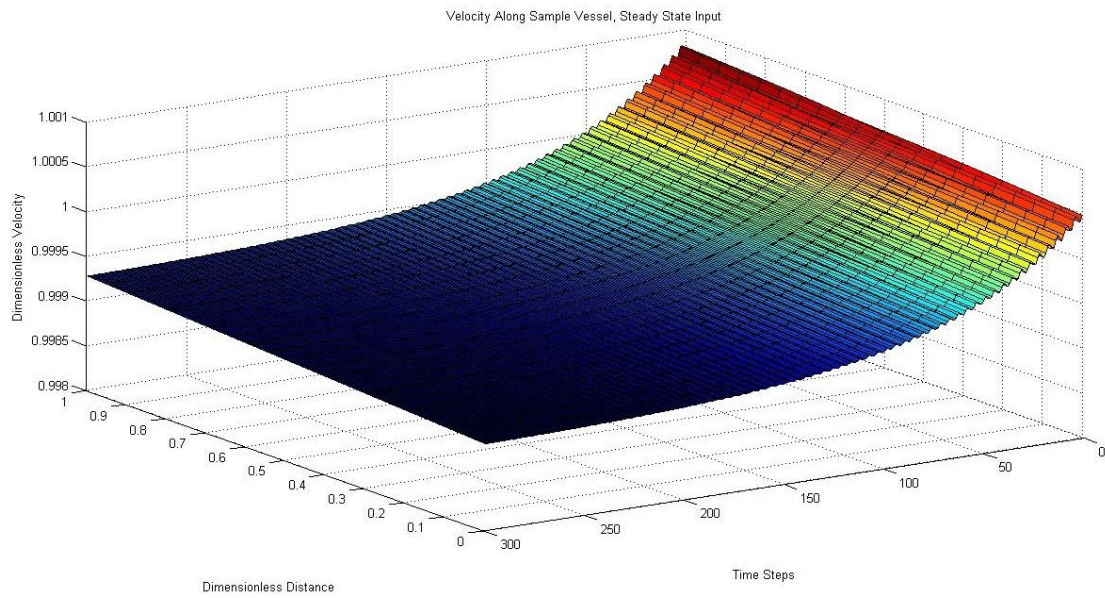


Figure 10: Numerical solution for fluid velocity, steady state boundary conditions

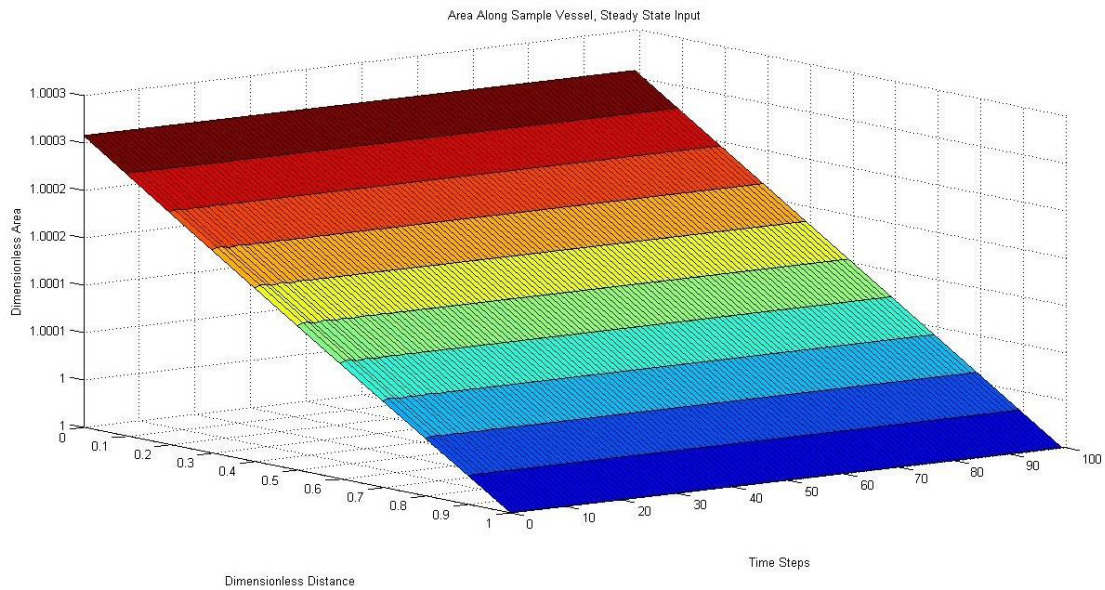


Figure 11: Numerical solution for area, steady state boundary conditions

The results are just as expected. The pressure drops along the vessel equal to the Poiseuille pressure drop used as input. The area drops along the vessel linearly, but only very slightly. The velocity increases very slightly along the length of the vessel. We can see that due to the initial guesses being a little off from the true value, the plots of pressure and velocity start out a bit jagged. They quickly smooth out and converge to the steady state value, however. An interesting result is that the correction via the perturbation expansion causes the numerical steady states to be a small percentage off of the Poiseuille solution. These are precisely the effects we want to capture with this method. Additionally, to see the velocity to converge to the new steady state, we used three times our normal period of the input. This allowed the velocity enough time to flatten out.

6.2.2 Simple Oscillatory Input

We next test the transient code on a simple oscillatory boundary condition before implementing the full time dependent pulse. The same three plots are generated for these new inputs. Additionally, the derivatives of the pressure conditions used for this case are also plotted (these go directly into the \underline{z} vector).

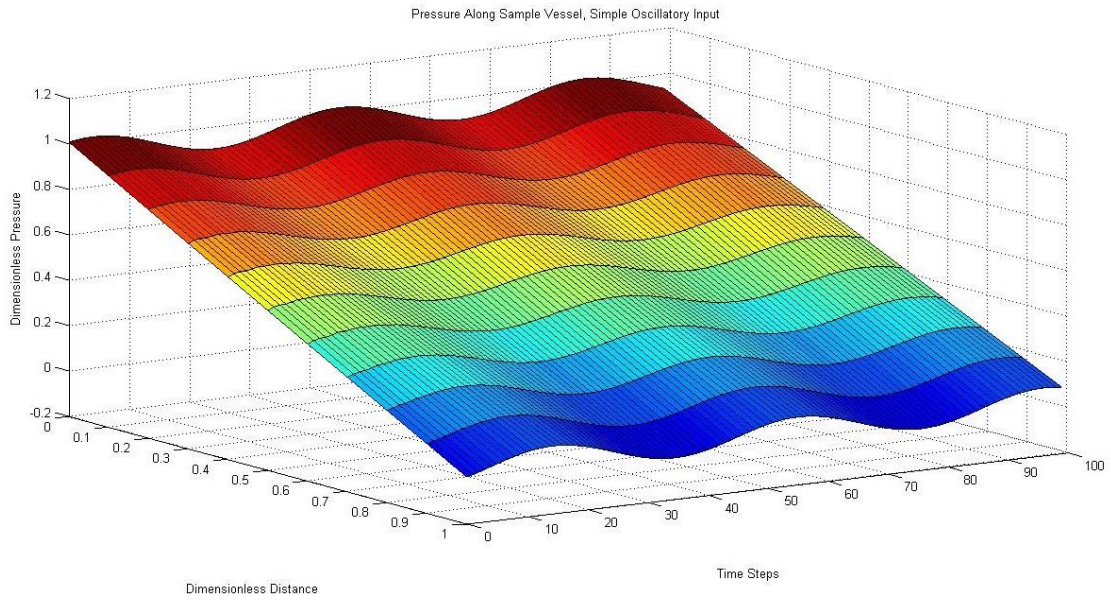


Figure 12: Numerical solution for pressure, oscillatory boundary conditions

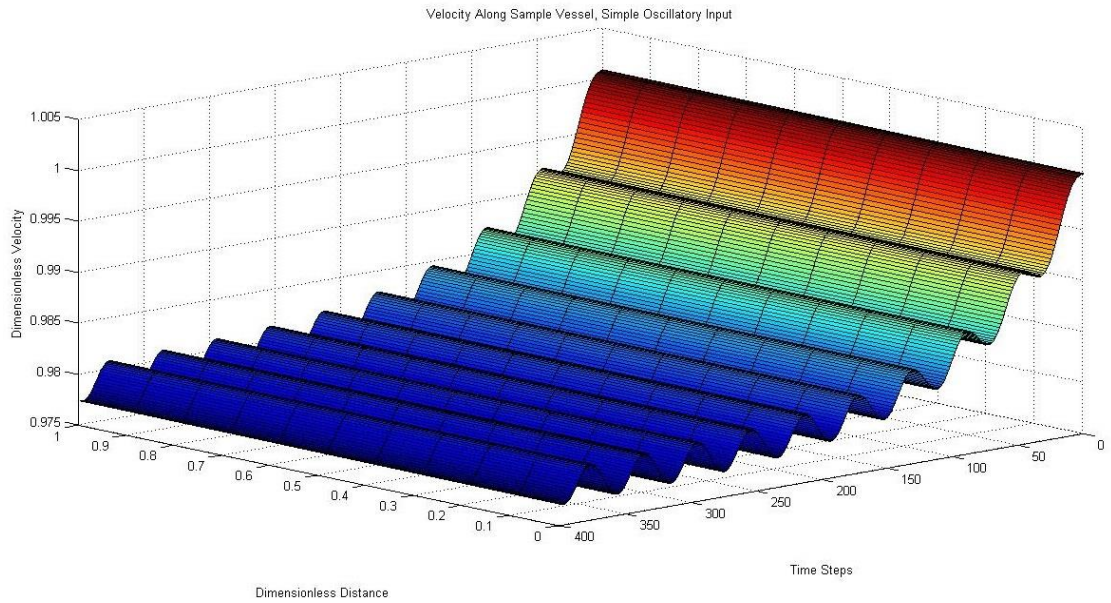


Figure 13: Numerical solution for fluid velocity, oscillatory boundary conditions

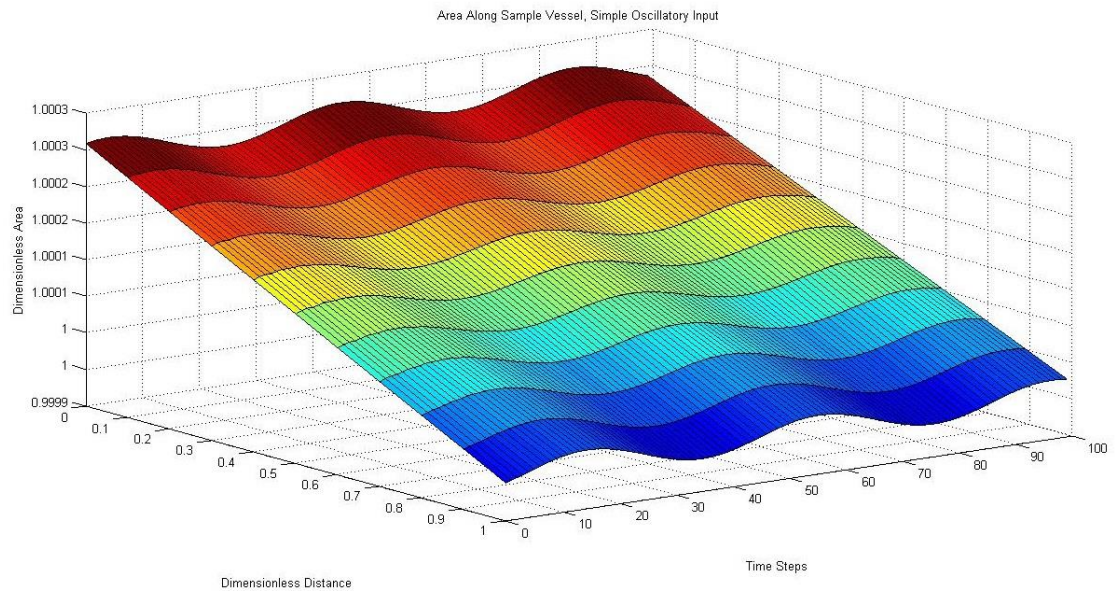


Figure 14: Numerical solution for area, oscillatory boundary conditions

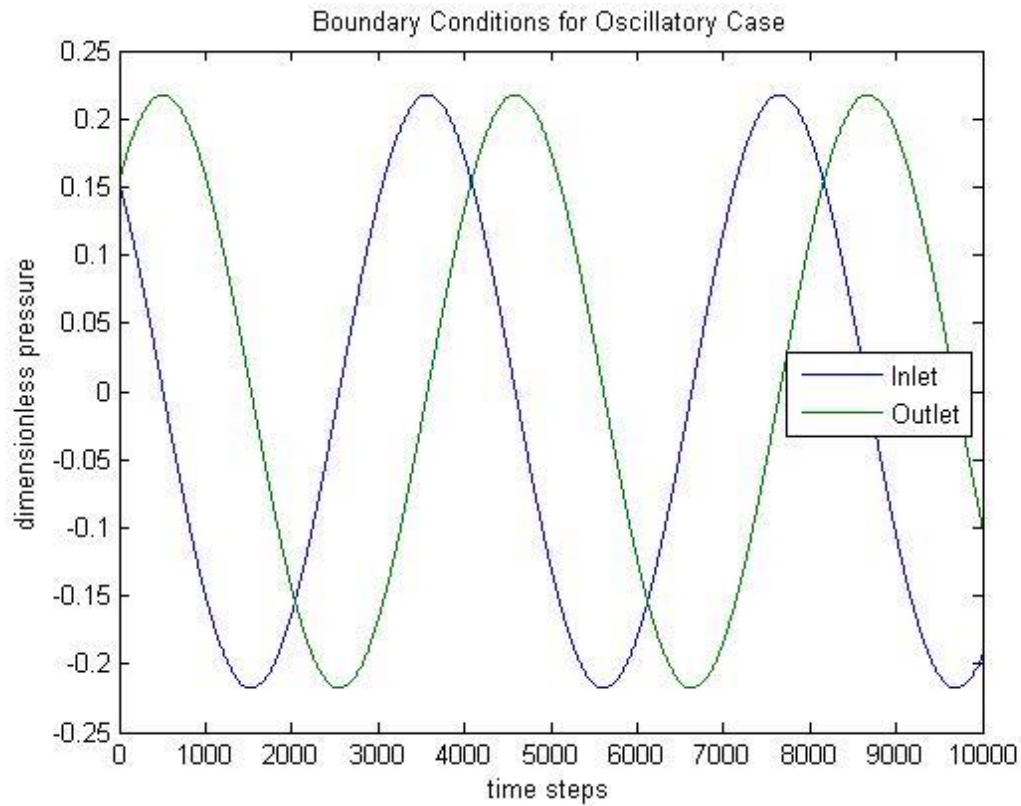


Figure 15: Boundary conditions for \underline{z} vector, oscillatory case

Several facts should be noted about this case. First, the plot for velocity contains four times as many time points as the pressure and area plots. This is because the velocity takes longer to converge to the new steady state, so more time had to be added. Also, the plot of the pressure boundary conditions (Figure 15) is the *derivative* of the actual imposed conditions. This explains why the curves fluctuate around zero.

6.2.3 Full Pulse Solution

We are now prepared to find the solution for the full pulse waveform. Figure 16 shows the pressure across the vessel for the full duration of our sample pulse.

Subsequent periods follow this behavior very closely, so only one period is shown here. The boundary conditions are also plotted in Figure 17. This plot is *not* the derivative; rather these are the actual values versus time. The values of the x -axis are arbitrary; the full period is split into 10,000 evenly spaced time intervals. The values are simply a way to keep track of the pressure wave.

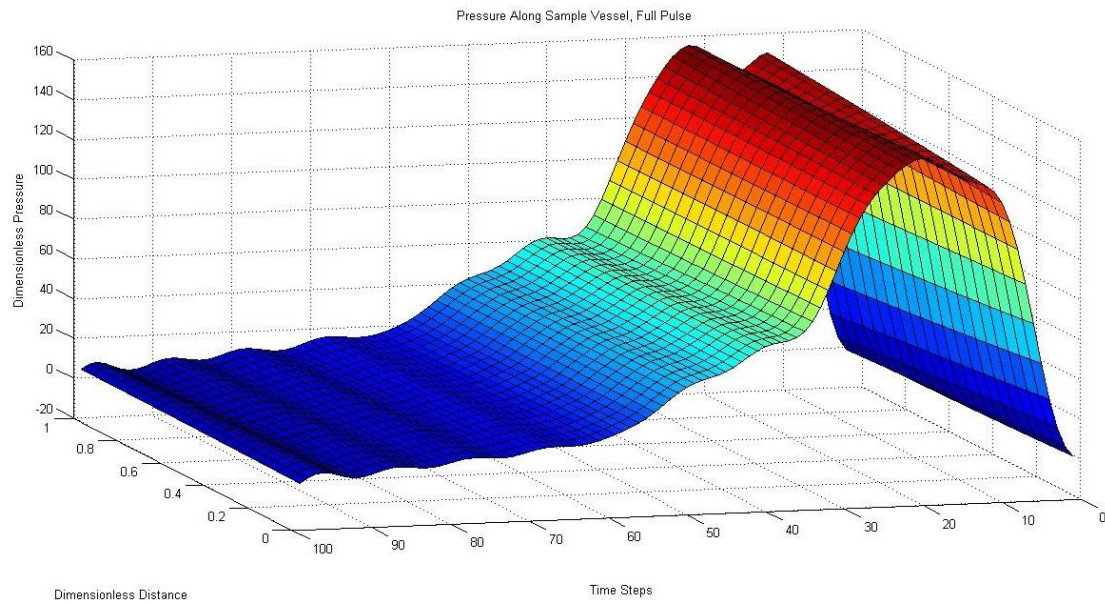


Figure 16: Numerical solution for pressure, full pulse

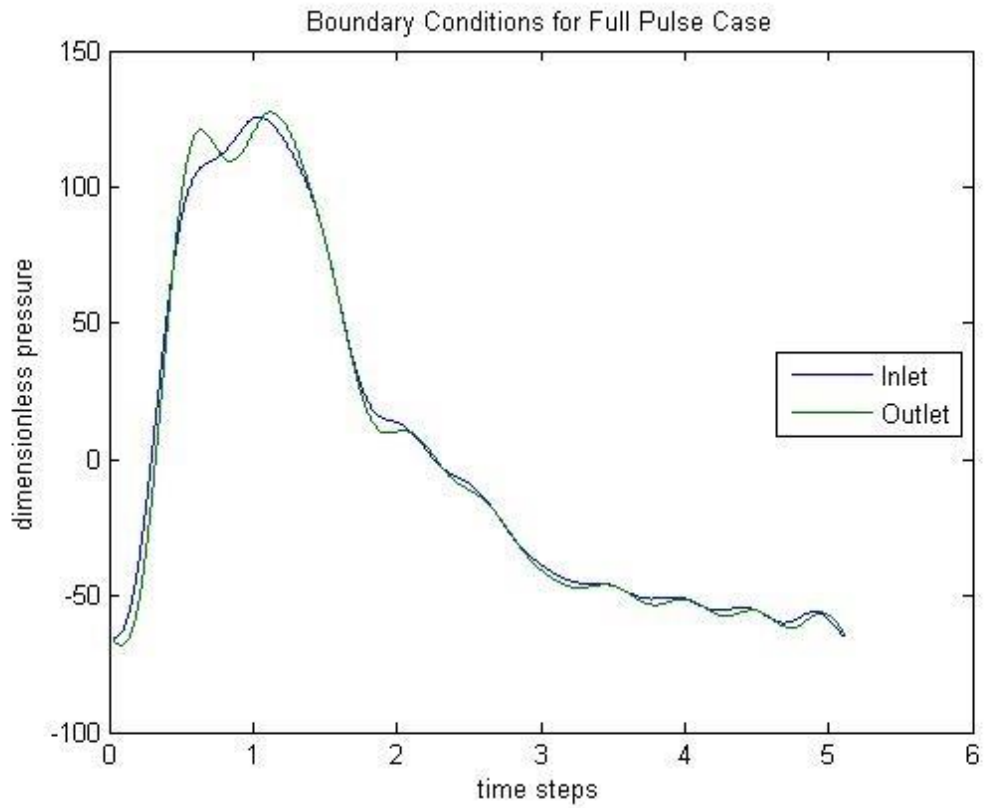


Figure 17: Pressure boundary conditions, full pulse

Figure 18 shows the solution for velocity over the first three periods. It is clear that the velocity has not converged after only three periods, so Figure 19 shows periods 4 through 6, indicating that the maximum converges around a dimensionless velocity value of 1.21.

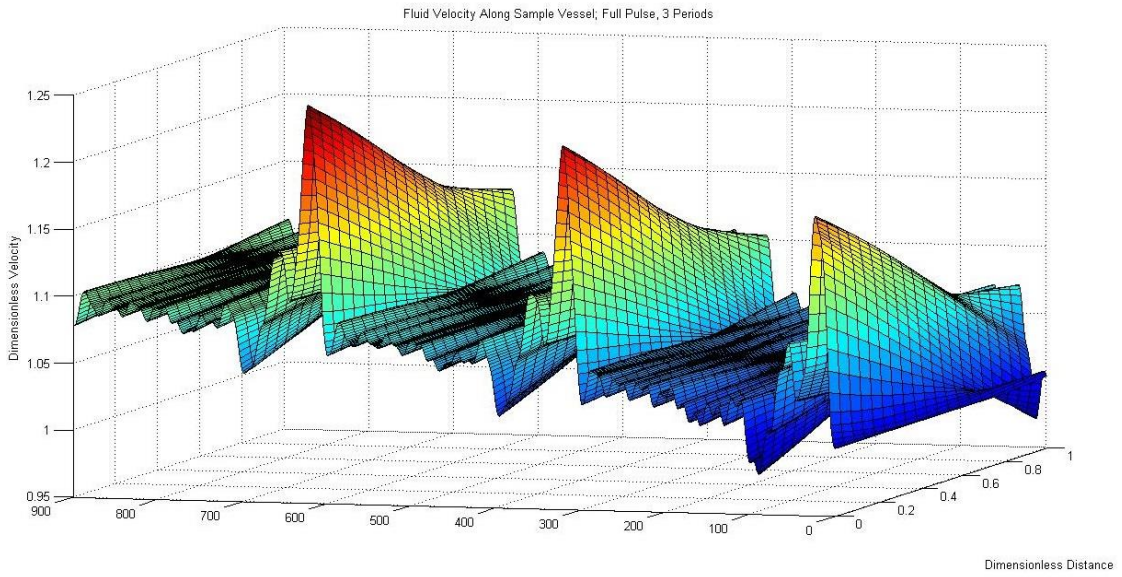


Figure 18: Numerical solution for fluid velocity, first three periods of full pulse

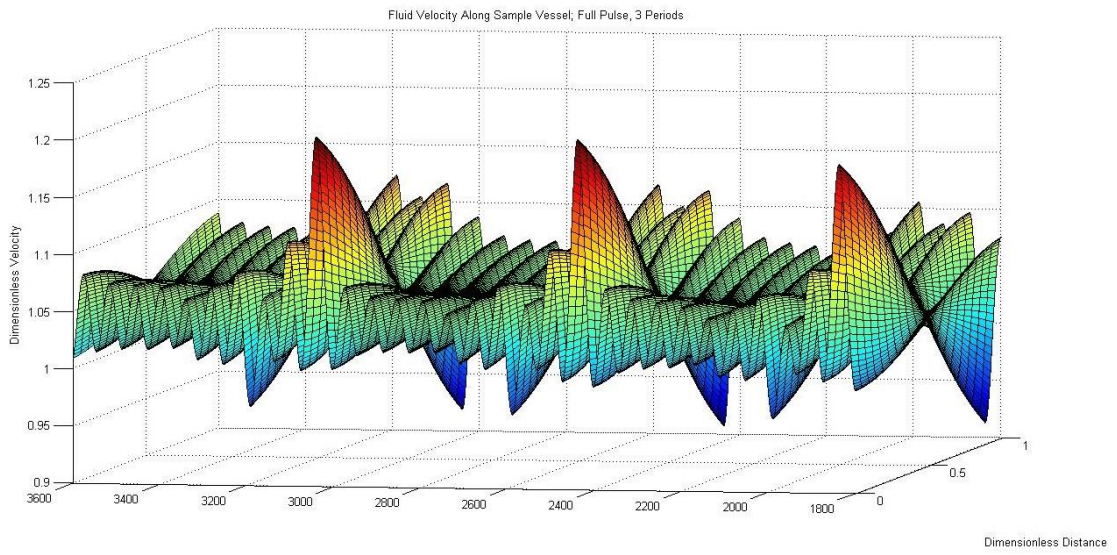


Figure 19: Numerical solution for fluid velocity, periods four through six of full pulse

Finally, Figure 20 shows the model solution for area, which matches the pressure behavior very closely.

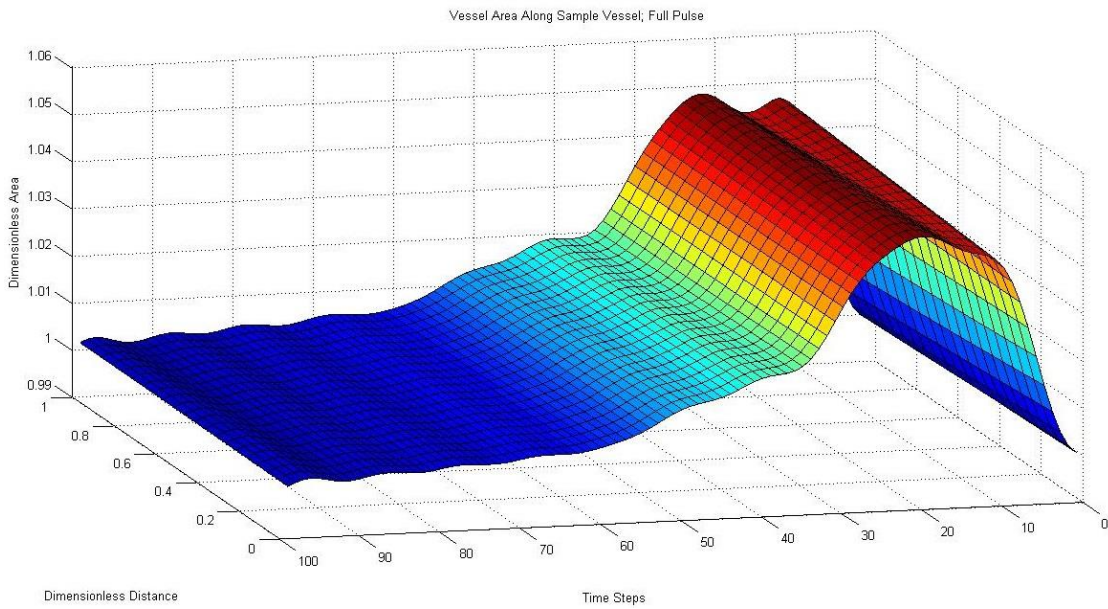


Figure 20: Numerical solution for area, full pulse

6.3 Model Comparison

The relevant steady state results are tabulated in Table 9.

Table 9: Model results obtained using both methods, steady state

| Variable | Original | Numerical | Units |
|---------------|----------|-----------|-------|
| Pressure Drop | 29.00 | 29.00 | Pa |
| Flow Rate | 1.5188 | 1.5196 | L/min |

The old technique results in a solution for flow rate that is only 0.05% smaller than the numerical solution. The pressure conditions were imposed, so these results are exactly the same.

We next compare the transient solutions. The following two figures plot volumetric flowrate versus time at the center point and two end points using the Womersley-like and numerical methods, respectively. The differences in the y-axis should be noted when comparing the two. Additionally, the Womersley solution is necessarily periodic, but we include several periods of the numerical solution to show convergence.

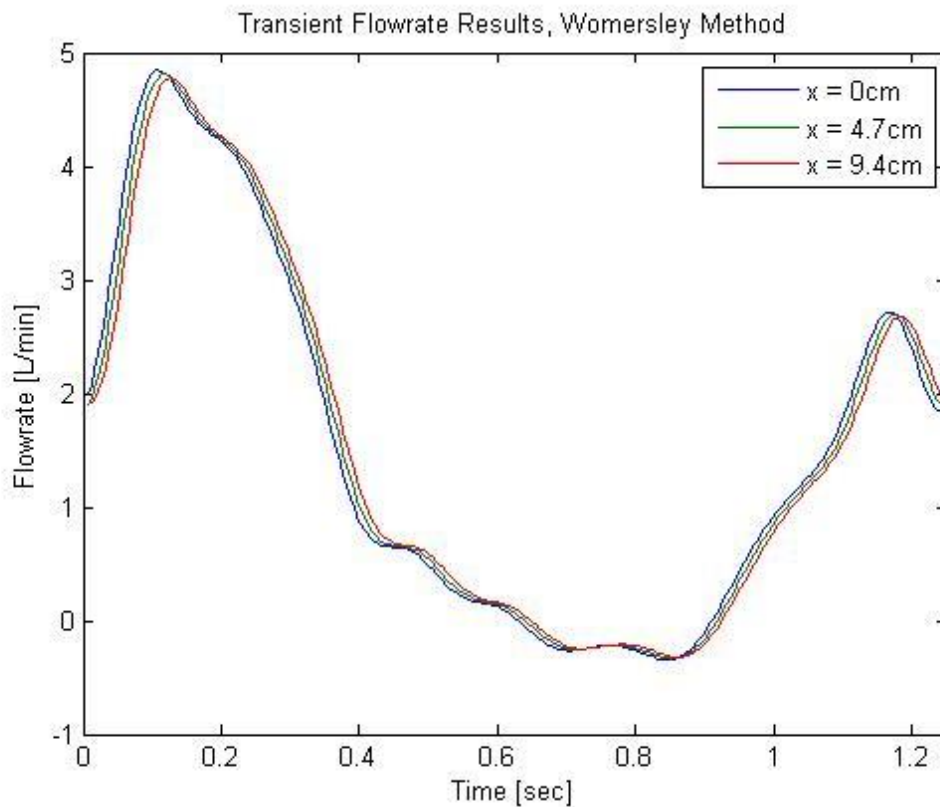


Figure 21: Transient flowrate results, Womersley method

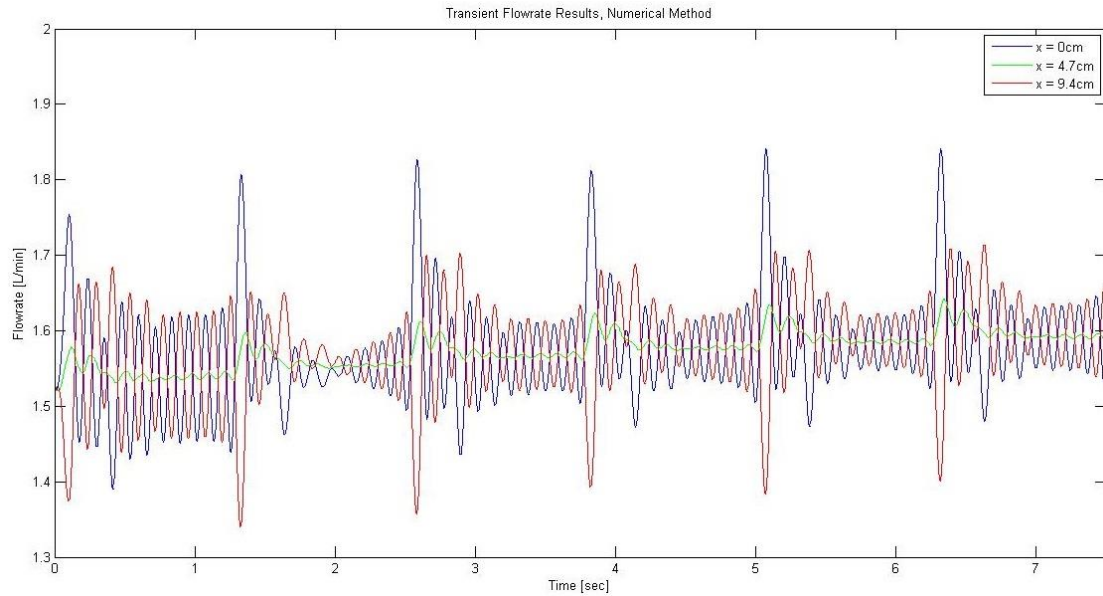


Figure 22: Transient flowrate results, numerical method

The average transient flowrate values for both methods are found in Table 10.

Table 10: Average flowrate values, both methods

| Method | Avg. Flowrate (L/min) | % difference |
|-----------|-----------------------|--------------|
| Womersley | 1.5188 | 3.7 |
| Numerical | 1.5750 | |

6.3.1 Single Harmonic Comparison

The drastic differences between the two flowrate solutions could potentially be accounted for by the incorporation of many harmonics in the pulse waves. We now conduct a similar test, but with only a single harmonic of the transient system. This example should show more clearly any differences between the two methods. Indeed, in Figures 23 and 24 we can see the smooth curve of the Womersley solution versus

the oscillatory solution of the numerical method, respectively. These results confirm the different behaviors of the two methods as seen above.

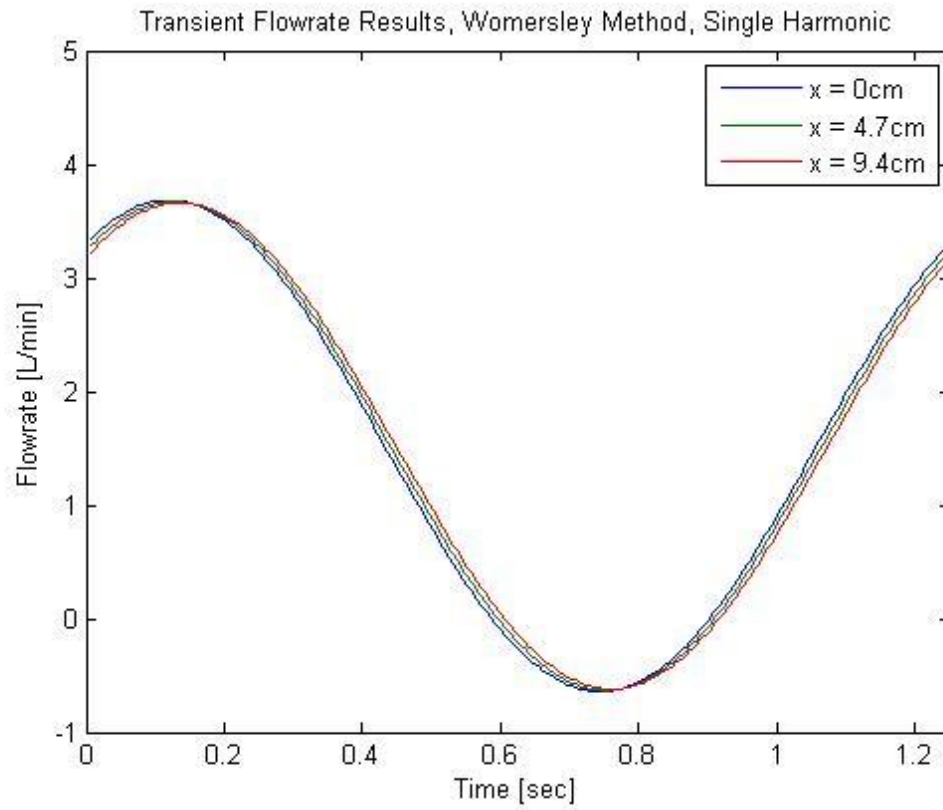


Figure 23: Single harmonic solution of the Womersley method, full pulse.

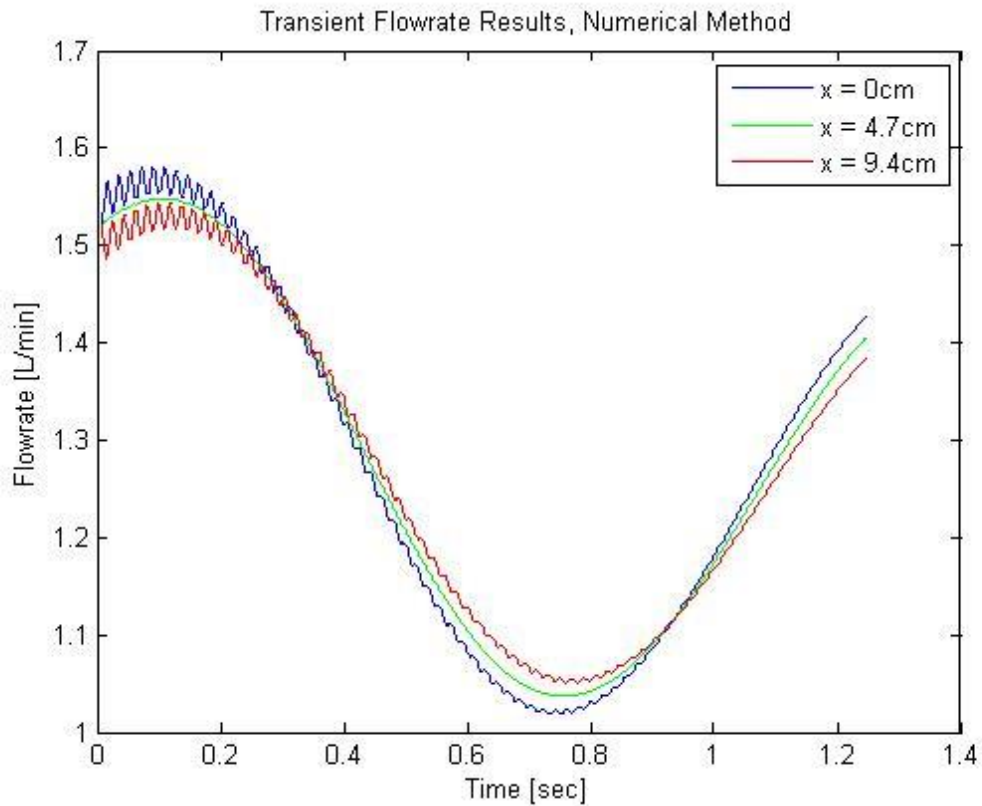


Figure 24: Single harmonic solution of the numerical method, full pulse.

Lastly, we run a simulation to see if these differences are due to inertial effects or some other factor. Inertial effects can be significant in large arteries, such as our test vessel, where the Reynolds number is ≥ 1 . In smaller vessels, where the Reynolds number is ≤ 0.1 , inertial effects are often neglected. We now reduce both the length and radius of the test vessel by an order of magnitude, thus reducing the Reynolds number by a factor of 100. The results for three periods are shown below for both methods. The jagged areas in the numerical plot arise because the pressure signal is not perfectly periodic; however, it quickly converges back to the correct solution.

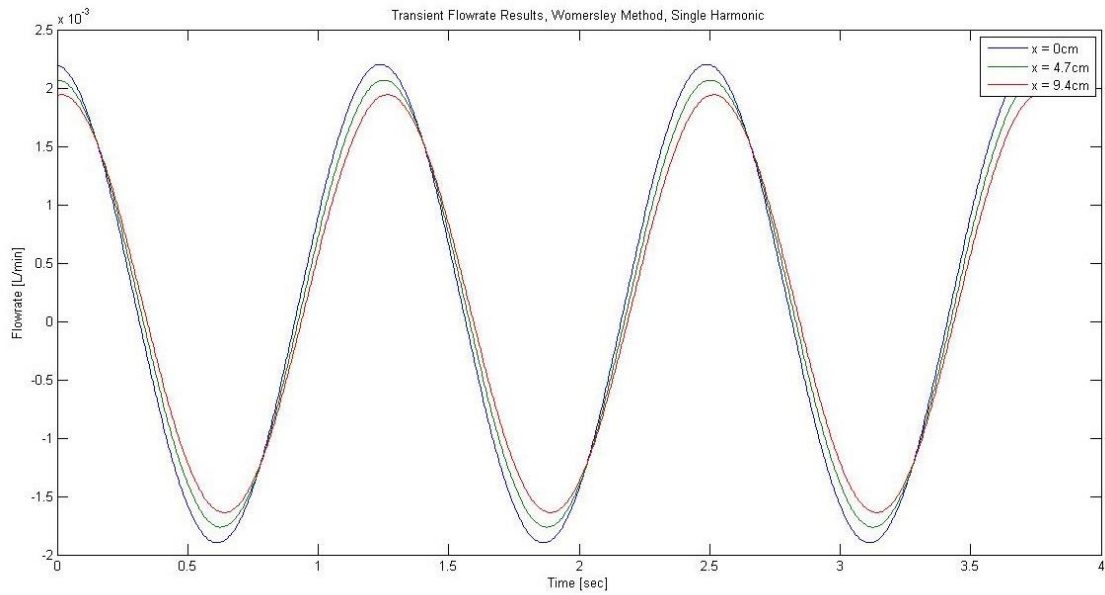


Figure 25: Womersley solution for the low Reynolds number case, three periods

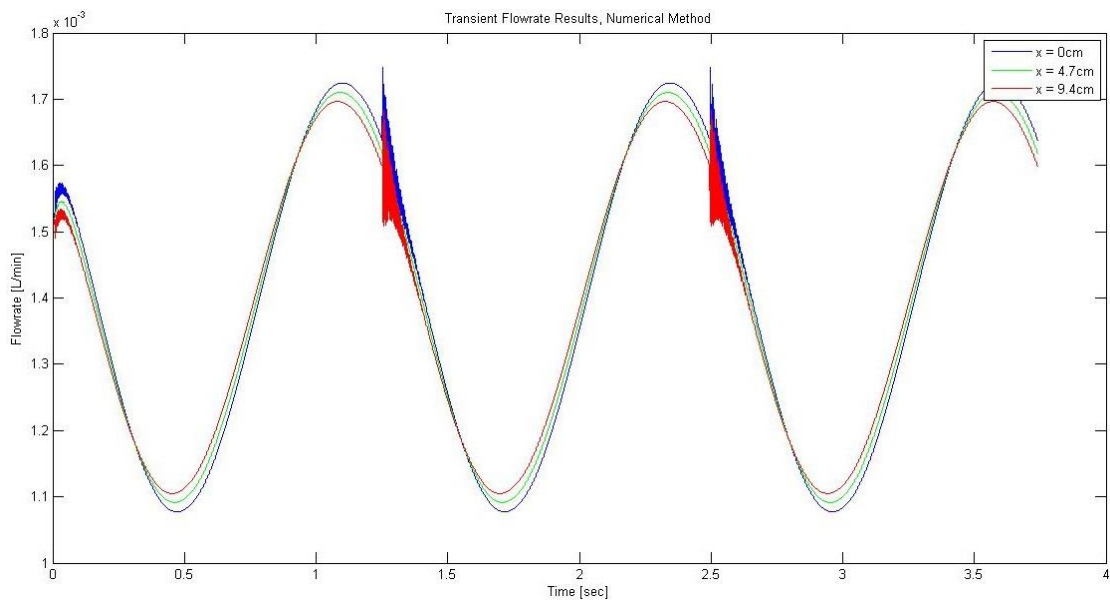


Figure 26: Numerical solution for the low Reynolds number case, three periods

6.4 Discussion

It is obvious that the numerical method we employ is picking up effects not captured by the original model. Specifically, these effects seem to be inertial in nature. This is evidenced by the fact that we see large deviations for a large Reynolds number. However, once the Reynolds number is reduced by multiple orders of magnitude, the two methods show good agreement in both magnitude and phase. The differences in the former case are present even though the same input information is being used to generate the solutions.

It is also evident that oscillations are very scarce in Figure 26. This fact indicates that flowrates at low Reynolds numbers may not require such a fine mesh to converge.

While the Womersley method lacks incorporation of (apparently very important) inertial effects, the numerical method does not account for radial changes, which are included in the Womersley case by way of Bessel functions. Thus, although we have bolstered the argument that the approximations used in many linearization techniques over-simplify the blood flow problem, more analysis should be done to assess the accuracy of this numerical method as well.

Chapter 7

CONCLUSIONS AND RECOMMENDATIONS FOR FUTURE WORK

7.1 Conclusions

The numerous additions and updates to our blood flow model have significantly improved its potential for application in fields such as diagnostics and research. It can successfully read in information on a single vessel or an entire network, generate trustworthy results, and display them in a user friendly fashion. It can handle cases involving recirculation of blood, which is present in areas of interest such as the brain. We have also implemented an entirely new method of solution, which can be used to validate our previous model.

The tests we have run indicate that at low Reynolds numbers, the two methods agree well. However, at high Reynolds numbers there did indeed exist underlying effects, specifically inertial effects, that the original model was unable to capture. These effects will be better characterized as more vessels and small networks are analyzed.

7.2 Recommendations for Future Work

We now have the capability of running our model on any vessel, or network of vessels, that we so choose. Thus, the two methods should be compared for different vessel sizes and rheological parameters, as well as at vessel bifurcations. Once a vast amount of data has been obtained, we can attempt to identify exactly where the assumptions of the original model break down and inertial effects gain substantial

importance. Similarly, we can identify where the numerical method needs to incorporate radial variations. This distinction is especially important in the cerebral arteries, where blood is able to recirculate around the Circle of Willis. We desire to better understand the flow patterns that occur here, so the CoW should definitely be the focus of further simulations.

REFERENCES

- Alastruey, J., K. H. Parker, J. Peiró, S. M. Byrd, and S. J. Sherwin. "Modelling the Circle of Willis to Assess the Effects of Anatomical Variations and Occlusions on Cerebral Flows." *Journal of Biomechanics* 40.8 (2007): 1794-805.
- American Heart Association, Heart Disease and Stroke Statistics (2014 Update), <http://circ.ahajournals.org/content/125/1/e2.full>
- Apostolidis, Alex J. and Antony N. Beris. "Modeling of the Blood Rheology in Steady-state Shear Flows." *Journal of Rheology* 58 (2014): 607-633.
- Barbee, James Henry. "The Flow of Human Blood Through Capillary Tubes with the Inside Diameters Between 8.7 and 221 Microns." Diss. California Institute of Technology, 1971.
- Batzel, Jerry J., Franz Kappel, Daniel Schneditz, and Hien T. Tran. "Cardiovascular and Respiratory Systems." (2007)
- Bevan, R. L. T., P. Nithiarasu, R. Van Loon, I. Sazonov, H. Luckraz, and A. Garnham. "Application of a Locally Conservative Galerkin (LCG) Method for Modelling Blood Flow through a Patient-specific Carotid Bifurcation." *International Journal for Numerical Methods in Fluids Int. J. Numer. Meth. Fluids* 64.10-12 (2010): 1274-295.
- Bird, R. Byron. *Dynamics of Polymeric Liquids*. 2nd ed. Vol. 1. New York: Wiley, 1987.
- Boutsianis, Evangelos, Sumeet Gupta, Kevin Boomsma, and Dimos Poulikakos. "Boundary Conditions by Schwarz-Christoffel Mapping in Anatomically Accurate Hemodynamics." *Annals of Biomedical Engineering Ann Biomed Eng* 36.12 (2008): 2068-084.
- Brinkman, A. M., P. B. Baker, W. P. Newman, R. Vigorito, and M. H. Friedman. "Variability of Human Coronary Artery Geometry: An Angiographic Study of the Left Anterior Descending Arteries of 30 Autopsy Hearts." *Annals of Biomedical Engineering Ann Biomed Eng* 22.1 (1994): 34-44.

- Bureau, M., J. C. Healy, D. Bourgoïn, and M. Joly. "Etude Expérimentale *in vitro* Du Comportement Rhéologique Du Sang En Régime Transitoire à Faible Vitesse De Cisaillement." *Rheologica Acta Rheol Acta* 17.6 (1978): 612-25.
- Chandran, K. B., Stanley E. Rittgers, and A. P. Yoganathan. *Biofluid Mechanics: The Human Circulation*. Boca Raton: CRC/Taylor & Francis, 2007.
- Changizi, Mark A., and Christopher Cherniak. "Modeling the Large-scale Geometry of Human Coronary Arteries." *Can. J. Physiol. Pharmacol. Canadian Journal of Physiology and Pharmacology* 78.8 (2000): 603-11.
- Cheer, A. Y., and Van Dam C. P. *Fluid Dynamics in Biology*. Providence: American Mathematical Society, 1993.
- Cheer, A. Y., and Van Dam C. P. *Fluid Dynamics in Biology: Proceedings of an AMS-IMS-SIAM Joint Summer Research Conference Held July 6-12, 1991 with Support from the National Science Foundation and NASA Headquarters*. Providence, RI: American Mathematical Society, 1993.
- Clipp, R. B., and B. N. Steele. "Impedance Boundary Conditions for the Pulmonary Vasculature Including the Effects of Geometry, Compliance, and Respiration." *IEEE Transactions on Biomedical Engineering IEEE Trans. Biomed. Eng.* 56.3 (2009): 862-70.
- Drzewiecki, Gary M., and John Li. *Analysis and Assessment of Cardiovascular Function*. New York: Springer-Verlag, 1998.
- Duan, B., and M. Zamir. "Viscous Damping in One-dimensional Wave Transmission." *The Journal of the Acoustical Society of America J. Acoust. Soc. Am.* 92.6 (1992): 3358.
- Fahy, Paul, Patrick Delassus, Peter Mccarthy, Sheriff Sultan, Niamh Hynes, and Liam Morris. "An In Vitro Assessment of the Cerebral Hemodynamics Through Three Patient Specific Circle of Willis Geometries." *Journal of Biomechanical Engineering J Biomech Eng* 136.1 (2013): 011007.
- Formaggia, Luca, Daniele Lamponi, and Alfio Quarteroni. "One-dimensional Models for Blood Flow in Arteries." *Journal of Engineering Mathematics* 47.3/4 (2003): 251-76.
- Formaggia, L., Alfio Quarteroni, and A. Veneziani. *Cardiovascular Mathematics: Modeling and Simulation of the Circulatory System*. Vol. 1. Milan: Springer, 2009.

- Frauenfelder, Thomas, Evangelos Boutsianis, Thomas Schertler, Lars Husmann, Sebastian Leschka, Dimos Poulikakos, Borut Marincek, and Hatem Alkadhi. "In-vivo Flow Simulation in Coronary Arteries Based on Computed Tomography Datasets: Feasibility and Initial Results." *Eur Radiol European Radiology* 17.5 (2006): 1291-300.
- Friedman, M. "Relationship between the Geometry and Quantitative Morphology of the Left Anterior Descending Coronary Artery." *Atherosclerosis* 125.2 (1996): 183-92.
- Fung, Y. C. *Biomechanics*. New York: Springer, 1997.
- Galdi, Giovanni P. *Hemodynamical Flows: Modeling, Analysis, and Simulation*. Basel: Birkhäuser 2008.
- Gay, Mickaël, and Lucy T. Zhang. "Numerical Studies of Blood Flow in Healthy, Stenosed, and Stented Carotid Arteries." *International Journal for Numerical Methods in Fluids Int. J. Numer. Meth. Fluids* 61.4 (2009): 453-72.
- Gijsen, F.j.h., E. Allanic, F.n. Van De Vosse, and J.d. Janssen. "The Influence of the Non-Newtonian Properties of Blood on the Flow in Large Arteries: Unsteady Flow in a 90° Curved Tube." *Journal of Biomechanics* 32.7 (1999): 705-13.
- Gohil, Trushar, Robert H. P. Mcgregor, Dominik Szczerba, Kathrin Burckhardt, Krishnamurthy Muralidhar, and Gábor Székely. "Simulation of Oscillatory Flow in an Aortic Bifurcation Using FVM and FEM: A Comparative Study of Implementation Strategies." *International Journal for Numerical Methods in Fluids Int. J. Numer. Meth. Fluids* 66.8 (2010): 1037-067.
- Goldsmith, Harry L., Giles R. Cokelet, and Peter Gaehtgens. "Robin Fåhræus: Evolution of his Concepts in Cardiovascular Physiology." *Journal of American Physiology* (1989): H1005-H1014
- Grinberg, Leopold, and George Em Karniadakis. "Outflow Boundary Conditions for Arterial Networks with Multiple Outlets." *Annals of Biomedical Engineering Ann Biomed Eng* 36.9 (2008): 1496-514.
- Hutchins, G. M., M. M. Miner, and J. K. Boitnott. "Vessel Caliber and Branch-angle of Human Coronary Artery Branch-points." *Circulation Research* 38.6 (1976): 572-76.

- Johnson, David A., Justin R. Spaeth, William C. Rose, Ulhas P. Naik, and Antony N. Beris. "An Impedance Model for Blood Flow in the Human Arterial System. Part I: Model Development and MATLAB Implementation." *Computers & Chemical Engineering* 35.7 (2011): 1304-316.
- Johnson, David A., William C. Rose, Jonathan W. Edwards, Ulhas P. Naik, and Antony N. Beris. "Application of 1D Blood Flow Models of the Human Arterial Network to Differential Pressure Predictions." *Journal of Biomechanics* 44.5 (2011): 869-76.
- Kamenskiy, Alexey V., Jason N. Mactaggart, Iraklis I. Pipinos, Jai Bikhchandani, and Yuris A. Dzenis. "Three-Dimensional Geometry of the Human Carotid Artery." *Journal of Biomechanical Engineering J. Biomech. Eng.* 134.6 (2012): 064502.
- Kato, Masaya, Keigo Dote, Koichi Nakaoka, Kenji Goto, Hiroaki Takemoto, and Seiji Habara. "Clinical Implication of Carotid Artery Remodeling in Acute Coronary Syndrome: Ultrasonographic Assessments of Positive Remodeling." *Journal of the American College of Cardiology* 41.6 (2003): 287.
- Korteweg, D. J. "Ueber Die Fortpflanzungsgeschwindigkeit Des Schalles in Elastischen Röhren." *Ann. Phys. Chem. Annalen Der Physik Und Chemie* 241.12 (1878): 525-42.
- Lee, S.-W., and D.a. Steinman. "On the Relative Importance of Rheology for Image-based CFD Models of the Carotid Bifurcation." *Journal of Biomechanics* 39 (2006)
- Li JK-J, *The Arterial Circulation: Physical Principles and Clinical Applications*. Humana Press: Totowa,NJ. 2000.
- Li, John K-J. *Dynamics of the Vascular System*. River Edge, NJ: World Scientific, 2004
- Merrill, Edward W., Chon S. Cheng, and Gerard A. Pelletier. "Yield Stress of Normal Human Blood as a Function of Endogenous Fibrinogen." *Journal of Applied Physiology* 26.1 (1969): 1-3.
- Mill, C. C. *Rheology of Disperse Systems*. New York: Symposium Publications Division, Pergamon, 1959.

- Milner, Jaques S., Jennifer A. Moore, Brian K. Rutt, and David A. Steinman. "Hemodynamics of Human Carotid Artery Bifurcations: Computational Studies with Models Reconstructed from Magnetic Resonance Imaging of Normal Subjects." *Journal of Vascular Surgery* 28.1 (1998): 143-56.
- Moens, A. *Die Pulscurve*. Leiden: E.J. Brill, 1878.
- Moore, S., T. David, J.G. Chase, J. Arnold, and J. Fink. "3D Models of Blood Flow in the Cerebral Vasculature." *Journal of Biomechanics* 39.8 (2006): 1454-463.
- Morbiducci, Umberto, Diego Gallo, Diana Massai, Raffaele Ponzini, Marco A. Deriu, Luca Antiga, Alberto Redaelli, and Franco M. Montevvecchi. "On the Importance of Blood Rheology for Bulk Flow in Hemodynamic Models of the Carotid Bifurcation." *Journal of Biomechanics* 44.13 (2011): 2427-438.
- Nguyen, Kien T., Christopher D. Clark, Thomas J. Chancellor, and Dimitrios V. Papavassiliou. "Carotid Geometry Effects on Blood Flow and on Risk for Vascular Disease." *Journal of Biomechanics* 41.1 (2008): 11-19.
- Nichols, Wilmer W., and Michael F. O'Rourke. *MacDonald's Blood Flow in Arteries: Theoretical, Experimental and Clinical Principles*. London: Arnold, 1998.
- Nissen, S. E., J. C. Gurley, C. L. Grines, D. C. Booth, R. McClure, M. Berk, C. Fischer, and A. N. Demaria. "Intravascular Ultrasound Assessment of Lumen Size and Wall Morphology in Normal Subjects and Patients with Coronary Artery Disease." *Circulation* 84.3 (1991): 1087-099.
- Olufsen, M. S. "Modeling Flow and Pressure in the Systemic Arteries." In: Ottesen, J. T., Olufsen, M. S., & Larsen, J. K. (Eds.) *Applied Mathematical Models in Human Physiology*, Philadelphia: SIAM, 2004.
- Passerini, Tiziano, Mariarita De Luca, Luca Formaggia, Alfio Quarteroni, and Alessandro Veneziani. "A 3D/1D Geometrical Multiscale Model of Cerebral Vasculature." *Journal of Engineering Mathematics J Eng Math* 64.4 (2009): 319-30.
- Peattie, Robert, Robert Fisher, Joseph Bronzino, and Donald Peterson. "Transport Phenomena in Biomedical Engineering." (2012)
- Pedley, T. J. *The Fluid Mechanics of Large Blood Vessels*. Cambridge: CambridgeUP, 1980.

- Perktold, K., M. Hofer, G. Rappitsch, M. Loew, B.d Kuban, and M.h Friedman. "Validated Computation of Physiologic Flow in a Realistic Coronary Artery Branch." *Journal of Biomechanics* 31.3 (1997): 217-28.
- Pries, A. R., T. W. Secomb, P. Gaetgens, and J. F. Gross. "Blood Flow in Microvascular Networks. Experiments and Simulation." *Circulation Research* 67.4 (1990): 826-34.
- Pries, Axel R., and Timothy W. Secomb. "Blood Flow in Microvascular Networks." *Comprehensive Physiology* (2011)
- Quarteroni, Alfio, and Alessandro Veneziani. "Analysis of a Geometrical Multiscale Model Based on the Coupling of ODE and PDE for Blood Flow Simulations." *Multiscale Modeling & Simulation Multiscale Model. Simul.* 1.2 (2003): 173-95.
- Ramaswamy, S. D., S. C. Vigmostad, A. Wahle, Y. -G. Lai, M. E. Olszewski, K. C. Braddy, T. M. H. Brennan, J. D. Rossen, M. Sonka, and K. B. Chandran. "Fluid Dynamic Analysis in a Human Left Anterior Descending Coronary Artery with Arterial Motion." *Annals of Biomedical Engineering Ann Biomed Eng* 32.12 (2004): 1628-641.
- Reymond, P., F. Merenda, F. Perren, D. Rufenacht, and N. Stergiopoulos. "Validation of a One-dimensional Model of the Systemic Arterial Tree." *AJP: Heart and Circulatory Physiology* 297.1 (2009): H208-222.
- Reymond, Philippe, Fabienne Perren, François Lazeyras, and Nikos Stergiopoulos. "Patient-specific Mean Pressure Drop in the Systemic Arterial Tree, a Comparison between 1-D and 3-D Models." *Journal of Biomechanics* 45.15 (2012): 2499-505.
- Rindt, C. C. M., and A. A. V. Steenhoven. "Unsteady Flow in a Rigid 3-D Model of the Carotid Artery Bifurcation." *Journal of Biomechanical Engineering J. Biomech. Eng.* 118.1 (1996): 90.
- Seo, Taewon. "Numerical Simulations of Blood Flow in Arterial Bifurcation Models." *Korea-Australia Rheology Journal Korea-Aust. Rheol. J.* 25.3 (2013): 153-61.
- Seron, Francisco J., Elsa Garcia, and Jorge Del Pico. "MOTRICO Project – Geometric Construction and Mesh Generation of Blood Vessels by Means of the Fusion of Angiograms and IVUS." *Pattern Recognition and Image Analysis Lecture Notes in Computer Science* (2003): 951-61.

- Seshadri, V., R.M. Hochmuth, P.A. Croce, and S.P. Suter. "Capillary Blood Flow." *Microvascular Research* 2.4 (1970): 434-42.
- Spilker, Ryan L., Jeffrey A. Feinstein, David W. Parker, V. Mohan Reddy, and Charles A. Taylor. "Morphometry-Based Impedance Boundary Conditions for Patient-Specific Modeling of Blood Flow in Pulmonary Arteries." *Annals of Biomedical Engineering Ann Biomed Eng* 35.4 (2007): 546-59.
- Steinman, David A., Jonathan B. Thomas, Hanif M. Ladak, Jaques S. Milner, Brian K. Rutt, and J. David Spence. "Reconstruction of Carotid Bifurcation Hemodynamics and Wall Thickness Using Computational Fluid Dynamics and MRI." *Magnetic Resonance in Medicine Magn. Reson. Med.* 47.1 (2001): 149-59.
- Taylor, Charles A., Thomas J. R. Hughes, and Christopher K. Zarins. "Finite Element Modeling of Three-Dimensional Pulsatile Flow in the Abdominal Aorta: Relevance to Atherosclerosis." *Annals of Biomedical Engineering* 26.6 (1998): 975-87.
- Torii, Ryo, Nigel B. Wood, Nearchos HadjiIoizou, Andrew W. Dowsey, Andrew R. Wright, Alun D. Hughes, Justin Davies, Darrel P. Francis, Jamil Mayet, Guang-Zhong Yang, Simon A. Mcg. Thom, and X. Yun Xu. "Fluid-structure Interaction Analysis of a Patient-specific Right Coronary Artery with Physiological Velocity and Pressure Waveforms." *Communications in Numerical Methods in Engineering Commun. Numer. Meth. Engng.* 25.5 (2009): 565-80.
- Truskey, G. A., F. Yuan, and D. F. Katz. *Transport Phenomena in Biological Systems*. Upper Saddle River: Prentice Hall, 2004.
- Turitto, Vincent T. *The Measurement of the Transport Kinetics of Platelets in Flowing Blood*. Ann Arbor, MI: U Microfilms, 1982.
- Valencia, Alvaro, Alvaro Zarate, Marcelo Galvez, and Lautaro Badilla. "Non-Newtonian Blood Flow Dynamics in a Right Internal Carotid Artery with a Saccular Aneurysm." *International Journal for Numerical Methods in Fluids Int. J. Numer. Meth. Fluids* 50.6 (2006): 751-64.
- Vosse, Frans N. Van De, and Nikos Stergiopoulos. "Pulse Wave Propagation in the Arterial Tree." *Annu. Rev. Fluid Mech. Annual Review of Fluid Mechanics* 43.1 (2011): 467-99.
- Waite, Lee, and Jerry Michael Fine. *Applied Biofluid Mechanics*. New York: McGraw-Hill, 2007.

- Wake, Amanda K., John N. Oshinski, Allen R. Tannenbaum, and Don P. Giddens. "Choice of In Vivo Versus Idealized Velocity Boundary Conditions Influences Physiologically Relevant Flow Patterns in a Subject-Specific Simulation of Flow in the Human Carotid Bifurcation." *Journal of Biomechanical Engineering J. Biomech. Eng.* 131.2 (2009): 021013.
- Wang, Sheng-Zhang, Jia-Liang Chen, Guang-Hong Ding, Gang Lu, and Xiao-Long Zhang. "Non-newtonian Computational Hemodynamics in Two Patient-specific Cerebral Aneurysms with Daughter Saccules." *Journal of Hydrodynamics, Ser. B* 22.5 (2010): 639-46.
- West, Geoffrey B., James H. Brown, and Brian J. Enquist. "A General Model for the Origin of Allometric Scaling Laws in Biology." *Science* 276.5309 (1997): 122-26.
- West, Geoffrey B. "The Origin of Universal Scaling Laws in Biology." *Physica A Statistical Mechanics and Its Applications* 263.1-4 (1999): 104-13.
- Womersley, J. R. "Method for the Calculation of Velocity, Rate of Flow and Viscous Drag in Arteries When the Pressure Gradient Is Known." *The Journal of Physiology* 127.3 (1955): 553-63.
- Womersley, J. R. "Oscillatory Flow in Arteries: The Constrained Elastic Tube as a Model of Arterial Flow and Pulse Transmission." *Physics in Medicine and Biology Phys. Med. Biol.* 2.2 (1957): 178-87.
- Xu, X. Y., Q. Long, M. W. Collins, M. Bourne, and T. M. Griffith. "Reconstruction of Blood Flow Patterns in Human Arteries." *Proceedings of the Institution of Mechanical Engineers, Part H: Journal of Engineering in Medicine* 213.5 (1999): 411-21.
- Zamir, M. *The Physics of Pulsatile Flow*. New York: AIP, 2000.

Appendix

RECIRCULATION MATLAB CODE

```
% FillenwarthFullModelSolution.m, taken from Main_PressureInput.m
% Calculates Steady State and Transient Pressures and Flows in
Arterial
% Network; Includes Changes in Viscosity, Wall Stress Effects, and
Tapering
% Vessels; Input pressure location is specified by user (inart)

% Revised code by John Fillenwarth with Prof. Antony Beris

% Necessary files:
%   Text files:
%       p2dec.txt (or similar file with heartbeat pressure info)
%   Data files:
%       vessel_data.mat
%       connectivity_data_uptodate.mat
%   Function files:
%       steadyiterate_P_density_SS_new.m
%       aortapressure_density_SS_new.m
% Additional files (currently commented out):
%   vesselPressure_compute_vs_Time.m (P vs. t in main arteries)
%   vesselFlow_compute_vs_Time.m (Q vs. t in main arteries)
%   aorta_3D_Pressure_profile.m (P vs. t and length along aortic
trunk - 3D plot)

clear
clear global

global rho rhogen          % blood density [kg/m^3]
global mu muSS            % blood viscosity  1 kg/(m-s)=10 g/(cm-s)=10
Poise=1000 cP
global nu w                % fundamental freq, vector of harmonic
frequencies [Hz]
global b1 b2 b3           % parameters to compute beta=vessel pseudo-
compliance
global inart              % vessel that receives input pressure
global N                  % length of time, pressure input arrays
global numModes           % number of Fourier harmonics
global vesselLengths     % [m]
global vesselProxRadii   % [m]
global vesselDistRadii   % [m]
```

```

delE1 = 1*0.15/(4*pi*0.8);
% delE1 = 0.2;
% delE2 = 0.5;
% delE3 = 0.5;
delE2=delE1;
delE3=delE1;
Eadj=1;
nscale2=2;      % bifurcating scaling factor for subnetworks
nscale3=3;      % trifurcating scaling factor for subnetworks

% Get input (filenames, etc) from user & read in data to analyze.
% The inlet pressure profile from Olufsen (2004) is named p2dec.txt
for the
% aorta, so the input artery is "1" for the model

inletPdata=load('p2dec.txt','-ascii');      %col.1=time[s],
col.2=pres[mmHg]
% allArts=input('Enter 1 to compute & save pressures in all arteries
and trees: ');
allArts = 1;

load('vessel_data.mat');
% HctD =      discharge hematocrit (dimensionless)
% Nbar =      number of generations from capillary where cubic
scaling
%           law is used for radii of arterial tree vessels
% PEnd =      pressure at capillary level (usually about 2000 Pa)
% Temp =      absolute temperature of experiment
%           (for human body approx. 309.65K)
% b1, b2, b3 = pseudo-compliance factors
% cap_LoverD = capillary length-to-diameter ratio (dimensionless)
% cf = 0.1    fibrinogen concentration [g/dl]
%           (APPROXIMATION - MUST BE CHANGED WHEN AN ACCURATE
%           EXPRESSION IS FOUND)
% inart =     artery where input pressure is located
%           (usually 1 for ascending aorta)
% muP =       viscosity of blood plasma [Pa s] (at reference Temp)
% nscale =    number of daughter vessels for each parent in sub-
networks
% numArt =    number of main vessels in network
% rhoP =      blood plasma density [kg/m^3]
% rhoRBC =    red blood cell density [kg/m^3]
% rmincap =   minimum capillary radius [m]
% sigma =     Poisson Ratio
% vesselLengths = single column array with vessel lengths in [m]
% vesselProxRadii = single column array with proximal vessel radii in
[m]
% vesselDistRadii = single column array with distal vessel radii in
[m]

Hctc = 0.3126*cf^2-0.468*cf+0.1764; % critical hematocrit
Temp0=296.16; % reference temperature for muP [K]

```

```

muPabs=muP*exp(-7.0276*(1-Temp0/Temp)); % corrected plasma viscosity
for j=1:numArt
    vesselAvgRadii(j)=(vesselProxRadii(j)+vesselDistRadii(j))/2;
    LRcap_ratio(j)=2*cap_LoverD; % capillary L/r ratio (adjustable)
end

terminal_brain_arteries=[57,58,64,65,71,72,74,75,76,78,80,82,84,86,88
,90,91,92,93,94,100,102];
for j=1:length(terminal_brain_arteries)
    LRcap_ratio(terminal_brain_arteries(j))=50;
end

load('connectivity_data_uptodate.mat');
% numArtConnected = matrix of all numbered vessels attached to given
node
maxVesselsConnected=length(numArtConnected(1,:));
% maximum number of main vessels connecting to a single node

numNodes=length(numArtConnected(:,1));
% total number of nodes connecting main arteries
% (includes terminal nodes and input pressure node)

% numNodesConnected = 2 column matrix denoting which nodes are
connected to
% given main vessel
numNodesConnected=zeros(max(max(numArtConnected(:,:))),2);
for j=1:numNodes
    for m=1:maxVesselsConnected
        if numArtConnected(j,m)~=0
            if numNodesConnected(numArtConnected(j,m),1)==0
                numNodesConnected(numArtConnected(j,m),1)=j;
            else
                numNodesConnected(numArtConnected(j,m),2)=j;
            end
        end
    end
end

% howmanynodesconnected = # of other nodes sharing a main vessel with
given node
howmanynodesconnected=zeros(numNodes,1);
howmanynodesconnected(1)=1;
for j=2:numNodes
    nnum=0;
    for m=1:maxVesselsConnected
        if numArtConnected(j,m)>0
            nnum=nnum+1;
        end
        if howmanynodesconnected(j)==1
            howmanynodesconnected(j)=2;
        else

```

```

        howmanynodesconnected(j)=nnum;
    end
end
end

parentvessel=zeros(numArt,1);
for j=2:numNodes
    if numArtConnected(j,2)==0
        parentvessel(numArtConnected(j,1))=1;
    end
end
% The parentvessel array returns 1 if the specified vessel is the
direct
% parent of a secondary network, or 0 if the vessel is instead
connected
% only to other numbered vessels

% time and pressure data come directly from p2dec input file
time=inletPdata(:,1);           %time increments of inlet
pressure wave
pressure=inletPdata(:,2)*133.322; %pressure at each time increment
(converted to [Pa])
Pmean=mean(pressure);           %mean pressure (used in SS calcs)
N=length(pressure);             %length of pressure and time
arrays
nu=(N-1)/(N*(time(N)-time(1))); %HR [Hz]
fprintf('%d point pairs loaded; fundamental frequency = %g
Hz.\n',N,nu);

%Fraction of input wave power accounted for by # of harmonics used
will be
%displayed for user. Increase numModes if <99% of power is accounted
for.

numModes=10;                    % # of Fourier harmonics
w=2*pi*nu*(1:numModes);         % frequency of each harmonic

majarts=[1 15 21 22 52]; % major arteries
% (aorta, L. common carotid, L. brachial, L. radial, L. femoral)
if isempty(allArts) || (allArts~=1)
    allArts=0;
    arteries=majarts;           %calc pressure, flow in these arteries
else
    arteries=[1:numArt];       %calc pressure, flow in all arteries
end

% Calculate Viscosity in Each Main Artery, Based on Bottom Radius
for j=1:numArt
    D=2*vesselDistRadii(j)*1e6; % diameter, must be converted to
microns for calculation

```

```

    HctT(j) = HctD*(HctD+(1-HctD)*(1+1.7*exp(-0.415*D)-0.6*exp(-
0.011*D)));
    % local hematocrit - volume fraction of red blood cells
    (dimensionless)
    alp = 4/(1+exp(-0.593*(D-6.74)));
    mu(j) = muPabs*(1 + ((exp(HctD*alp)-1)/(exp(0.45*alp)-
1))*(110*exp(-1.424*D)+3-3.45*exp(-0.035*D))); % local viscosity
    rho(j) = rhoP*(1-HctT(j)) + rhoRBC*HctT(j); % local density
    muSS(j) = muPabs*(1+2.0703*HctT(j)+3.7222*HctT(j)^2);
    tauw(j) = 1; % wall stress (will be corrected later)
end

% M-K Wave Speed, Pulse Wave Veloc, Impedance, Resistance (no
entrance effects)
% (for main vessels)
for j=1:numArt
    %Beta=E*h/r0, based on empirical fit to variation of beta with R
across arteries
    if vesselAvgRadii(j) > 5e-4
        Beta(j)=b1*exp(b2*vesselAvgRadii(j))+b3; %[kg/(m-s2)] Pseudo-
Compliance
    else
        Beta(j)=b1*exp(b2*5e-4)+b3;
    end

    if vesselAvgRadii(j) > 2e-4
        h = 0.07;
        %
        E = (Beta(j)*Ravg(j)/h) +
i*0.15*(Beta(j)*Ravg(j)/h)/(2*pi*2);
        E(j) = Eadj*(Beta(j)*vesselAvgRadii(j)/h) +
i*nu*(Beta(j)*vesselAvgRadii(j)/h)*delE1;
        Beta(j) = E(j)*h/vesselAvgRadii(j);
    elseif vesselAvgRadii(j) > 2e-5
        h = 0.4;
        %
        E = (Beta(j)*Ravg(j)/h) +
i*0.15*(Beta(j)*Ravg(j)/h)/(2*pi*2);
        E(j) = Eadj*(Beta(j)*vesselAvgRadii(j)/h) +
i*nu*(Beta(j)*vesselAvgRadii(j)/h)*delE2;
        Beta(j) = E(j)*h/vesselAvgRadii(j);
        fprintf('error')
    else
        h = 0.17;
        %
        E = (Beta(j)*Ravg(j)/h) +
i*0.15*(Beta(j)*Ravg(j)/h)/(2*pi*2);
        E(j) = Eadj*(Beta(j)*vesselAvgRadii(j)/h) +
i*nu*(Beta(j)*vesselAvgRadii(j)/h)*delE3;
        Beta(j) = E(j)*h/vesselAvgRadii(j);
        fprintf('error')
    end
end

```

```

Comp(j)=(3/2)*pi*vesselLengths(j)*((vesselDistRadii(j)^2+vesselProxRadii(j)^2)/3)/Beta(j);
c0(j)=sqrt(Beta(j)/(2*rho(j))); % [m/s] Moens-Korteweg Wave
Velocity
    for n=1:numModes
        alpha(j,n)=sqrt(w(n)*rho(j)/mu(j))*vesselAvgRadii(j); %
Womersley Number
        c(j,n)=c0(j)*sqrt(-(1/(1-
sigma^2))*(besselj(2,i^(3/2)*alpha(j,n)))/(besselj(0,i^(3/2)*alpha(j
,n)))));
        % ^Complex Wavespeed [m/s]
        Z(j,n)=(1/(1-
sigma^2))*(c0(j))^2*rho(j)/(pi*(vesselAvgRadii(j))^2*c(j,n)); %
Characteristic (Local) Impedance
        Zphase0(j,n)=atan2(imag(Z(j,n)),real(Z(j,n)));
        Zmag0(j,n)=real(Z(j,n))/cos(Zphase0(j,n));
    end
end
Emodulus=real(E);
% Lubrication Integration of Resistance for Tapered Vessels
for j=1:numArt
    if vesselProxRadii(j)==vesselDistRadii(j) % (vessel does not
change radius/does not taper)

PoisRes(j)=8*muSS(j)*vesselLengths(j)/(pi*vesselProxRadii(j)^4);
%[Pa-s/m^3]
        K(j)=0; % exponential factor not needed
    else

K(j)=log(vesselDistRadii(j)/vesselProxRadii(j))/vesselLengths(j);

PoisRes(j)=8*muSS(j)/(pi*((vesselProxRadii(j)+vesselDistRadii(j))/2)^
4)*(exp(-4*K(j)*vesselLengths(j))-1)/(-4*K(j));
        % ^Correction for tapering
    end
end

% Scaling Trees Attached to Each Terminal Main Artery %
global lgen %lengths of vessels in generations stemming from terminal
numbered arteries
for j=1:numArt
    Gentotal(j)=0; % number of generations after terminal main vessel
    if parentvessel(j,1)==1
        % First check critical radius
        rbar(j)=rmincap/(nscale3^(-Nbar/3));
        if rbar(j)>=vesselDistRadii(j) % (scaling immediately follows
cubic law)
            kbar(j)=0;
            Gentotal(j)=fix(-
3*log(rmincap/vesselDistRadii(j))/log(nscale3));
        else % (scaling follows square root up to kbar)

```

```

        kbar(j)=fix(-
2*log(rbar(j)/vesselDistRadii(j))/log(nscale2));
        Gentotal(j)=Nbar+kbar(j);
    end
    % Radii will scale by factor of 1/2 for generations < kbar,
then
    % change to factor of 1/3
    for m=1:Gentotal(j)
        if m<=kbar
            if m==1
                Rgen(j,m)=vesselDistRadii(j)*nscale2^(-1/2);
            else
                Rgen(j,m)=Rgen(j,m-1)*nscale2^(-1/2);
            end
        else
            if m==1
                Rgen(j,m)=vesselDistRadii(j)*nscale3^(-1/3);
            else
                Rgen(j,m)=Rgen(j,m-1)*nscale3^(-1/3);
            end
        end
    end
    % Back-calculate lengths based on ratio of capillary
length/radius
    % and move up through subnetworks
    Lgen(j,Gentotal(j))=LRcap_ratio(j)*Rgen(j,Gentotal(j));
    for m=1:min(Nbar,Gentotal(j)-1)
        Lgen(j,Gentotal(j)-m)=Lgen(j,Gentotal(j)-
m+1)*nscale3^(1/3);
    end
    if Gentotal(j)>Nbar+1 % (or if kbar(j)>0)
        for m=1:kbar(j)-1
            Lgen(j,kbar(j)-m)=Lgen(j,kbar(j)-m+1)*nscale2^(1/3);
        end
    end
end
end
end

% Calculate Viscosity in Arterial Trees %
for j=1:numArt
    if parentvessel(j,1)==1
        for m=1:Gentotal(j)
            D=2*Rgen(j,m)*1e6; % diameter of mth generation of jth
terminal artery in microns
            HctTgen(j,m) = HctD*(HctD+(1-HctD)*(1+1.7*exp(-0.415*D)-
0.6*exp(-0.011*D))); % local hematocrit of mth generation
            alp = 4/(1+exp(-0.593*(D-6.74)));
            mugen(j,m) = muPabs*(1 + ((exp(HctD*alp)-
1)/(exp(0.45*alp)-1))*(110*exp(-1.424*D)+3-3.45*exp(-0.035*D))); %
local viscosity of mth generation
            rhogen(j,m) = rhoP*(1-HctTgen(j,m)) +
rhoRBC*HctTgen(j,m); % local density of mth generation
        end
    end
end

```

```

        mugenSS(j,m) =
muPabs*(1+2.0703*HctTgen(j,m)+3.7222*HctTgen(j,m)^2);
        tauwgen(j,m) = 1; % wall stress (will correct later)
    end
end
end

% M-K Wave Speed, Pulse Wave Veloc, Impedance, Resistance (no
entrance effects)
% (for sub-networks)
for j=1:numArt
    if parentvessel(j,1)==1
        for m=1:Gentotal(j)

PoisResgen(j,m)=Lgen(j,m)*8*mugenSS(j,m)/(pi*Rgen(j,m)^4); %[Pa-
s/m^3]

            if Rgen(j,m) > 5e-4
Beta=E*h/r0
                Betagen(j,m)=b1*exp(b2*Rgen(j,m))+b3;    %[kg/m-s^2]
            else
                Betagen(j,m)=b1*exp(b2*5e-4)+b3;
            end

            if Rgen(j,m) > 2e-4
                h = 0.07;
                %
                E = (Betagen(j,m)*Rgen(j,m)/h) +
i*0.15*(Betagen(j,m)*Rgen(j,m)/h)/(2*pi^2);
                E = Eadj*(Betagen(j,m)*Rgen(j,m)/h) +
i*nu*(Betagen(j,m)*Rgen(j,m)/h)*delE1;
                Betagen(j,m) = E*h/Rgen(j,m);
            elseif Rgen(j,m) > 2e-5
                h = 0.4;
                %
                E = (Betagen(j,m)*Rgen(j,m)/h) +
i*0.15*(Betagen(j,m)*Rgen(j,m)/h)/(2*pi^2);
                E = Eadj*(Betagen(j,m)*Rgen(j,m)/h) +
i*nu*(Betagen(j,m)*Rgen(j,m)/h)*delE2;
                Betagen(j,m) = E*h/Rgen(j,m);
            else
                h = 0.17;
                %
                E = (Betagen(j,m)*Rgen(j,m)/h) +
i*0.15*(Betagen(j,m)*Rgen(j,m)/h)/(2*pi^2);
                E = Eadj*(Betagen(j,m)*Rgen(j,m)/h) +
i*nu*(Betagen(j,m)*Rgen(j,m)/h)*delE3;
                Betagen(j,m) = E*h/Rgen(j,m);
            end

            c0gen(j,m)=sqrt(Betagen(j,m)/(2*rhogen(j,m)));    %[m/s]
            for n=1:numModes

alphagen(j,m,n)=sqrt(n^2*pi*nu*rhogen(j,m)/mugen(j,m))*Rgen(j,m);

```

```

        cgen(j,m,n)=c0gen(j,m)*sqrt(-
        ((besselj(2,i^(3/2)*alphagen(j,m,n)))/(besselj(0,i^(3/2)*alphagen(j,m
        ,n)))));    %[m/s]

Zgen(j,m,n)=(c0gen(j,m))^2*rhogen(j,m)/(pi*(Rgen(j,m))^2*cgen(j,m,n))
;

Compgen(j,m)=(3/2)*pi*Lgen(j,m)*Rgen(j,m)^2/Betagen(j,m);
        end
    end
end

% Iterate to find entrance resistances and wall stress values that
% give convergence
[Rentrance,Rentrancegen,Pmeanao,tauw,tauwgen,muSSeff,mugenSSeff,FlowF
rac,LCC,LR,RCA]=...

steadyiterate_P_density_SS_new(parentvessel,Gentotal,kbar,numArt,numN
odes,howmanyodesconnected,numArtConnected,...

numNodesConnected,Pmean,PEnd,vesselAvgRadii,vesselProxRadii,rho,rhoge
n,Lgen,vesselLengths,Rgen,...

vesselDistRadii,inart,Hctc,HctT,HctTgen,tauw,tauwgen,muSS,mugenSS,cf,
nscale2,nscale3);

% Final Resistance = Final Entrance Resistance + Poiseuille
Resistance
% TotRes will contain resistances of numbered vessels in SI units
for j=1:numArt
    if HctT(j) > Hctc
        tau0 = 0.1*((HctT(j)-Hctc)^2)*((0.5084*cf+0.4517)^2);
        eps = 1-((1/21)*(tau0/tauw(j))^4)-
        ((16/7)*(tau0/tauw(j))^0.5)+((4/3)*(tau0/tauw(j)));
        TotRes(j)=PoisRes(j)/eps+Rentrance(j);    %[Pa-s/m^3]
    else
        tau0 = 0;
        TotRes(j)=PoisRes(j)+Rentrance(j);    %[Pa-s/m^3]
    end
end
end

% Final Resistance = Final Entrance Resistances + Poiseuille
Resistance (secondary networks)
% TotResgen will contain individual resistances of vessels in each
generation (SI units)
for j=1:numArt
    if parentvessel(j,1)==1
        for m=1:Gentotal(j)
            if HctTgen(j,m) > Hctc
                tau0 = 0.1*((HctTgen(j,m)-
                Hctc)^2)*((0.5084*cf+0.4517)^2);

```

```

        if tauwgen(j,m) == 0
            eps=1;
        else
            eps = 1-((1/21)*(tau0/tauwgen(j,m))^4)-
((16/7)*(tau0/tauwgen(j,m))^0.5)+((4/3)*(tau0/tauwgen(j,m)));
        end
        TotResgen(j,m)=PoisResgen(j,m)/eps+Rentrancegen(j,m);
    %[Pa-s/m^3]
    else
        tau0 = 0;
        TotResgen(j,m)=PoisResgen(j,m)+Rentrancegen(j,m);
    %[Pa-s/m^3]
    end
end
end
end

% Equivalent Resistances of Each Vessel in Secondary Networks
% Rcumgen(j,m) will contain the cumulative resistance from the start
of
% generation m in sub-network j, out to the capillary level, taking
into
% account the entrance resistances and series/parallel combinations
of all
% downstream vessels.
for j=1:numArt
    if parentvessel(j,1)==1
        Rcumgen(j,Gentotal(j))=TotResgen(j,Gentotal(j));
        for m=1:(Gentotal(j)-1)
            if (Gentotal(j)-m)>kbar(j)
                Rcumgen(j,Gentotal(j)-m)=TotResgen(j,Gentotal(j)-
m)+Rcumgen(j,Gentotal(j)-m+1)/nscale3;
            else
                Rcumgen(j,Gentotal(j)-m)=TotResgen(j,Gentotal(j)-
m)+Rcumgen(j,Gentotal(j)-m+1)/nscale2;
            end
        end
    end
end

% System of Equations to find SS Pressures at each Node
PdropEffective=Pmean-PEnd;      % [Pa], accounts for actual capillary
pressure
a=zeros(numNodes,numNodes);
b=zeros(numNodes,1);
a(1,1)=1;
b(1,1)=PdropEffective;
for j=2:numNodes
    for m=1:howmanynodesconnected(j)
        if numArtConnected(j,m)==0
            if kbar(j)==0

```

```

        a(j,j)=a(j,j)-
        (nscale3/Rcumgen(numArtConnected(j,1),1)); % trifurcation
    else
        a(j,j)=a(j,j)-
        (nscale2/Rcumgen(numArtConnected(j,1),1)); % bifurcation
    end
else
PairNode=numNodesConnected(numArtConnected(j,m),1)+numNodesConnected(
numArtConnected(j,m),2)-j;
    a(j,PairNode)=1/TotRes(numArtConnected(j,m));
    a(j,j)=a(j,j)-(1/TotRes(numArtConnected(j,m)));
end
end
end
Pstar=a\b; % Effective pressures at every node
Poutcome=a*Pstar-b; % check - should be effectively zero for every
node

% Steady State Flow in all vessels
for j=1:numArt
    SteadyFlow(j)=abs(Pstar(numNodesConnected(j,1))-
Pstar(numNodesConnected(j,2)))/TotRes(j);
    if parentvessel(j)==1
        for m=1:Gentotal(j)
            if m==1
                if m<=kbar(j)
                    SteadyFlowgen(j,m)=SteadyFlow(j)/nscale2;
                else
                    SteadyFlowgen(j,m)=SteadyFlow(j)/nscale3;
                end
            else
                if m<=kbar(j)
                    SteadyFlowgen(j,m)=SteadyFlowgen(j,m-1)/nscale2;
                else
                    SteadyFlowgen(j,m)=SteadyFlowgen(j,m-1)/nscale3;
                end
            end
        end
    end
end
end

% termflux = sum of flows at each terminal node
% (should equal total cardiac output)
termflux=0;
for j=1:numArt
    if parentvessel(j)==1
        termflux=termflux+abs((Pstar(numNodesConnected(j,1))-
Pstar(numNodesConnected(j,2)))/TotRes(j));
    end
end
end

```

```

% Total Steady Flow, Pressure Drop, & Cumulative Resistance
Calculation
Flowtotal=(Pstar(1)-Pstar(2))/TotRes(1);    % Total Cardiac Output
(overall flow) based on pressure drop along first vessel [m^3/s]
Rcum=(PdropEffective/Flowtotal);           % Cumulative Resistance
of network

% vesselflow gives flux through any main vessel [m^3/s]
vesselflow=zeros(numArt,1);
for j=1:numArt
    vesselflow(j)=abs((Pstar(numNodesConnected(j,1))-
Pstar(numNodesConnected(j,2)))/TotRes(j));
end

% flowtobrain gives total flux to the brain, taking into account
flows through
% common carotid and vertebral arteries [L/min]
flowtobrain=(vesselflow(5)+vesselflow(6)+vesselflow(15)+vesselflow(20
))*6e4;

fprintf('Total pressure drop = %f Pa\n',PdropEffective)
fprintf('Total Cardiac Output = %f L/min\n',Flowtotal*6e4)
fprintf('Total Blood Flow to Brain = %f L/min\n',flowtobrain)
fprintf('Cumulative Resistance of Network = %f dyne/(cm^5
sec)\n',Rcum*1e-5)

% Determine Reflection Ratios (Alpha) in Arterial Trees
for j=1:numArt
    if parentvessel(j,1)==1
        for n=1:numModes
            for m=1:Gentotal(j)
                k=Gentotal(j)-m+1; % (k counts backward to 1)
                if k==Gentotal(j)
                    Ztermgen=Zgen(j,k,n); % assume perfect
termination at capillaries
                elseif k>=kbar(j)
                    Ztermgen=InputZgen(j,k+1,n)/nscale3;
                else
                    Ztermgen=InputZgen(j,k+1,n)/nscale2;
                end
                Alphagen(j,k,n)=(Ztermgen-
Zgen(j,k,n))/(Ztermgen+Zgen(j,k,n));
                InputZgen(j,k,n)=Zgen(j,k,n)*...    % Input Impedance
((1+Alphagen(j,k,n)*exp(-
2*i*w(n)*Lgen(j,k)/cgen(j,k,n)))/...
(1-Alphagen(j,k,n)*exp(-
2*i*w(n)*Lgen(j,k)/cgen(j,k,n)))));
            end
        end
    end
end
end

```

```

% Determine Reflection Ratios (Alpha) in Terminal Main Arteries
for j=1:numArt
    if parentvessel(j,1)==1
        for n=1:numModes
            if kbar(j)==0
                Zterm(j,n)=InputZgen(j,1,n)/nscale3;
            else
                Zterm(j,n)=InputZgen(j,1,n)/nscale2;
            end
            Alpha(j,n)=(Zterm(j,n)-Z(j,n))/(Zterm(j,n)+Z(j,n));
            InputZ(j,n)=Z(j,n)*((1+Alpha(j,n))*exp(-
2*i*w(n)*vesselLengths(j)/c(j,n)))/...
            (1-Alpha(j,n))*exp(-
2*i*w(n)*vesselLengths(j)/c(j,n))); % Input Impedance
            % (^see Milnor reference (7.20) in Johnson et al. 2011)
        end
    end
end

% System of Equations to find Forward and Backward Pressure Waves
(complex) for each Vessel
% A(j,1)*PstarTrans(1,n)+A(j,2)*PstarTrans(2,n)+...=B(j) for each
harmonic
PstarTrans=zeros(2*numArt,numModes);
for n=1:numModes
    A=zeros(2*numArt);
    B=zeros(2*numArt,1);
    A(1,1)=1;
    A(1,2)=1;
    B(1)=1; % all pressures are relative to Ptot (calculated by
aortaP below)
    ncounter=2;
    for j=2:numNodes
        if howmanynodesconnected(j)==2
            % terminal network section
            termVesselNumber=numArtConnected(j,1);
            A(ncounter,2*termVesselNumber-
1)=Alpha(termVesselNumber,n);
            A(ncounter,2*termVesselNumber)=-1;
            ncounter=ncounter+1;
        else
            k=howmanynodesconnected(j);
            % assign coefficients for forward and backward pressure
waves
            % by setting total flux at node = 0
            for m=1:k
                vesselNumber=numArtConnected(j,m);
                if numNodesConnected(vesselNumber,1)==j
                    % node is effectively at beginning of vessel
                    A(ncounter,2*vesselNumber-1)=-
1/Z(vesselNumber,n);

```

```

        A(ncounter,2*vesselNumber)=exp(-
i*w(n)*vesselLengths(vesselNumber)/c(vesselNumber,n))/Z(vesselNumber,
n);
        else
            % node is effectively at end of vessel
            A(ncounter,2*vesselNumber-1)=exp(-
i*w(n)*vesselLengths(vesselNumber)/c(vesselNumber,n))/Z(vesselNumber,
n);
            A(ncounter,2*vesselNumber)=-1/Z(vesselNumber,n);
        end
        % weight coefficients to avoid singularity problems
        % bring coefficients much closer to order of 1
        if m==1
            weight=1/A(ncounter,2*vesselNumber-1);
        end
        A(ncounter,2*vesselNumber-
1)=A(ncounter,2*vesselNumber-1)*weight;
A(ncounter,2*vesselNumber)=A(ncounter,2*vesselNumber)*weight;
    end
    ncounter=ncounter+1;
    for m=1:k-1
        % set all total pressures just outside of node equal
        vesselNumber1=numArtConnected(j,1);
        if numNodesConnected(vesselNumber1,1)==j
            % node is effectively at beginning of vessel
            A(ncounter,2*vesselNumber1-1)=1;
            A(ncounter,2*vesselNumber1)=exp(-
i*w(n)*vesselLengths(vesselNumber1)/c(vesselNumber1,n));
        else
            % node is effectively at end of vessel
            A(ncounter,2*vesselNumber1-1)=exp(-
i*w(n)*vesselLengths(vesselNumber1)/c(vesselNumber1,n));
            A(ncounter,2*vesselNumber1)=1;
        end
        vesselNumber2=numArtConnected(j,m+1);
        if numNodesConnected(vesselNumber2,1)==j
            % node is effectively at beginning of vessel
            A(ncounter,2*vesselNumber2-1)=-1;
            A(ncounter,2*vesselNumber2)=-exp(-
i*w(n)*vesselLengths(vesselNumber2)/c(vesselNumber2,n));
        else
            % node is effectively at end of vessel
            A(ncounter,2*vesselNumber2-1)=-exp(-
i*w(n)*vesselLengths(vesselNumber2)/c(vesselNumber2,n));
            A(ncounter,2*vesselNumber2)=-1;
        end
        ncounter=ncounter+1;
    end
end
end
PstarTrans(:,n)=A\B;

```

```

        %Pf for vessel j = PstarTrans(2*j-1,n)
        %Pb for vessel j = PstarTrans(2*j,n)
    end

    % Find Reflection Ratios (Alpha) for non-terminal main vessels
    for j=1:numArt
        if parentvessel(j,1)~=1
            for n=1:numModes
                Alpha(j,n)=PstarTrans(2*j,n)/PstarTrans(2*j-
1,n)*exp(i*w(n)*vesselLengths(j)/c(j,n));
            end
        end
    end

    % aortaPressure.m computes aortic forward pressure wave harmonics
    % also plots floward and backward components of pressure and flow in
    aorta
    [Ptot,Pfao]=aortaPressure_density_SS_new(pressure,time,Flowtotal,vess
elLengths,Pmeanao,Pmean,Alpha,c,Z,inart);

```